Final report for the ONR award "Numerical Methods for Computing Turbulence-Induced Noise"

ONR Grant No. 00014-02-1-0425

Performance Period: 04/01/02-09/30/05

Assad A. Oberai
Department of Aerospace and Mechanical Engineering
Center for Computational Science
Boston University
Boston, MA 02215

Prepared for
Dr. Luise Couchman
Office of Naval Research
Ballston Center Tower One
800 North Quincy Street
Arlington VA 22217-5660

REPORT DOCUMENTATION PAGE

Form Approved
OMB No. 0704-0188

1. REPORT DATE *(DD-MM-YYYY)*	2. REPORT TYPE	3. DATES COVERED *(From - To)*
16-12-2005	Final	April 2002- Sept. 2005

4. TITLE AND SUBTITLE
Numerical Methods for Computing Turbulence-Induced Noise

5a. CONTRACT NUMBER

5b. GRANT NUMBER
00014-02-1-0425

5c. PROGRAM ELEMENT NUMBER

6. AUTHOR(S)
Oberai, Assad, A.

5d. PROJECT NUMBER

5e. TASK NUMBER

5f. WORK UNIT NUMBER

7. PERFORMING ORGANIZATION NAME(S) AND ADDRESS(ES)
The Trustees of Boston University, Office of Sponsored Programs 881 Commowealth Avenue Boston MA 02215

8. PERFORMING ORGANIZATION REPORT NUMBER

9. SPONSORING/MONITORING AGENCY NAME(S) AND ADDRESS(ES)
Office of Naval Resarch Ballston Center Tower One 800 North Quincy Street Arlington, VA 22217-5660

10. SPONSOR/MONITOR'S ACRONYM(S)
ONR

11. SPONSOR/MONITOR'S REPORT NUMBER(S)

12. DISTRIBUTION/AVAILABILITY STATEMENT
Approved for Public Release

13. SUPPLEMENTARY NOTES

14. ABSTRACT
The prediction of noise generated by hydrodynamic sources is a significant problem of interest to the U.S. Navy. This proposal describes a program of research aimed at developing and testing computational techniques for formulating and solving structural acoustics problems driven by hydrodynamic sources.

15. SUBJECT TERMS
hydroacoustics; turbulence modeling; large eddy simulation

16. SECURITY CLASSIFICATION OF:			17. LIMITATION OF ABSTRACT	18. NUMBER OF PAGES	19a. NAME OF RESPONSIBLE PERSON
a. REPORT	b. ABSTRACT	c. THIS PAGE			Assad A. Oberai
U	U	U	UU		19b. TELEPHONE NUMBER *(Include area code)* 617 353 7381

Contents

Chapter 1

Introduction

The prediction of noise generated by hydrodynamic sources is a significant problem of interest to the U.S. Navy. This proposal describes a program of research aimed at developing and testing computational techniques for formulating and solving structural acoustics problems driven by hydrodynamic sources.

The typical parameters associated with the problems of interest to the Navy are low Mach numbers and high Reynolds numbers. This regime naturally leads to the application of Lighthill's acoustic analogy to solve the problem [1, 2]. In this approach the original problem is decomposed into two parts, one that involves the solution of the Navier-Stokes equations to determine the unsteady fluid variables, and another that involves the solution of an acoustic problem driven by *quadrupole* sources whose distribution is determined by the components of Lighthill's turbulence tensor. This tensor is constructed from the unsteady flow field computed in the fluid calculation. In our previous work [3, 4], we have developed a methodology that uses large eddy simulation (LES) to calculate Lighthill's tensor and a variational formulation of Lighthill's acoustic analogy to solve the acoustic problem. The effectiveness of this method was demonstrated in [4], where we calculated the noise generated by turbulent flow over an airfoil, while fully accounting for its geometry. Previous studies [5–11] have had to make simplifications to render the problem tractable. In the same paper, it was found that the computational costs of the overall methodology were dominated by the turbulent calculation. This meant that better and more efficient LES models were required to extend the applicability of the proposed methodology to higher Reynolds number. With this in mind a parallel effort aimed at developing new LES models based on the *variational multiscale formulation* was undertaken (see [12, 13]). The proposed research extends these ideas in new directions.

A significant component of the research is aimed at improving the variational multiscale formulation of LES [12–14]. This is accomplished by developing a *dynamic* version of this method, wherein the eddy viscosity is calculated during the numerical simulation and is not fixed *a-priori*. For this purpose the dynamic Smagorinsky model [15] is revisited, and a variational version of the Germano identity is derived. This is done in the context of an abstract variational problem in Chapter 2. It is found that this leads to a formulation which may be used to determine unknown parameters in a generic numerical method.

Thereafter the variational Germano identity is applied to solve problems posed as conservation laws. The specialization of this identity to account for spectral discretizations

is developed and the effectiveness of this formulation in solving problems with discontinuities (shocks) is demonstrated. These developments are presented in Chapter 3.

In Chapter 4, the variational Germano identity is applied to the large eddy simulation of incompressible turbulent flows, and it is demonstrated that it is more accurate and robust than the filtered counterpart.

Finally in Chapter 5, the performance of this identity in predicting the far-field noise generated by homogeneous turbulence is assessed. It is found that in conjunction with the variational multiscale formulation it outperforms the current state of art.

The results of this research have been published in refereed journals in the following articles [16–19].

Chapter 2

Variational Germano Identity

2.1 Introduction

Consider the weak form of an abstract (possibly non-linear) partial differential equation, viz., find $\boldsymbol{u} \in \mathcal{V}$, such that

$$B(\boldsymbol{w}, \boldsymbol{u}) = (\boldsymbol{w}, \boldsymbol{f}), \qquad \forall \boldsymbol{w} \in \mathcal{V}. \tag{2.1}$$

Here $B(\cdot, \cdot) : \mathcal{V} \times \mathcal{V} \to \mathbb{R}$ is a semi-linear form that is linear in its first slot, $\mathcal{V}$ is the space of weighting functions and trial solutions, and $f \in L^2(\Omega)$ is the prescribed forcing function. The Galerkin approximation to the weak form is given by: find $\boldsymbol{u}^h \in \mathcal{V}^h$, such that

$$B(\boldsymbol{w}^h, \boldsymbol{u}^h) = (\boldsymbol{w}^h, f), \qquad \forall \boldsymbol{w}^h \in \mathcal{V}^h, \tag{2.2}$$

where $\mathcal{V}^h \subset \mathcal{V}$ is a finite dimensional subspace.

In several applications the Galerkin method does not yield good numerical solutions. In such cases, other numerical methods with solutions that are close to an "optimal" representation of the continuous solution in $\mathcal{V}^h$, are derived (see for example [20, 21]). That is methods with solutions $\boldsymbol{u}^h$,

$$\boldsymbol{u}^h \approx \boldsymbol{v}^h \equiv \mathbb{P}^h \boldsymbol{u}, \tag{2.3}$$

where $\boldsymbol{v}^h$ is the optimal representation of $\boldsymbol{u}$ in $\mathcal{V}^h$, and $\mathbb{P}^h : \mathcal{V} \to \mathcal{V}^h$ is an appropriate mapping. Several definitions of $\mathbb{P}^h$ and hence $\boldsymbol{v}^h$ may be considered. For example, in a finite element context, $\boldsymbol{v}^h$ may be the nodal interpolant, or the L^2 or H^1 projection of $\boldsymbol{u}$ on to $\mathcal{V}^h$. A large class of such numerical methods may be formally expressed as: find $\boldsymbol{u}^h \in \mathcal{V}^h$, such that

$$B(\boldsymbol{w}^h, \boldsymbol{u}^h) + M(\boldsymbol{w}^h, \boldsymbol{u}^h, \boldsymbol{f}; h, \boldsymbol{c}) = (\boldsymbol{w}^h, \boldsymbol{f}), \qquad \forall \boldsymbol{w}^h \in \mathcal{V}^h. \tag{2.4}$$

Here $M^h(\cdot, \cdot, \cdot; \cdot, \cdot) : \mathcal{V} \times \mathcal{V} \times L^2(\Omega) \times \mathbb{R} \times \mathbb{R}^P \to \mathbb{R}$ is the model term, which is a functional of the weighting function $\boldsymbol{w}^h$, the trial solution $\boldsymbol{u}^h$, and the forcing function $\boldsymbol{f}$. It also depends on the grid or mesh size h, and a vector of parameters $\boldsymbol{c} = [c_1, \cdots, c_P] \in \mathbb{R}^P$. Note that the solution of (2.4) is different form the Galerkin solution (solution of (2.2)).

In this manuscript we consider a numerical method (such as the one in (2.4)) with unknown parameters $\boldsymbol{c}$, and derive a methodology for determining these dynamically. This is achieved by requiring the solution of the numerical method to be equal to the optimal representation of the continuous solution on $\mathcal{V}^h$ *and its subspaces.* The result is an expression for $\boldsymbol{c}$ in terms of $\boldsymbol{u}^h$, $\boldsymbol{f}$, the mesh size associated with $\mathcal{V}^h$ and its subspaces, and the analog of the operator $\mathbb{P}^h$ on each subspace. Similar methods for computing numerical parameters have been developed by several researchers (see for example [22–25]). However, these methods typically involve either analytical or numerical solution of a simplified version of the original or an auxiliary (usually the adjoint) PDE. In contrast to these, the proposed method does not require such a solution. Instead it requires restrictions of the numerical solution on to coarse function spaces. These restrictions are easily computed and do not add significantly to the overall computational cost of the method.

The starting point of our development is the variational counterpart of the Germano identity. The Germano identity is a popular tool for computing the magnitude of the eddy viscosity in the large eddy simulation of turbulent flows. It was initially derived for the *filtered* Navier-Stokes equations in [15]. In this manuscript we propose a generalization of the variational form of this identity, and describe how it may be used to design better numerical methods. We first apply it to the linear advection-diffusion equation to dynamically evaluate the mesh-dependent diffusivity for the finite element approximation of this equation. Thereafter we apply it to evaluate the Smagorinsky coefficient in the large eddy simulation (LES) of the decay of homogeneous isotropic turbulence. In both cases the resulting numerical method is found to perform well. For the advection-diffusion equation, the results compare favorably with the Streamline Upwind Petrov-Galerkin (SUPG) method, which produces nodally exact solutions. For the turbulent flow problem, the results are generally more accurate than the constant-coefficient and the traditional dynamic Smagorinsky models. It is remarkable that the same formulation leads to accurate methods for these two significantly different problems.

The format of this chapter is as follows: In Section 2, we describe the variational Germano identity and derive its extension. In Section 3, we use this extension to derive an expression for the unknown parameters in a numerical method, which is the main result of this chapter. In Section 4, we apply this result to the linear advection diffusion to derive a non-linear *dynamic diffusivity method*, and compare the performance of this method with the streamline-upwind Petrov-Galerkin (SUPG) method. In Section 5 we apply the same methodology to compute the Smagorinsky coefficient in the LES of the decay of homogeneous isotropic turbulence in three dimensions, and compare our results with the constant-coefficient and the traditional dynamic Smagorinsky models. We end with concluding remarks in Section 6.

2.2 The Variational Germano Identity

In the context of the filtered Navier-Stokes equations the Germano identity is derived in [15]. In this section we apply its variational counterpart to the abstract PDE given by (2.4).

We begin by requiring the solution of the numerical method ($\boldsymbol{u}^h$) to be equal to $\boldsymbol{v}^h$.

Recall that $\boldsymbol{v}^h = \mathbb{P}^h \boldsymbol{u}$, is the optimal representation of $\boldsymbol{u}$ in $\mathcal{V}^h$. Setting $\boldsymbol{u}^h = \boldsymbol{v}^h$ in (2.4),

$$M(\boldsymbol{w}^h, \boldsymbol{v}^h, f; h, \boldsymbol{c}) = -\Big(B(\boldsymbol{w}^h, \boldsymbol{v}^h) - (\boldsymbol{w}^h, f)\Big), \qquad \forall \boldsymbol{w}^h \in \mathcal{V}^h. \tag{2.5}$$

This equation may be considered as a condition on the model term that is necessary for the numerical solution to be equal to the optimal representation of the continuous solution (that is $\boldsymbol{u}^h = \boldsymbol{v}^h$). Now consider the finite dimensional subspace $\mathcal{V}^{h_1} \subset \mathcal{V}^h$. Let $\boldsymbol{v}^{h_1} = \mathbb{P}^{h_1} \boldsymbol{u}$ be the optimal representation of $\boldsymbol{u}$ in $\mathcal{V}^{h_1}$ and $\mathbb{P}^{h_1} : \mathcal{V} \to \mathcal{V}^{h_1}$ be the appropriate mapping. We consider the following numerical method which is obtained by replacing h with h_1 in (2.4). Find $\boldsymbol{u}^{h_1} \in \mathcal{V}^{h_1}$, such that

$$B(\boldsymbol{w}^{h_1}, \boldsymbol{u}^{h_1}) + M(\boldsymbol{w}^{h_1}, \boldsymbol{u}^{h_1}, \boldsymbol{f}; h_1, \boldsymbol{c}) = (\boldsymbol{w}^{h_1}, f), \qquad \forall \boldsymbol{w}^{h_1} \in \mathcal{V}^{h_1}. \tag{2.6}$$

We assume that the solution of this numerical method is equal to the optimal representation of $\boldsymbol{u}$ in $\mathcal{V}^{h_1}$. That is, the same functional form of the model that leads to the optimal solution on $\mathcal{V}^h$, also leads to the optimal solution on $\mathcal{V}^{h_1}$. Thus, requiring $\boldsymbol{u}^{h_1} = \boldsymbol{v}^{h_1}$ in (2.6)

$$M(\boldsymbol{w}^{h_1}, \boldsymbol{v}^{h_1}, \boldsymbol{f}; h_1, \boldsymbol{c}) = -\Big(B(\boldsymbol{w}^{h_1}, \boldsymbol{v}^{h_1}) - (\boldsymbol{w}^{h_1}, f)\Big), \qquad \forall \boldsymbol{w}^{h_1} \in \mathcal{V}^{h_1}. \tag{2.7}$$

Subtracting (2.5) from (2.7) we arrive at the variational counterpart of the Germano identity, viz.

$$M(\boldsymbol{w}^{h_1}, \boldsymbol{v}^{h_1}, \boldsymbol{f}; h_1, \boldsymbol{c}) - M(\boldsymbol{w}^{h_1}, \boldsymbol{v}^h, \boldsymbol{f}; h, \boldsymbol{c}) = -\Big(B(\boldsymbol{w}^{h_1}, \boldsymbol{v}^{h_1}) - B(\boldsymbol{w}^{h_1}, \boldsymbol{v}^h)\Big), \quad \forall \boldsymbol{w}^{h_1} \in \mathcal{V}^{h_1}. \tag{2.8}$$

Note that (2.8) holds for weighting functions chosen from the intersection of the spaces of weighting functions for (2.5) and (2.7), that is $\mathcal{V}^h \bigcap \mathcal{V}^{h_1} = \mathcal{V}^{h_1}$. Equation (2.8), which may be interpreted as a consistency condition on model terms at two different scales, involves only the finite dimensional representations $\boldsymbol{v}^h$ and $\boldsymbol{v}^{h_1}$ of the exact solution $\boldsymbol{u}$ and not $\boldsymbol{u}$ itself.

Remark. The model term may be viewed as a sub-grid model by replacing the second term on the right hand side of (2.5) with $B(\boldsymbol{w}^h, \boldsymbol{u})$. This yields

$$M(\boldsymbol{w}^h, \boldsymbol{v}^h, \boldsymbol{f}; h, \boldsymbol{c}) = -\Big(B(\boldsymbol{w}^h, \boldsymbol{v}^h) - B(\boldsymbol{w}^h, \boldsymbol{u})\Big), \qquad \forall \boldsymbol{w}^h \in \mathcal{V}^h. \tag{2.9}$$

The right-hand side of (2.9) represents the effect of that part of $\boldsymbol{u}$ which is not contained in $\boldsymbol{v}^h$.

2.2.1 Extension of the Variational Germano Identity

In some circumstances (for models with more than one parameter) the variational Germano identity may not yield sufficient relations to determine the parameters of a model. For these cases we need to generalize (2.8).

Consider a hierarchy of finite dimensional function spaces $\mathcal{V}^{h_J} \subset \mathcal{V}^{h_{J-1}} \subset \cdots \subset \mathcal{V}^{h_2} \subset \mathcal{V}^{h_1} \subset \mathcal{V}^h$. For a given space $\mathcal{V}^{h_j}, j \in \mathbb{N}(1, J)$, let $\boldsymbol{v}^{h_j} = \mathbb{P}^{h_j} \boldsymbol{u}$ be the optimal representation

of the continuous solution and $\mathbb{P}^{h_j} : \mathcal{V} \rightarrow \mathcal{V}^{h_j}$ be the appropriate mapping. Following the procedure described in the previous section, and assuming that the same functional form of the model yields optimal solutions for the numerical method posed on all subspaces of $\mathcal{V}^h$, we arrive at the generic Germano identity viz,

$$M(\boldsymbol{w}^{h_j}, \boldsymbol{v}^{h_j}, \boldsymbol{f}; h_j, \boldsymbol{c}) - M(\boldsymbol{w}^{h_j}, \boldsymbol{v}^h, \boldsymbol{f}; h, \boldsymbol{c}) = -\Big(B(\boldsymbol{w}^{h_j}, \boldsymbol{v}^{h_j}) - B(\boldsymbol{w}^{h_j}, \boldsymbol{v}^h)\Big), \quad \forall \boldsymbol{w}^{h_j} \in \mathcal{V}^{h_j}, \qquad j = 1, \cdots, J \tag{2.10}$$

Note that for a given j, (2.10) holds for weighting functions chosen from the intersection of the spaces $\mathcal{V}^h \bigcap \mathcal{V}^{h_j} = \mathcal{V}^{h_j}$.

2.3 Application Of The Variational Germano Identity

In this section we describe how (2.10) may be used to derive an expression for $\boldsymbol{c}$.

For arbitrary weighting functions the variational Germano identity (2.10) represents a relation that involves the functions $\boldsymbol{v}^h, \boldsymbol{f}, \boldsymbol{v}^{h_1}, \cdots, \boldsymbol{v}^{h_J}$, and the parameters $\boldsymbol{h}$ and $\boldsymbol{c}$. Here

$$\boldsymbol{h} \equiv \{h, h_1, \cdots, h_J\}. \tag{2.11}$$

The dependence on $\boldsymbol{v}^{h_1}, \cdots, \boldsymbol{v}^{h_J}$ may be eliminated by expressing $\boldsymbol{v}^{h_j}$ in terms of $\boldsymbol{v}^h$. This is possible if

$$\mathbb{P}^{h_j}\mathbb{P}^h = \mathbb{P}^{h_j}, \tag{2.12}$$

since this implies $\boldsymbol{v}^{h_j} = \mathbb{P}^{h_j}\boldsymbol{v}^h$. Assuming $\mathcal{V}^{h_j} \subset \mathcal{V}^h$, it can be verified that (2.12) is satisfied *at least* for the following cases:

1. When $\mathbb{P}^h$ and $\mathbb{P}^{h_j}$ are interpolation operators.
2. When $\mathcal{V}^h \subset H^m(\Omega)$, and $\mathbb{P}^h$ and $\mathbb{P}^{h_j}$ are $H^n(\Omega)$-projections from $\mathcal{V}$ to $\mathcal{V}^h$ and $\mathcal{V}^{h_j}$ respectively, with $n \leq m$.

Using (2.12), (2.10) is reduced to

$$M(\boldsymbol{w}^{h_j}, \mathbb{P}^{h_j}\boldsymbol{v}^h, \boldsymbol{f}; h_j, \boldsymbol{c}) - M(\boldsymbol{w}^{h_j}, \boldsymbol{v}^h, \boldsymbol{f}; h, \boldsymbol{c}) = -\Big(B(\boldsymbol{w}^{h_j}, \mathbb{P}^{h_j}\boldsymbol{v}^h) - B(\boldsymbol{w}^{h_j}, \boldsymbol{v}^h)\Big), \quad \forall \boldsymbol{w}^{h_j} \in \mathcal{V}^{h_j}, \qquad j = 1, \cdots, J \tag{2.13}$$

In this form, for an arbitrary weighting function, the variational Germano identity represents a relation that involves the functions $\boldsymbol{v}^h$ and f, the parameters $\boldsymbol{h}$ and $\boldsymbol{c}$, and the set of operators $\mathbf{P}$, given by

$$\mathbf{P} \equiv \{\mathbb{P}^{h_1}, \cdots, \mathbb{P}^{h_J}\}. \tag{2.14}$$

Let $N^{h_j} = \dim(\mathcal{V}^{h_j})$. Then for every j (2.13) represents N^{h_j} relations. Experience with the Germano identity has shown that these relations should be interpreted in a global sense. This may be accomplished by either of the following methods.

Dissipation method This approach involves choosing $\boldsymbol{w}^{h_j} = \boldsymbol{v}^{h_j} = \mathbb{P}^{h_j}\boldsymbol{v}^h$ in (2.13). This yields

$$M(\mathbb{P}^{h_j}\boldsymbol{v}^h, \mathbb{P}^{h_j}\boldsymbol{v}^h, \boldsymbol{f}; h_j, \boldsymbol{c}) - M(\mathbb{P}^{h_j}\boldsymbol{v}^h, \boldsymbol{v}^h, \boldsymbol{f}; h, \boldsymbol{c}) = -\Big(B(\mathbb{P}^{h_j}\boldsymbol{v}^h, \mathbb{P}^{h_j}\boldsymbol{v}^h) - B(\mathbb{P}^{h_j}\boldsymbol{v}^h, \boldsymbol{v}^h)\Big), \quad j = 1, \cdots, J. \tag{2.15}$$

Equation (2.15) is motivated by previous work in the context of filtered Navier-Stokes equations [15]. In that case the model contribution in (2.15) (that is the left hand side of the equation) represents the difference in the dissipation of the total turbulent kinetic energy induced by LES models acting at two different scales. For this reason we refer to this approach as the *dissipation method.*

Equation (2.15) represents a set of J scalar equations for the P parameters $\boldsymbol{c} = [c_1, \cdots, c_P]$ that involve $\boldsymbol{v}^h$, f, $\boldsymbol{h}$ and $\mathbf{P}$. When $J = P$, these equations may be solved to determine the model parameters. Assuming this is feasible the result is a relation of the form

$$\boldsymbol{c} = \boldsymbol{\pi}(\boldsymbol{v}^h, \boldsymbol{f}; \boldsymbol{h}; \mathbf{P}). \tag{2.16}$$

Least-squares method An alternate approach, which is motivated by the work of Ghosal et al. [26] and Lilly [27] involves selecting $\boldsymbol{w}^{h_j}$ as

$$\boldsymbol{w}^{h_j} = \boldsymbol{\phi}_A^{h_j}(\boldsymbol{x}) \tag{2.17}$$

where $\boldsymbol{\phi}_A^{h_j}, A = 1, \cdots, N^{h_j}$ are functions that span $\mathcal{V}^{h_j}$. Using (2.17) in (2.13),

$$M(\boldsymbol{\phi}_A^{h_j}, \mathbb{P}^{h_j}\boldsymbol{v}^h, \boldsymbol{f}; h_j, \boldsymbol{c}) - M(\boldsymbol{\phi}_A^{h_j}, \boldsymbol{v}^h, \boldsymbol{f}; h, \boldsymbol{c}) = -\Big(B(\boldsymbol{\phi}_A^{h_j}, \mathbb{P}^{h_j}\boldsymbol{v}^h) - B(\boldsymbol{\phi}_A^{h_j}, \boldsymbol{v}^h)\Big), \quad A = 1, \cdots, N^{h_j}, \quad j = 1, \cdots, J. \tag{2.18}$$

The equation above represents $N = \sum_{j=1}^{J} N^{h_j}$, scalar relations. An expression that is formally identical to (2.16) may be obtained from this equation by finding the parameters $\boldsymbol{c}$ that minimize the square of the residual of these relations.

Once an expression for $\boldsymbol{\pi}$ is derived using either the dissipation or the least-squares method, the numerical method may be written as

$$B(\boldsymbol{w}^h, \boldsymbol{u}^h) + M(\boldsymbol{w}^h, \boldsymbol{u}^h, \boldsymbol{f}; h, \boldsymbol{c}) = (\boldsymbol{w}^h, \boldsymbol{f}), \qquad \forall \boldsymbol{w}^h \in \mathcal{V}^h \tag{2.19}$$

$$\boldsymbol{c} = \boldsymbol{\pi}(\boldsymbol{u}^h, \boldsymbol{f}; \boldsymbol{h}; \mathbf{P}), \tag{2.20}$$

By construction, this method has one of the following special properties:

1. When the parameters are determined using the dissipation method, a subset of the conditions that are necessary for the solution of the numerical method on $\mathcal{V}^h, \mathcal{V}^{h_1}, \cdots, \mathcal{V}^{h_J}$ to be equal to the optimal representation of the continuous solution, are satisfied.

2. When the parameters are determined using the least-squares method, the conditions that are necessary for the solution of the numerical method on $\mathcal{V}^h, \mathcal{V}^{h_1}, \cdots, \mathcal{V}^{h_J}$ to be equal to the optimal representation of the continuous solution, are satisfied in a least-squares sense.

The following additional remarks may be made about the numerical method (2.19)-(2.20).

Remarks

1. During a numerical simulation, each quantity that appears in (2.20) is known, hence this expression closes the numerical method.
2. π is typically non-linear in $\boldsymbol{u}^h$, and hence the resulting numerical method is also *non-linear.*
3. The fact that π depends on $\mathbf{P}$, which in turn depends on the definition of the optimal solution, indicates that different numerical methods are obtained for different choices of the optimal solution.
4. Evaluating π using either the dissipation or the least-squares method, and hence implementing the proposed numerical method, does not require the analytical solution of the continuous problem. Thus this method may be used for solving complex non-linear partial differential equations where such solutions are unavailable.
5. In the development above, for simplicity, we have assumed that $\boldsymbol{c}$ is constant in Ω. When this is not the case a piecewise-constant approximation to $\boldsymbol{c}$ may be used and the procedure described above repeated on individual subdomains where $\boldsymbol{c}$ is constant.

2.4 Linear Advection Diffusion Equation

In this section we apply the methodology developed in the previous section for solving the linear advection-diffusion problem. For this equation a model term that yields nodally exact solutions in one dimension can be derived analytically. Hence the results of (2.19)-(2.20) may be compared with this "ideal" model.

2.4.1 Problem Description

We consider the advection diffusion equation in $\Omega = (0,1)$, with homogeneous Dirichlet boundary conditions and forcing f. The strong form of the problem is given by

$$\begin{aligned} \mathcal{L}u \equiv -\nu u_{,xx} + a u_{,x} &= f, \qquad x \in (0,1) && (2.21) \\ u(0) = u(1) &= 0. && (2.22) \end{aligned}$$

where ν is the diffusivity, assumed constant in Ω, $a \equiv 1$, is the prescribed velocity, and f is the forcing function given by

$$f(x) = \langle x - x_0 \rangle = \begin{cases} 0, & x < x_0 \\ x - x_0, & x \geq x_o \end{cases} \qquad (2.23)$$

We have experimented with several values of x_0 and have obtained results that are insensitive to it. As a representative value we choose $x_0 = 1/2$.

An equivalent weak or variational form of (2.21) and (2.22) is given by (2.1), where

$$B(w,u) = \nu(w_{,x},u_{,x}) - a(w_{,x},u), \tag{2.24}$$

$$(w,f) = \int_0^1 wf\,dx, \tag{2.25}$$

and $\mathcal{V} = \{v | v \in H^1(\Omega), v(0) = v(1) = 0\}$.

2.4.2 Variational Germano Identity

Preliminaries

Model term The finite dimensional approximation of (2.21)–(2.22) inclusive of a model is given by (2.4). For the model we choose a residual-based term given by

$$M(w^h,u^h,f;h,\mathbf{c}) = c_1 h^{c_2}(w^h_{,x},\mathcal{L}u^h - f)_{\tilde{\Omega}}, \tag{2.26}$$

where $\tilde{\Omega}$ is the union of all element interiors, h is the element size of the finite element discretization, and $\mathbf{c} = \{c_1, c_2\}$ are the parameters that will be determined using (2.15). Since the number of unknown parameters $P = 2$, we select the number of subspaces of $\mathcal{V}^h$, denoted by $J = 2$ also.

Function spaces To solve (2.4) we use a uniform mesh of *linear finite elements*. With this specification the model term (2.26) reduces to

$$M(w^h,u^h,f;h,\mathbf{c}) = c_1 h^{c_2}(w^h_{,x},u^h_{,x} - f). \tag{2.27}$$

The spaces $\mathcal{V}^h, \mathcal{V}^{h_1}$ and $\mathcal{V}^{h_2}$ are constructed from shape functions associated with a uniform mesh of linear finite elements of size $h, 2h$ and $4h$ respectively. Thus $\boldsymbol{h} = \{h, 2h, 4h\}$. It easily verified that this choice satisfies $\mathcal{V}^{h_2} \subset \mathcal{V}^{h_1} \subset \mathcal{V}^h$.

Operators Since $J = 2$, the set $\mathbf{P} = \{\mathbb{P}^{h_1}, \mathbb{P}^{h_2}\}$. The operators $\mathbb{P}^h, \mathbb{P}^{h_1}$ and $\mathbb{P}^{h_2}$ are chosen to be the nodal interpolation operators at scales h, $2h$ and $4h$ respectively. Note that this choice satisfies (2.12).

Determining π

We now specialize (2.15) to the advection-diffusion problem. Using (2.27) in (2.15), recognizing that $B(\cdot,\cdot)$ is a bilinear form, and that for our choices of $\mathcal{V}^{h_j}$ and $\mathbb{P}^{h_j}$,

$$(w^{h_j}_{,x}, v^h_{,x} - f) = (w^{h_j}_{,x}, (\mathbb{P}^{h_j} v^h)_{,x} - f), \quad \forall w^{h_j} \in \mathcal{V}^{h_j}, \quad j = 1,2, \tag{2.28}$$

we arrive at

$$c_1 h^{c_2}((h_j/h)^{c_2} - 1) = F(v^h, f; \mathbb{P}^{h_j}), \quad j = 1,2, \tag{2.29}$$

where

$$F(v^h, f; \mathbb{P}^{h_j}) \equiv \frac{B(\mathbb{P}^{h_j} v^h, v^h - \mathbb{P}^{h_j} v^h)}{((\mathbb{P}^{h_j} v^h)_{,x}, (\mathbb{P}^{h_j} v^h)_{,x} - f)}. \tag{2.30}$$

Solving (2.29) for c_1 and c_2 yields

$$c_2 = \pi_2(v^h, f; \boldsymbol{h}; \mathbf{P})|_{\boldsymbol{h}=\{h,2h,4h\}} = \bar{\pi}_2(v^h, f; h; \mathbf{P}) = \ln\Big(\frac{F(v^h, f; \mathbb{P}^{h_2})}{F(v^h, f; \mathbb{P}^{h_1})} - 1\Big)(\ln 2)^{-1} \tag{2.31}$$

$$c_1 = \pi_1(v^h, f; \boldsymbol{h}; \mathbf{P})|_{\boldsymbol{h}=\{h,2h,4h\}} = \bar{\pi}_1(v^h, f; h; \mathbf{P}) = \frac{F(v^h, f; \mathbb{P}^{h_1})}{h^{\bar{\pi}_2}(2^{\bar{\pi}_2} - 1)}. \tag{2.32}$$

2.4.3 Numerical Solution

Nonlinearity The numerical method (2.19)-(2.20) specializes to

$$B(w^h, u^h) + \nu^h(w^h_{,x}, u^h_{,x} - f) = (w^h, f), \forall w^h \in \mathcal{V}^h \tag{2.33}$$

$$\begin{aligned} \nu^h &= g^h(u^h, f; h; \mathbf{P}) \\ &= \bar{\pi}_1(u^h, f; h; \mathbf{P}) h^{\bar{\pi}_2(u^h, f; h; \mathbf{P})} \end{aligned} \tag{2.34}$$

where $B(\cdot,\cdot)$ is defined in (2.24), and $\bar{\pi}_1$ and $\bar{\pi}_2$ are given by (2.32) and (2.31). We term this method the *dynamic diffusivity method*, since the numerical diffusivity is not determined *a-priori*, but is determined based on the solution.

To solve this nonlinear problem we introduce an artificial "time" variable t, and instead of (2.34) we solve

$$\frac{d\nu^h}{dt} = g^h(u^h, f; h; \mathbf{P}) - \nu^h, \tag{2.35}$$

with $\nu^h(0) = 0$. The steady state solution of this equation is the solution to (2.34). We use the following simple scheme to discretize this equation in time.

$$\nu^h(t + \Delta t) = \frac{1}{1 + \Delta t}\nu^h(t) + \frac{\Delta t}{1 + \Delta t}|g^h(u^h(t), f; h; \mathbf{P})| \tag{2.36}$$

where $u^h(t)$ is solution to (2.33). This scheme corresponds to a forward Euler step in the non-linear term and a backward Euler step in the linear term. We have used the absolute value of g^h in this equation, in order to avoid the scheme from diverging whenever (rarely) a negative value of g^h is encountered. Similar precautions are taking when evaluation eddy viscosities in turbulence models [15,26]. For the examples shown below we choose $\Delta t = 3/7$.

Results The diffusivity that renders the numerical solution nodally exact is given by

$$\nu^e = \frac{ah}{2}\xi^e, \tag{2.37}$$

where the non-dimensional parameter ξ^e is given by

$$\xi^e = \coth\alpha - \frac{1}{\alpha}, \tag{2.38}$$

and $\alpha = \frac{ah}{2\nu}$ is the mesh Peclet number. Using this diffusivity in (2.33) leads to the SUPG method [28].

First, we study the convergence of the dynamic diffusivity ν^h, obtained by solving (2.33) and (2.35) to ν^e. In particular we compare ξ^h with ξ^e, where ξ^h is given by

$$\xi^h = \frac{\nu^h(T)}{ah/2}, \tag{2.39}$$

where $\nu^h(T)$ is the converged or the steady-state value of ν^h. The results of this comparison are shown in Figure 2.1 for $\alpha \in (3.2 \times 10^{-2}, 3.2 \times 10^3)$. For all results $h = 1/52$. We observe that the values of ξ^h and ξ^e are in agreement in both the advective and diffusive limits ($\alpha \to \infty$ and $\alpha \to 0$ respectively). There are some noticeable differences in the diffusive limit with dynamic diffusivity being slightly larger than the analytical value. However, it is worth noting that in this limit the numerical diffusivity is much smaller than the molecular diffusivity (same for every method), which dominates the solution.

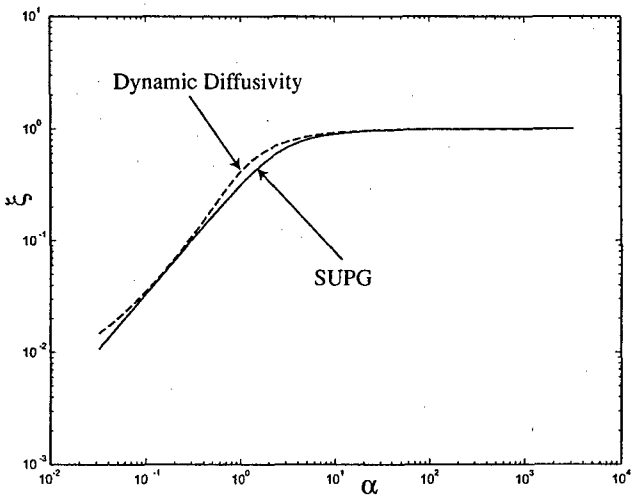

Figure 2.1: Variation of the non-dimensional viscosity for SUPG (ξ^e) and the dynamic diffusivity method (ξ^h) as a function of the mesh Peclet number (α).

In Figures 2.2 through 2.5, we have plotted the Galerkin, the SUPG (which is also the nodal interpolant of the exact solution) and the dynamic diffusivity solutions for different values of mesh Peclet number. Figure 2.2 corresponds to a value of $\alpha = 3.2 \times 10^{-2}$. We observe that all solutions including the Galerkin solution are very accurate. In Figure 2.3 we have plotted the solutions corresponding to $\alpha = 1.0$. We can now observe differences in the Galerkin solution and other solutions. There is a bump in the Galerkin solution at $x = 0.97$ which is absent from the SUPG (the nodal interpolant) and the dynamic diffusivity solution. In Figure 2.4 we have plotted the solutions for $\alpha = 3.2 \times 10^3$. This represents the advective limit. We observe that the Galerkin solution has large spurious oscillations that are absent from the SUPG and dynamic diffusivity method. In order to compare the dynamic method with the SUPG method, we have plotted these solutions in Figure 2.5 without the Galerkin solution. We observe that the solutions are virtually indistinguishable.

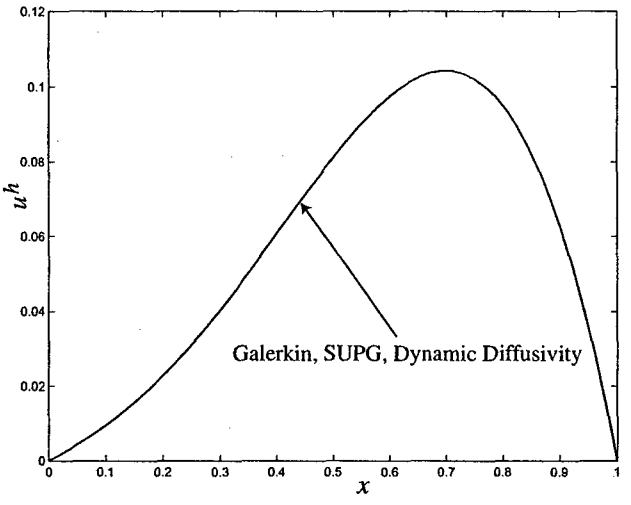

Figure 2.2: Galerkin, SUPG and dynamic diffusivity solutions for $\alpha = 3.2 \times 10^{-2}$.

In Figure 2.6, we present the convergence of the diffusivity of the dynamic method as a function of iteration number, for different values of Peclet numbers. For all cases we start with no diffusivity (that is the Galerkin method) and within about 10 iterations converge to the SUPG method.

2.5 Incompressible Navier-Stokes Equation

In this section we apply the variational Germano identity to the more challenging problem of solving turbulent flows governed by the incompressible Navier-Stokes equations on grids for which the mesh size is much larger than the dissipation length scale.

2.5.1 Problem Description

We consider the problem in $Q = \Omega \times]T_1, T_2[$, where $\Omega = [0, 2\pi]^3$ is the spatial domain and $]T_1, T_2[$ is the time period of interest. The strong form of the problem is given by

$$\mathcal{L}\boldsymbol{U} \equiv \begin{cases} \boldsymbol{u}_{,t} + \nabla \cdot (\boldsymbol{u} \otimes \boldsymbol{u}) + \nabla p - \nu \nabla^2 \boldsymbol{u} &= \boldsymbol{0}, \text{ in } Q \\ \nabla \cdot \boldsymbol{u} &= 0, \text{ in } Q \end{cases} \tag{2.40}$$

In the above equations $\boldsymbol{U} = [\boldsymbol{u}, p]^T$, where $\boldsymbol{u}$ is the fluid velocity field and p is the pressure. In addition, ν is the kinematic viscosity and the symbol $\otimes$ denotes the outer product of two vectors. The boundary of Ω is denoted by $\partial\Omega$. It is comprised of six faces, $\Gamma_j(0)$, $\Gamma_j(2\pi)$, $j = 1, 2, 3$, where

$$\Gamma_j(c) = \{\boldsymbol{x} \in \partial\Omega \mid x_j = c\} \tag{2.41}$$

It is assumed the solution is periodic, that is

$$\boldsymbol{u}(\boldsymbol{x} + 2\pi \boldsymbol{e}_j, t) = \boldsymbol{u}(\boldsymbol{x}, t), \quad \boldsymbol{x} \in \Gamma_j(0), \quad t \in]T_1, T_2[\tag{2.42}$$

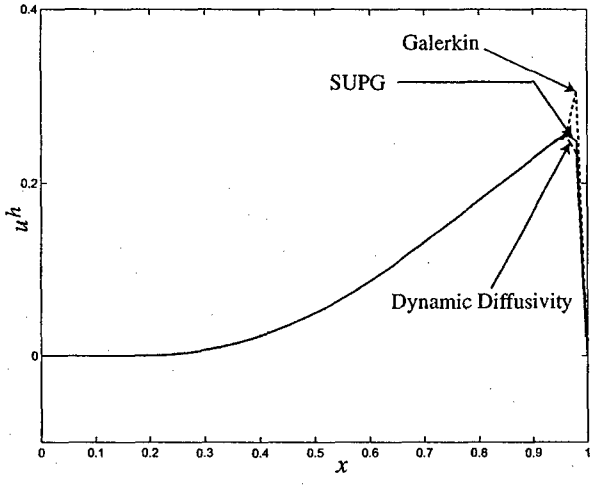

Figure 2.3: Galerkin, SUPG and dynamic diffusivity solutions for $\alpha = 1$.

where $\boldsymbol{e}_j$ is the Cartesian basis vector in the x_j direction. The initial, divergence-free velocity field is given by

$$\boldsymbol{u}(\boldsymbol{x}, 0) = \boldsymbol{u}_0(\boldsymbol{x}). \tag{2.43}$$

When seeking approximate numerical solutions to the Navier-Stokes equations one may either (a) develop and approximate a spatial variational formulation of the problem to arrive at a set of coupled ordinary differential equations and solve these using a standard time marching scheme, or (b) discretize the space-time domain into slabs, and develop and approximate a space-time variational formulation using the discontinuous Galerkin method, leading to a set of coupled algebraic equations. Methods based on approach (a) are commonly referred to as semi-discrete methods, and those based on approach (b) are referred to as fully discrete space-time methods. In our work we consider the more commonly used semi-discrete method. A direct consequence of this choice is that numerical method developed in Section 2 (which is directly applicable to space-time methods) must be modified. These modifications are described in the following paragraphs.

The weak formulation (in Ω) of (4.1), (4.30) and (4.3) is given by (see [29] for example): Find $\boldsymbol{u}(\cdot, t) \in \mathcal{V}$, such that

$$B(\boldsymbol{w}, \boldsymbol{u}) = 0, \qquad \forall \boldsymbol{w} \in \mathcal{V}, \forall t \in]T_1, T_2[, \tag{2.44}$$

where the semi-linear form $B(\cdot, \cdot)$ is defined as

$$B(\boldsymbol{w}, \boldsymbol{u}) \;=\; (\boldsymbol{w}, \boldsymbol{u}_{,t}) - (\nabla \boldsymbol{w}, \boldsymbol{u} \otimes \boldsymbol{u}) + 2\nu(\nabla^S \boldsymbol{w}, \nabla^S \boldsymbol{u}) + (\nabla \cdot \boldsymbol{w}, \nabla^{-2}(\nabla \cdot \nabla \cdot \boldsymbol{u} \otimes \boldsymbol{u})) \tag{2.45}$$

Note that the pressure and the divergence terms are absent from the definition of the semi-linear form. This is because the divergence-free constraint for the velocity field is built into the definition of the function space $\mathcal{V}$,

$$\mathcal{V} = \Big\{ v | v = \sum_{\boldsymbol{k} \in \mathbb{Z}^3} \hat{\boldsymbol{v}}_{\boldsymbol{k}} e^{i\boldsymbol{k}\cdot\boldsymbol{x}};\; \hat{\boldsymbol{v}}^*_{-\boldsymbol{k}} = \hat{\boldsymbol{v}}_{\boldsymbol{k}};\; \sum_{\boldsymbol{k} \in \mathbb{Z}^3} |\hat{\boldsymbol{v}}_{\boldsymbol{k}}|^2 (1 + |\boldsymbol{k}|^2) < \infty \Big\}. \tag{2.46}$$

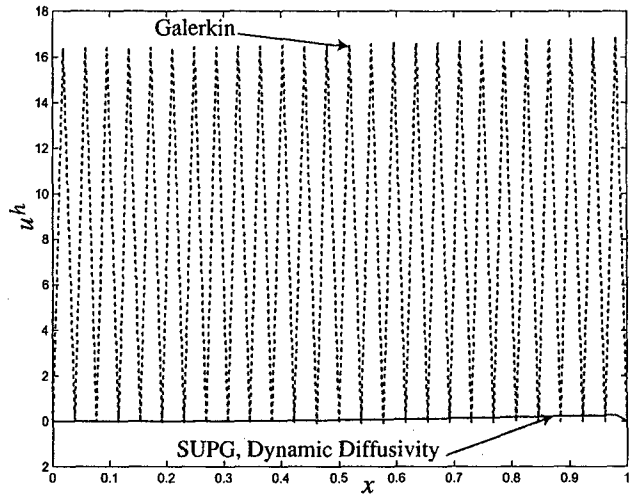

Figure 2.4: Galerkin, SUPG and dynamic diffusivity solutions for $\alpha = 3.2 \times 10^3$.

In the equation above, $\hat{\boldsymbol{v}}_{\boldsymbol{k}}$ is the Fourier-coefficient of $\boldsymbol{v}$, $\boldsymbol{k}$ is the corresponding wave-vector, and the superscript $*$ denotes the complex-conjugate of a quantity. The terms within the curly brackets imply that vector fields contained in $\mathcal{V}$ are real-valued, divergence-free and belong to $H^1(\Omega)$ (the energy and the enstrophy of the flow are finite for $t \in]T_1, T_2[$). The periodic boundary conditions are also built into the definition of $\mathcal{V}$.

2.5.2 Variational Germano Identity

Model term The finite dimensional approximation of (4.11) and (4.3), inclusive of a model, is given by: Find $\boldsymbol{u}^h(\cdot, t) \in \mathcal{V}^h$ such that

$$B(\boldsymbol{w}^h, \boldsymbol{u}^h) + M(\boldsymbol{w}^h, \boldsymbol{u}^h; h, \boldsymbol{c}) = 0, \qquad \forall \boldsymbol{w}^h \in \mathcal{V}^h, \forall t \in]T_1, T_2[. \tag{2.47}$$

For the model we choose the Smagorinsky eddy viscosity model [30] given by,

$$M(\boldsymbol{w}^h, \boldsymbol{u}^h; h, \boldsymbol{c}) = 2(c_1 h)^2 (\nabla^S \boldsymbol{w}^h, |\nabla^S \boldsymbol{u}^h| \nabla^S \boldsymbol{u}^h), \tag{2.48}$$

where h is the grid (or mesh) size, and $c_1(t)$ is the time-dependent viscosity coefficient that will be determined using the methodology developed in Section 2.

For the semi-discrete approximation of the Navier-Stokes equations considered herein, the variational Germano identity may be derived using arguments that are analogous to those used in Sections 2 and 3. The end result is (2.13), which now holds $\forall t \in]T_1, T_2[$. The application of the dissipation and the least squares method to this equation results in (2.15) and (2.18) respectively, which now hold $\forall t \in]T_1, T_2[$. Consequently, these equations may be used to determine the *time-dependent* parameters in the model term. In the following development, for the Smagorinsky model, we use (2.15) to determine c_1 as a function of time.

Function spaces Since the number of unknown parameters is one ($P = 1$), we select the number of subspaces of $\mathcal{V}^h$ also to be one ($J = 1$). We use a finite-dimensional Fourier-spectral basis to approximate our solution in Ω. Formally, the spaces $\mathcal{V}^h$ and $\mathcal{V}^{h_1}$ are given

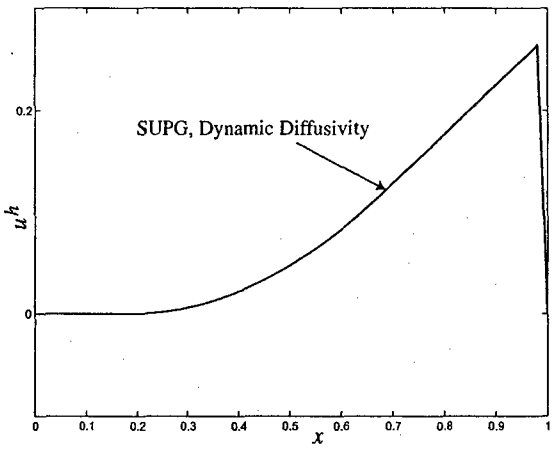

Figure 2.5: SUPG and dynamic diffusivity solutions for $\alpha = 3.2 \times 10^3$.

by

$$\mathcal{V}^h = \{v \in \mathcal{V}; \boldsymbol{v}_{\boldsymbol{k}} = \boldsymbol{0}, |\boldsymbol{k}|_\infty > k^h\} \tag{2.49}$$

$$\mathcal{V}^{h_1} = \{v \in \mathcal{V}; \boldsymbol{v}_{\boldsymbol{k}} = \boldsymbol{0}, |\boldsymbol{k}|_\infty > k^{h_1}\}, \tag{2.50}$$

where $|\boldsymbol{k}|_\infty \equiv \max\{|k_1|, |k_2|, |k_3|\}$, and $k^h = \pi/h$, and $k^{h_1} = \pi/h_1$ are the cut-off wavenumbers. In particular, we choose $k^h = 16$, and $k^{h_1} = 8$.

Operators Since $J = 1$, the set $\mathbf{P} = \{\mathbb{P}^{h_1}\}$. The operators $\mathbb{P}^h$ and $\mathbb{P}^{h_1}$ are chosen to be the $H^1(\Omega)$ projections of functions in $\mathcal{V}$ into $\mathcal{V}^h$ and $\mathcal{V}^{h_1}$ respectively. Note that these projections satisfy the following property.

Let $\boldsymbol{u}(\cdot, t) \in \mathcal{V}$ be represented in terms of the infinite series

$$\boldsymbol{u}(\boldsymbol{x}, t) = \sum_{\boldsymbol{k}} \hat{\boldsymbol{u}}_{\boldsymbol{k}}(t) e^{i\boldsymbol{k}\cdot\boldsymbol{x}}, \tag{2.51}$$

where $\hat{\boldsymbol{u}}_{\boldsymbol{k}}(t)$ are the Fourier-coefficients of $\boldsymbol{u}$. Then $\mathbb{P}^h \boldsymbol{u}$ is given by

$$\mathbb{P}^h \boldsymbol{u}(\boldsymbol{x}, t) = \sum_{|\boldsymbol{k}|_\infty \le k^h} \hat{\boldsymbol{u}}_{\boldsymbol{k}}(t) e^{i\boldsymbol{k}\cdot\boldsymbol{x}}, \tag{2.52}$$

and likewise $\mathbb{P}^{h_1} \boldsymbol{u}$ is given by

$$\mathbb{P}^{h_1} \boldsymbol{u}(\boldsymbol{x}, t) = \sum_{|\boldsymbol{k}|_\infty \le k^{h_1}} \hat{\boldsymbol{u}}_{\boldsymbol{k}}(t) e^{i\boldsymbol{k}\cdot\boldsymbol{x}}. \tag{2.53}$$

In other words, these projections correspond to the sharp-cutoff filters in the wavenumber space.

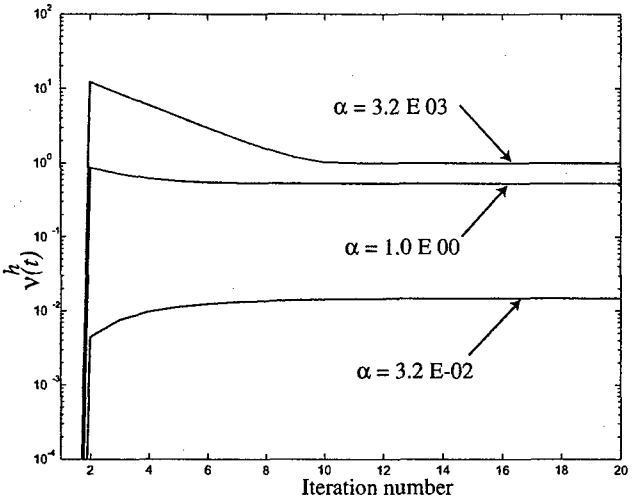

Figure 2.6: Variation of ν^h for the dynamic diffusivity method as a function of iteration number.

Determining π

We now specialize (2.15) to the incompressible Navier-Stokes equation. Using the definition of the model (2.48) and the semi-linear form (2.45) in (2.15), we have

$$\begin{aligned} c_1 &= \pi_1(\boldsymbol{v}^h, \boldsymbol{h}; \mathbb{P}^{h_1}) \\ &= \sqrt{\frac{1}{2}\frac{(\nabla \boldsymbol{v}^{h_1}, \boldsymbol{v}^{h_1} \otimes \boldsymbol{v}^{h_1}) - (\nabla \boldsymbol{v}^{h_1}, \boldsymbol{v}^h \otimes \boldsymbol{v}^h)}{h_1^2(\nabla^S \boldsymbol{v}^{h_1}, |\nabla^S \boldsymbol{v}^{h_1}|\nabla^S \boldsymbol{v}^{h_1}) - h^2(\nabla^S \boldsymbol{v}^{h_1}, |\nabla^S \boldsymbol{v}^h|\nabla^S \boldsymbol{v}^h)}}, \forall t \in]T_1, T_2[, \quad (2.54) \end{aligned}$$

where $\boldsymbol{v}^{h_1} = \mathbb{P}^{h_1}\boldsymbol{v}^h$. In deriving (2.54) we have utilized the fact that the contribution from terms in $B(\boldsymbol{w}, \boldsymbol{u})$ that are linear in $\boldsymbol{u}$ is zero due to the specific form of the basis functions and projection operators $\mathbb{P}^h$ and $\mathbb{P}^{h_1}$. We have also made use of the fact that $\boldsymbol{v}^h$ and $\boldsymbol{v}^{h_1}$ are divergence free.

2.5.3 Numerical Solution

The proposed numerical method for solving the incompressible Navier-Stokes equations is given by (2.47) and (2.48). The Smagorinsky parameter that appears in the model is given by (2.54) with v^h and v^{h_1} replaced by u^h and u^{h_1} respectively. That is

$$c_1 = \sqrt{\frac{1}{2}\frac{(\nabla \boldsymbol{u}^{h_1}, \boldsymbol{u}^{h_1} \otimes \boldsymbol{u}^{h_1}) - (\nabla \boldsymbol{u}^{h_1}, \boldsymbol{u}^h \otimes \boldsymbol{u}^h)}{h_1^2(\nabla^S \boldsymbol{u}^{h_1}, |\nabla^S \boldsymbol{u}^{h_1}|\nabla^S \boldsymbol{u}^{h_1}) - h^2(\nabla^S \boldsymbol{u}^{h_1}, |\nabla^S \boldsymbol{u}^h|\nabla^S \boldsymbol{u}^h)}}, \forall t \in]T_1, T_2[, \quad (2.55)$$

where $\boldsymbol{u}^{h_1} = \mathbb{P}^{h_1}\boldsymbol{u}^h$. We refer to the method implied by (2.47), (2.48) and (2.55) as the *variational dynamic Smagorinsky method.* These equations represent a closed system of ODEs which may be integrated in time to yield the velocity field in $]T_1, T_2[$.

Results To test the performance of the proposed numerical method we generate a well-resolved benchmark solution on a 256^3 mesh. For this solution we use a random initial condition with an energy spectrum (energy density in wavenumber space) given by $E(k) = (q^2/2A)(k^4/k_p^5)\exp(-2(k/k_p)^2)$, where the initial turbulent kinetic energy, $\frac{q^2}{2} = \frac{3}{2}$, and the spectrum is peaked at $k_p = 3$. The same spectrum was used in [31] to study the decay of low Reynolds number homogeneous isotropic turbulence. The phase of the modes for the initial velocity field is chosen randomly and each mode satisfies the divergence-free condition. The solution is allowed to evolve according to the Navier-Stokes equations till a spectra with a physical $k^{-5/3}$ range is obtained (see Figure 2.7). This corresponds to $t = T_1 \approx 2.2$. At this time the Taylor-microscale Reynolds number is ≈ 90. This state of the flow is chosen

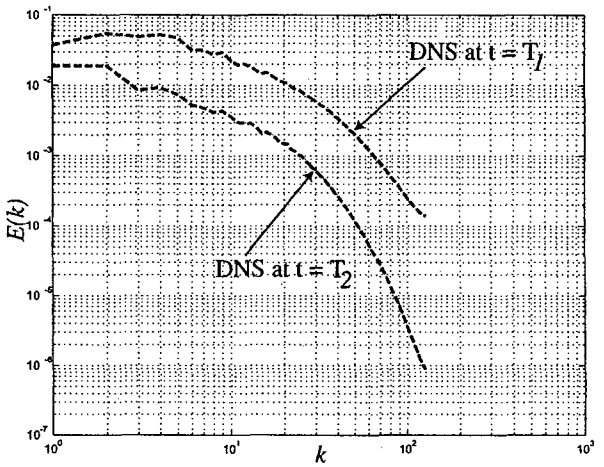

Figure 2.7: Energy spectra $E(k)$, for the DNS at initial and final time (T_1&T_2).

as an initial condition for all numerical solutions. In addition to the variational dynamic Smagorinsky method on a 32^3 grid, the following numerical methods are included in the comparison.

1. A well resolved Direct Numerical Simulation (DNS) solution on a 256^3 mesh. This corresponds to the Fourier-Galerkin method applied to the Navier-Stokes equations (that is (2.47) with the model term set to zero). The resolution is chosen such that the largest wavenumber is sufficient to capture the dissipation or the Kolmogorov length scale. This solution is treated as the benchmark solution. Note that the number of degrees of freedom in the well resolved DNS is 512 times more than the other simulations.

2. An under-resolved (coarse) DNS solution on a 32^3 mesh. This method is also given by (2.47) with the model term set to zero. However a coarse 32^3 mesh, on which the dissipation length scale is not represented, is utilized. This solution represents the coarse Fourier-Galerkin approximation of the Navier-Stokes equations.

3. A constant coefficient (static) Smagorinsky model on a 32^3 mesh. This numerical method is given by (2.47) and (2.48), where the Smagorinsky constant is set to

$c_1 = 0.16$, a value obtained by assuming an infinite inertial range (see [32]). The value of the coefficient is not changed during the simulation.

4. The traditional dynamic Smagorinsky model on a 32^3 mesh. This numerical method is given by (2.47) and (2.48). In (2.48), the Smagorinsky coefficient is calculated using the Germano identity [15] applied to the filtered Navier-Stokes equations. The coefficient is given by

$$c_1 = \sqrt{\frac{1}{2}\frac{(\nabla \boldsymbol{u}^h, \boldsymbol{u}^{h_1} \otimes \boldsymbol{u}^{h_1}) - (\nabla \boldsymbol{u}^{h_1}, \boldsymbol{u}^h \otimes \boldsymbol{u}^h)}{h_1^2(\nabla^S \boldsymbol{u}^h, |\nabla^S \boldsymbol{u}^{h_1}| \nabla^S \boldsymbol{u}^{h_1}) - h^2(\nabla^S \boldsymbol{u}^{h_1}, |\nabla^S \boldsymbol{u}^h| \nabla^S \boldsymbol{u}^h)}}, \forall t \in]T_1, T_2[. \quad (2.56)$$

   Note that in the above expression for c_1, u^h appears in the weighting function slot of the second term in the numerator and the denominator. Whereas in (2.55), which is derived from a variational standpoint, u^{h_1} appears in these slots. In the following section we will observe that this difference leads to a smaller value for c_1 when it is calculated using (2.55).

All the numerical methods described above lead to a set of coupled ODEs. These equations are advanced in time using a mixed integration scheme in which the exact integrating factor is used for the viscous term and a third-order Runge-Kutta method is used for the remaining terms (see for example [33]).

In Figure 2.8, we have plotted the Taylor microscale Reynolds number (Re_λ) as a function of time for the benchmark DNS solution. We observe that in the time period of interest (that is $t \in]2.2, 4.4[$), Re_λ falls from 90 to about 62.

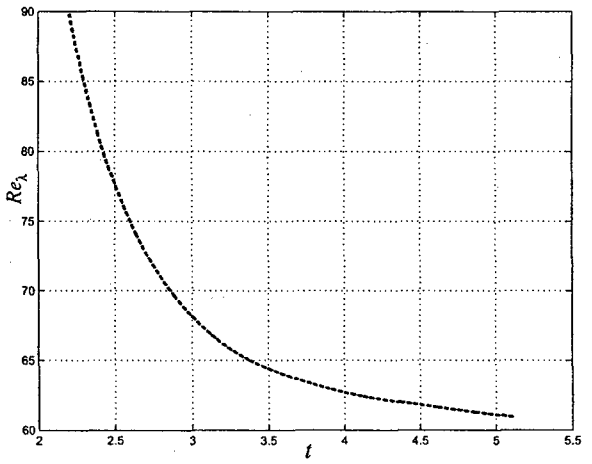

Figure 2.8: The Taylor microscale Reynolds number (Re_λ) for the DNS as a function of time.

In Figure 2.9, we have plotted the coefficient c_1 as a function of time for the static, the traditional dynamic and the variational dynamic Smagorinsky formulations. We observe that the coefficient for the static Smagorinsky formulation is the largest. For the traditional dynamic method the coefficient starts out high but settles to a lower value of 0.14. The

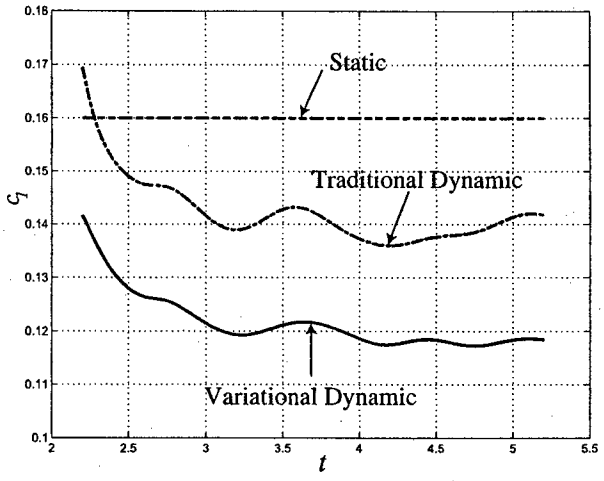

Figure 2.9: Variation of the Smagorinsky coefficient (c_1) as a function of time.

coefficient for the variational dynamic method is the smallest, and settles to a value of about 0.12.

In Figure 2.10, we have plotted the energy spectra for the benchmark DNS and the various numerical solutions at the final time (T_2). From this figure we observe that the coarse DNS solution is completely incorrect indicating that a model term is necessary to compute a reasonable approximation of the well-resolved DNS solution. The coarse DNS exhibits a cusp at large wavenumbers caused by the abrupt truncation of the energy cascade at the cut-off wavenumber. Further, through the coupling induced by the quadratic term, this accumulation of energy at high wavenumbers has led to an increased transfer of energy from the low wavenumbers, which has in turn resulted in an under-prediction of the energy at these wavenumbers. This error in the coarse DNS solution is rectified by the Smagorinsky model. However, for the static coefficient case we observe that the model has overcompensated to some extent: the large dissipation in the fine scales has led to a drop-off in the spectrum at the cutoff wavenumber, which has in turn caused a net decrease in the transfer of energy from the coarse scales, leading to a pile-up of energy at the these scales. The traditional dynamic Smagorinsky formulation, which has a smaller viscosity, is seen to improve these results somewhat. The most accurate spectrum is achieved by the variational dynamic formulation, which has the smallest Smagorinsky coefficient.

In Figure 2.11, we have plotted the resolved turbulent kinetic energy in the flow as a function of time. We observe that with the exception of the coarse DNS solution, all solutions match the DNS data quite well. In particular, the variational dynamic Smagorinsky and the constant coefficient Smagorinsky methods are very accurate at initial and intermediate times respectively.

Finally in Figure 2.12, we have plotted the resolved enstrophy (L^2 norm of vorticity) as a function of time. We observe that the coarse DNS solution severely over-predicts this quantity, while both the constant coefficient and the traditional dynamic Smagorinsky solutions under-predict it. The variational dynamic formulation is once again the most accurate.

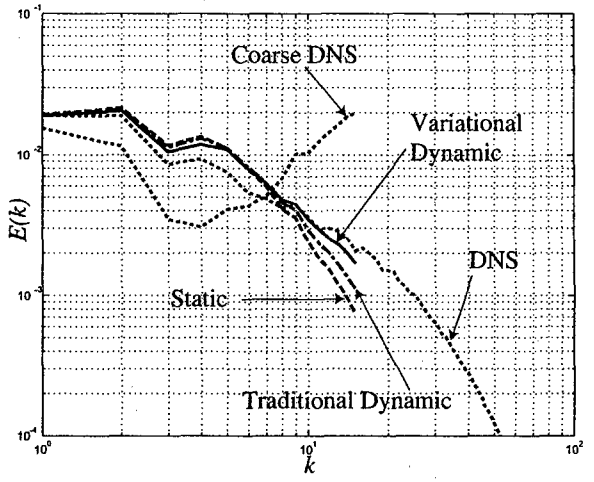

Figure 2.10: Energy spectra $E(k)$, for the benchmark DNS and the numerical methods at the final time $t = T_2$.

2.6 Conclusions

Using an extension of the variational counterpart of the Germano identity, we have derived a methodology for evaluating the parameters of a numerical method. The parameters obtained using this approach satisfy certain conditions necessary for the numerical method to yield optimal solutions over a set of finite dimensional subspaces. We have applied this approach to calculate the numerical diffusivity required for nodally exact solutions to the advection diffusion equation in one dimension. We have found that the resulting diffusivity, which is a non-linear function of the numerical solution, converges to the value obtained using the SUPG analysis. In addition we have applied the same approach for computing the Smagorinsky coefficient in the decay of homogeneous isotropic turbulence. In this case we have found that the resulting model produces results which are generally more accurate than the constant-coefficient and the traditional dynamic Smagorinsky models.

It is interesting to enumerate the differences between the advection-diffusion and the turbulence problems that were solved in this study: (1) the former was a linear PDE while the latter was a system of non-linear PDEs, (2) the former was posed in one spatial dimension while the latter was posed in three dimensions, (3) the latter exhibited chaotic solutions while the former did not, (4) the former was solved using the finite element method, while the latter was solved using a spectral method. Given these differences it is remarkable that the same methodology, namely the variational Germano identity, could be employed to design accurate numerical methods for these two problems. In the future we propose to explore the application of this identity to other physical systems.

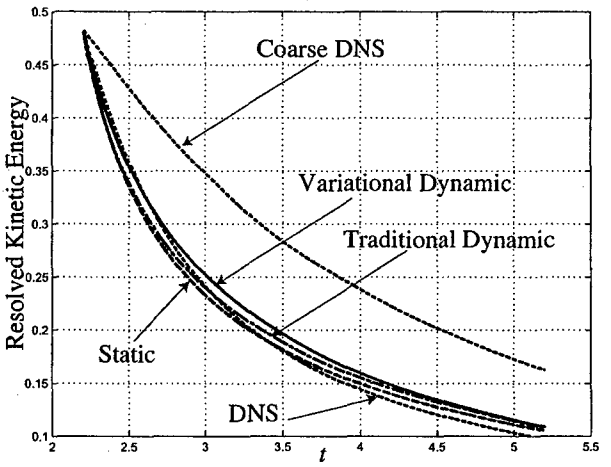

Figure 2.11: Total resolved kinetic energy (q^2) as a function of time.

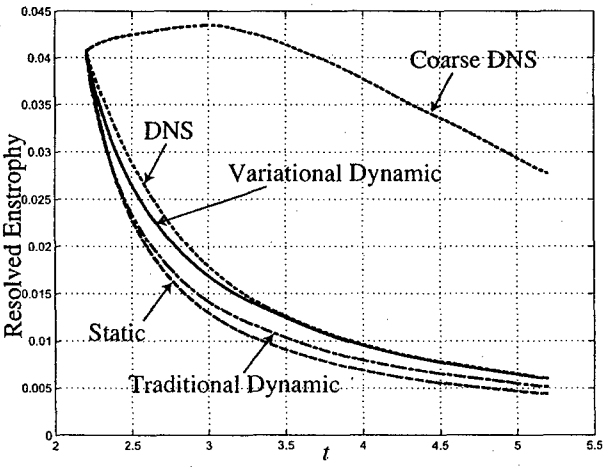

Figure 2.12: Total resolved enstrophy as a function of time.

Chapter 3

Variational Germano Identity Applied to the Spectral Discretization of a Conservation Law

3.1 Introduction

In this chapter we develop a numerical method for the spectral approximation of non-linear conservation laws. These laws describe a broad range of physical phenomena which include the dynamics of gasses, the flow of traffic and the propagation of shallow water and nonlinear acoustic waves. In all these systems we are interested in cases when the physical viscosity (or diffusivity) is small or zero. In the small viscosity case, the solution to such systems develops local regions of large spatial and temporal gradients called shocks. The width of a shock reduces with reducing viscosity, and in the limit of zero viscosity the solution becomes discontinuous. In fact, in this limit in order to ensure unique solutions, the conservation law must be supplemented with an entropy production inequality and conditions that relate jumps in conserved quantities across the shock [34, 35].

For small viscosities, the standard Fourier-Galerkin approximation to non-linear conservation laws becomes unstable if the shock width is smaller than the grid size. For a large class of problems the computational cost of employing a grid which is fine enough to resolve a shock is prohibitive and as a result this method finds limited application. Further, in the limit of zero viscosity, even with sufficient grid refinement, the Fourier-Galerkin solution does not converge to the unique "physical" solution which satisfies the entropy production inequality. To overcome these difficulties associated with the Fourier-Galerkin method, several methods have been proposed. A large proportion of these methods involve appending to the Fourier-Galerkin formulation a numerical viscosity term (see [36] for example). We choose to classify different numerical viscosity based methods on the basis of the equations in which the viscosity appears. To accomplish this, we introduce the concept of the *coarse* and the *fine scale equations* of a numerical approximation as follows.

In a Fourier-Galerkin method, the residual of the original partial differential equation is weighted by a Fourier mode, integrated over the domain, and the result is set to zero. This leads to a finite number of ordinary differential equations (ODEs), which may then be solved

to determine the coefficients in the Fourier expansion of the numerical solution (see [37] for example). Note that in a Galerkin method the same set of modes is used for the weighting functions and the trial solution. Given a set of modes that comprises the weighting function space, we select a scalar $\tilde{k}$ and label modes with wavenumbers k such that $|k| < \tilde{k}$ as the low wavenumber or the coarse scale modes, and the remaining modes as the high wavenumber or the fine scale modes. Then depending on whether an ODE in the numerical approximation is obtained from a coarse or a fine scale weighting function, we classify it as a coarse or a fine scale equation.

In several popular methods (such as the vanishing viscosity method [38]) that guarantee the convergence of the numerical solution to the unique entropy solution, the numerical viscosity is applied to both the coarse and the fine scale equations. On the other hand, in the vanishing spectral viscosity method proposed by Tadmor [39], the viscosity is applied only to the fine scale equations. As a result, this method retains the spectral accuracy of the coarse or the large scale modes while guaranteeing convergence to the entropy solution. It is interesting to note that in the context of the large eddy simulation (LES) of incompressible turbulent flows, the multiscale method of Hughes et al. [12, 14], also involves applying a numerical viscosity only to the fine scale equations.

Motivated by the class of methods where the viscosity appears only in the fine scale equations, we propose a method where *different numerical viscosities appear in the large and the small scale equations.* In addition, in contrast to the methods described above, these viscosities are not determined *a-priori*, instead they are calculated as part of the solution (dynamically). The equations that are used to determine the viscosities are derived from the condition that the resulting numerical method be optimal in a certain user-defined sense. We dub this method the dynamic multiscale viscosity method.

We remark that the equation used to dynamically determine the viscosities, is in effect the variational counterpart of the Germano identity. This identity has found widespread use in determining model parameters in the LES of turbulent flows [15]. Recently, we have demonstrated how it may be used as a tool for determining unknown parameters in a numerical method aimed at solving an abstract partial differential equation [16]. The work presented in this chapter is an application of this methodology to the spectral approximation of non-linear conservation laws. In particular we use it to develop the dynamic multiscale method for a generic non-linear conservation law and then apply it to the model case of one-dimensional Burgers equation to study its properties. We find that the dynamic multiscale method outperforms the vanishing spectral viscosity method.

An outline of the remainder of this chapter is as follows: In Section 2, we present the equations for a generic non-linear conservation law. In Section 3, we introduce its Fourier-Galerkin approximation. In Section 4, we introduce the multiscale viscosity method. In Section 5, we derive the necessary conditions that ensure the multiscale viscosity method is optimal in a user-defined sense. We employ these conditions in Section 6 to derive expressions for the multiscale viscosities. This completes the description of the dynamic multiscale method. In Section 7, we apply the proposed method to the one-dimensional Burgers equation, and compare the results with the Fourier-Galerkin and the spectral vanishing viscosity methods. We end with concluding remarks in Section 8.

3.2 Problem Statement

We represent a generic non-linear conservation law with the following quasi-linear partial differential equation in the space-time domain $Q = \Omega \times]0, T[$, where $\Omega = [0, 2\pi]$ is the spatial domain, and $]0, T[$ denotes the time period of interest: Given $\boldsymbol{f}$, $\boldsymbol{G}$, $\boldsymbol{D}$ and $\boldsymbol{u}_0$, find $\boldsymbol{u} : Q \to \mathbb{R}^n$, such that

$$\begin{aligned} \boldsymbol{u}_{,t} + \boldsymbol{G}(\boldsymbol{u})_{,x} - \boldsymbol{D}\boldsymbol{u}_{,xx} + \boldsymbol{f} &= \boldsymbol{0}, \qquad \text{in } Q \qquad (3.1) \\ \boldsymbol{u}(x, 0) &= \boldsymbol{u}_0(x), \quad \text{in } \Omega. \qquad (3.2) \end{aligned}$$

In the equations above, $\boldsymbol{u}_{,t}$ is the time derivative of $\boldsymbol{u}$, $\boldsymbol{G} : \mathbb{R}^n \to \mathbb{R}^n$ is a non-linear vector function of $\boldsymbol{u}$, $\boldsymbol{D} : \mathbb{R}^n \to \mathbb{R}^n$ is an $n \times n$ positive semi-definite matrix of viscosities given by $\boldsymbol{D} = \text{diag}\{\nu_1, \cdots, \nu_n\}$, and $\boldsymbol{u}_0$ is the initial condition. The form of equations (3.1-3.2) is representative of a large class of physical phenomena that includes the dynamics of gasses, models of traffic flow, non-linear water waves, and processes described by Burgers equation.

We consider periodic boundary conditions for $\boldsymbol{u}$ expressed as

$$\boldsymbol{u}(2\pi, t) = \boldsymbol{u}(0, t), \quad t \in]0, T[. \qquad (3.3)$$

For any $\boldsymbol{v} : Q \to \mathbb{R}^n$, we introduce a Fourier-series representation $\mathbb{P}^{(\alpha)}\boldsymbol{v}$, defined as

$$\mathbb{P}^{(\alpha)}\boldsymbol{v} = \sum_{0 \le |k| \le \alpha} \hat{\boldsymbol{v}}(k, t) e^{ikx}, \qquad (3.4)$$

where k is the wavenumber, and $\hat{\boldsymbol{u}}$ are the Fourier coefficients given by

$$\hat{\boldsymbol{v}}(k, t) = \frac{1}{2\pi} \int_\Omega \boldsymbol{v}(x, t) e^{-ikx}\, dx. \qquad (3.5)$$

It is easily verified that the operator $\mathbb{P}^{(\alpha)}$ commutes with spatial and temporal differentiation and that

$$\mathbb{P}^{(\alpha)}\mathbb{P}^{(\beta)} = \mathbb{P}^{(\beta)}\mathbb{P}^{(\alpha)} = \mathbb{P}^{(\min(\alpha,\beta))}. \qquad (3.6)$$

We will make use of this property in deriving the consistency conditions for the optimal numerical method in Section 5.

We are interested in spectral approximation of (3.1-3.2) for small viscosities ($|\boldsymbol{D}| \ll 1$) and in the limit of vanishing viscosities ($|\boldsymbol{D}| \to 0$). For small viscosities the solution to these equations is known to exhibit sharp variations in space and time called shocks. For $\boldsymbol{D} = \boldsymbol{0}$ the solution becomes discontinuous and multivalued. To ensure uniqueness, (3.1-3.2) must be supplemented with conditions that relate jumps in conserved quantities across a shock and an entropy production inequality. Another mechanism to arrive at the same physically relevant solution in this limit is to construct a solution with finite viscosity and then consider the limit $|\boldsymbol{D}| \to 0$.

3.3 Fourier-Galerkin Approximation

The Fourier-Galerkin approximation of (3.1-3.2) is a function $\boldsymbol{u}^{(N)}$

$$\boldsymbol{u}^{(N)} = \sum_{0 \le |k| \le N} \hat{\boldsymbol{u}}(k,t) e^{ikx} \tag{3.7}$$

such that

$$\begin{aligned} \mathbb{P}^{(N)}\left[\boldsymbol{u}^{(N)}_{,t} + \boldsymbol{G}(\boldsymbol{u}^N)_{,x} - \boldsymbol{D}\boldsymbol{u}^N_{,xx} + \boldsymbol{f}\right] &= \boldsymbol{0}, \qquad \text{in } Q & (3.8)\\ \mathbb{P}^{(N)}\boldsymbol{u}^{(N)}(x,0) &= \mathbb{P}^{(N)}\boldsymbol{u}_0(x), \quad \text{in } \Omega. & (3.9) \end{aligned}$$

Noting that $\mathbb{P}^{(N)}$ commutes with spatial and temporal differentiation, and that $\mathbb{P}^{(N)}\boldsymbol{u}^{(N)} = \boldsymbol{u}^{(N)}$, (3.8-3.9) may be simplified as

$$\begin{aligned} \boldsymbol{u}^{(N)}_{,t} + \left(\mathbb{P}^{(N)}[\boldsymbol{G}(\boldsymbol{u}^{(N)})]\right)_{,x} - \boldsymbol{D}\boldsymbol{u}^{(N)}_{,xx} + \mathbb{P}^{(N)}\boldsymbol{f} &= \boldsymbol{0}, \qquad \text{in } Q & (3.10)\\ \boldsymbol{u}^{(N)}(x,0) &= \mathbb{P}^{(N)}\boldsymbol{u}_0(x), \quad \text{in } \Omega. & (3.11) \end{aligned}$$

Using (3.7) in (3.10-3.11) and invoking the orthogonality of e^{ikx} in Ω, we have

$$\begin{aligned} \hat{\boldsymbol{u}}_{N,t} + ik\hat{\boldsymbol{G}}(\boldsymbol{u}^{(N)}) + k^2\boldsymbol{D}\hat{\boldsymbol{u}}^{(N)} + \hat{\boldsymbol{f}} &= \boldsymbol{0}, \qquad 0 \le |k| \le N, \text{ in }]0,T[& (3.12)\\ \hat{\boldsymbol{u}}^{(N)}(k,0) &= \hat{\boldsymbol{u}}_0(k), \quad 0 \le |k| \le N, & (3.13) \end{aligned}$$

Note that in (3.12), for notational convenience, we have omitted the explicit dependence of the Fourier coefficients (the hat terms) on k and t.

Equations (3.10-3.11) and (3.12-3.13) are both expressions of the Fourier-Galerkin approximation to the original partial differential equation. We wish to solve these equations in the limit of small or vanishing viscosities when the mesh size denoted by π/N is much larger than the shock width. In this case, the Fourier-Galerkin is known to produce large spurious oscillations and become unstable. Further, in the limit $\boldsymbol{D} = \boldsymbol{0}$, even with mesh refinement, that is $N \to \infty$, the Fourier-Galerkin solution is known *not to* converge to "physical" entropy solution. In order to address these issues, in the following section we propose a multiscale method based on adding numerical viscosities to the Fourier-Galerkin approximation.

3.4 Multiscale Viscosity Method

We augment the Fourier-Galerkin method with *multiscale* viscosities. The choice of using two distinct viscosities, one for the coarse scale equations, and another for the fine scale equations is motivated by the earlier work of several researchers [12,14,39,40]. The resulting method is given by

$$\boldsymbol{u}^{(N)}_{,t} + \left(\mathbb{P}^{(N)}[\boldsymbol{G}(\boldsymbol{u}^{(N)})]\right)_{,x} - (\boldsymbol{D} + \frac{\bar{\boldsymbol{D}}}{N}\mathbb{P}^{(\alpha N)} + \frac{\acute{\boldsymbol{D}}}{N}(\mathbb{I} - \mathbb{P}^{(\alpha N)}))[\boldsymbol{u}^{(N)}_{,xx}] + \mathbb{P}^{(N)}\boldsymbol{f} = \boldsymbol{0}, \quad \text{in } Q, \tag{3.14}$$

where $\alpha \in]0,1[$ is a real number, $\mathbb{I}$ is the identity operator, and $\bar{\boldsymbol{D}} = \text{diag}\{\bar{\nu}_1, \cdots, \bar{\nu}_n\}$ and $\acute{\boldsymbol{D}} = \text{diag}\{\acute{\nu}_1, \cdots, \acute{\nu}_n\}$ are matrices of numerical viscosities. The initial condition remains unaltered and is given by (3.11). Note that two distinct numerical viscosities, given by $\bar{\boldsymbol{D}}/N$ and $\acute{\boldsymbol{D}}/N$, appear in the equations for the coarse and fine scales respectively. This is clearly seen once equations for the Fourier coefficients of $\boldsymbol{u}^{(N)}$ are evaluated. That is, using (3.7) in (3.14),

$$\hat{\boldsymbol{u}}_{N,t} + ik\hat{\boldsymbol{G}}(\boldsymbol{u}^{(N)}) + k^2(\boldsymbol{D} + \frac{\bar{\boldsymbol{D}}}{N})\hat{\boldsymbol{u}}^{(N)} + \hat{\boldsymbol{f}} = \boldsymbol{0}, \quad 0 \leq |k| \leq \alpha N, \text{ in }]0,T[\tag{3.15}$$

$$\hat{\boldsymbol{u}}_{N,t} + ik\hat{\boldsymbol{G}}(\boldsymbol{u}^{(N)}) + k^2(\boldsymbol{D} + \frac{\acute{\boldsymbol{D}}}{N})\hat{\boldsymbol{u}}^{(N)} + \hat{\boldsymbol{f}} = \boldsymbol{0}, \quad \alpha N < |k| \leq N, \text{ in }]0,T[. \tag{3.16}$$

Since (3.15) is obtained from coarse scale weighting functions ($|k| \leq \alpha N$), and (3.16) is obtained from fine scale weighting functions we term these equations the *coarse and fine scale equations* respectively. As is apparent from these equations, the numerical viscosity that appears in the coarse and fine scale equations is given by $\bar{\boldsymbol{D}}/N$ and $\acute{\boldsymbol{D}}/N$ respectively.

While the proposed method is motivated by earlier works (see [12, 14, 39, 40]), there are two crucial differences

1. In the aforementioned methods the viscosity is applied only to the fine scale equations. The viscosity in the coarse scale equations is zero. In our method different but non-zero viscosities are applied to both the coarse and the fine scale equations.

2. In the aforementioned methods the viscosity is determined *a-priori*. In our method the viscosity is determined as a part of the calculation using an optimality argument. This development is described in the following section.

3.5 Consistency Conditions

We now derive a set of consistency conditions that are utilized in the next section to compute an explicit expression for evaluating the numerical viscosities. These conditions are motivated by the Germano identity, which is commonly used to evaluate parameters in subgrid models for the large eddy simulation of turbulent flows [15].

The main idea which is expressed in Theorem 5.1 below, is the following. We assume that it is possible to choose the viscosities in (3.14) such that the resulting solution is optimal in the sense that its Fourier coefficients exactly match the corresponding coefficients of the continuous solution. Note that other, user-defined definitions of an optimal solution are also possible. In addition, we assume that the same viscosities also yield optimal results for a coarser discretization. That is the solution of (3.14) with N replaced by M everywhere, where $M < N$, is also optimal in the manner described above. These assumptions lead to a set of conditions that must be satisfied by the numerical viscosities in order to yield optimal results. A key feature of these conditions is that they do not involve the continuous solution $\boldsymbol{u}$, and are expressed entirely in terms of the numerical solution $\boldsymbol{u}^N$. Hence they may be utilized with relative ease to determine the numerical viscosities.

Theorem 5.1: Let $\boldsymbol{u}^{(N)}$ and $\boldsymbol{u}^{(M)}$ be solutions of the multiscale viscosity method with modes up to N and M respectively, with $M < N$. If

$$\boldsymbol{u}^{(N)} = \mathbb{P}^{(N)}\boldsymbol{u} \tag{3.17}$$
$$\boldsymbol{u}^{(M)} = \mathbb{P}^{(M)}\boldsymbol{u} \tag{3.18}$$

where $\boldsymbol{u}$ is the solution of the continuous problem, then

$$\Big(\bar{\boldsymbol{D}}(\frac{\mathbb{P}^{(\alpha M)}}{M} - \frac{\mathbb{P}^{(\alpha N)}}{N}) + \acute{\boldsymbol{D}}(\frac{\mathbb{I} - \mathbb{P}^{(\alpha M)}}{M} - \frac{\mathbb{I} - \mathbb{P}^{(\alpha N)}}{N})\Big)[(\mathbb{P}^{(M)}\boldsymbol{u}^{(N)})_{,xx}] = \Big(\mathbb{P}^{(M)}[\boldsymbol{G}(\mathbb{P}^{(M)}\boldsymbol{u}^{(N)}) - \boldsymbol{G}(\boldsymbol{u}^{(N)})]\Big)_{,x}, \text{ in } Q. \tag{3.19}$$

Proof: $\boldsymbol{u}^{(M)}$ satisfies (3.14) with N replaced by M everywhere. Further, from (3.18)

$$\begin{aligned} \boldsymbol{u}^{(M)} &= \mathbb{P}^{(M)}\boldsymbol{u} \\ &= \mathbb{P}^{(M)}\mathbb{P}^{(N)}\boldsymbol{u} \quad \text{(from (3.6), and since } M < N) \\ &= \mathbb{P}^{(M)}\boldsymbol{u}^{(N)} \quad \text{(from (3.17)).} \end{aligned} \tag{3.20}$$

Using (3.20) in (3.14) written with N replaced by M, and rearranging terms so as to retain only the model term on the left-hand side, we arrive at

$$\Big(\frac{\bar{\boldsymbol{D}}}{M}\mathbb{P}^{(\alpha M)} + \frac{\acute{\boldsymbol{D}}}{M}(\mathbb{I} - \mathbb{P}^{(\alpha M)})\Big)[(\mathbb{P}^{(M)}\boldsymbol{u}^{(N)})_{,xx}] = \mathbb{P}^{(M)}\boldsymbol{u}^{(N)}_{,t} + \Big(\mathbb{P}^{(M)}[\boldsymbol{G}(\mathbb{P}^{(M)}\boldsymbol{u}^{(N)})]\Big)_{,x} - \boldsymbol{D}(\mathbb{P}^{(M)}\boldsymbol{u}^{(N)})_{,xx} + \mathbb{P}^{(M)}\boldsymbol{f}, \text{ in } Q. \tag{3.21}$$

By applying $\mathbb{P}^{(M)}$ to (3.14), assuming that $\mathbb{P}^{(M)}$ and spatial differentiation commute, using property (3.17), and rearranging terms so as to retain only the model term on the left hand side, we conclude that

$$\Big(\frac{\bar{\boldsymbol{D}}}{N}\mathbb{P}^{(\alpha N)} + \frac{\acute{\boldsymbol{D}}}{N}(\mathbb{I} - \mathbb{P}^{(\alpha N)})\Big)[(\mathbb{P}^{(M)}\boldsymbol{u}^{(N)})_{,xx}] = \mathbb{P}^{(M)}\boldsymbol{u}^{(N)}_{,t} + \Big(\mathbb{P}^{(M)}[\boldsymbol{G}(\boldsymbol{u}^{(N)})]\Big)_{,x} - \boldsymbol{D}\mathbb{P}^{(M)}\boldsymbol{u}^{(N)}_{,xx} + \mathbb{P}^{(M)}\boldsymbol{f} \text{ in } Q. \tag{3.22}$$

Subtracting (3.22) from (3.21) we have the desired result (viz. (3.19)) ■

Remark: The Fourier representation of (3.19) is given by

$$-k^2 \left\{ \begin{array}{ll} (\frac{\bar{\boldsymbol{D}}}{M} - \frac{\bar{\boldsymbol{D}}}{N})(\hat{\boldsymbol{u}}^{(N)}) & , 0 \le |k| \le \alpha M \\ (\frac{\acute{\boldsymbol{D}}}{M} - \frac{\bar{\boldsymbol{D}}}{N})(\hat{\boldsymbol{u}}^{(N)}) & , \alpha M \le |k| \le \beta \\ (\frac{\acute{\boldsymbol{D}}}{M} - \frac{\acute{\boldsymbol{D}}}{N})(\hat{\boldsymbol{u}}^{(N)}) & , \beta \le |k| \le M \end{array} \right\} = ik\Big(\hat{\boldsymbol{G}}(\mathbb{P}^{(M)}\boldsymbol{u}^{(N)}) - \hat{\boldsymbol{G}}(\boldsymbol{u}^{(N)})\Big) \text{ in }]0, T[\tag{3.23}$$

where

$$\beta = \min(\alpha N, M). \tag{3.24}$$

3.6 Evaluation of the Viscosity Parameters

Equation (3.19) (or (3.23)) represents as many relations as there are modes for which $|k| \leq M$. We wish to evaluate only the $2n$ parameters that appear in $\bar{\boldsymbol{D}}$ and $\acute{\boldsymbol{D}}$ using these relations. One mechanism of reducing (3.19) to $2n$ equations is to equate the L_2 inner product of its residual with the linearly independent functions

$$\mathbb{P}^{(\alpha M)} u_j^{(N)}, \quad j = 1, \cdots, n \tag{3.25}$$

and

$$(\mathbb{I} - \mathbb{P}^{(\alpha M)}) u_j^{(N)}, \quad j = 1, \cdots, n \tag{3.26}$$

to zero. This procedure leads to $2n$ scalar equations that are most conveniently expressed in terms of the Fourier coefficients of $\boldsymbol{u}^{(N)}$. For $j = 1, \cdots, n$ they are given by

$$-(\frac{\bar{\nu}_j}{M} - \frac{\bar{\nu}_j}{N}) \sum_{0 \leq |k| \leq \alpha M} k^2 |\hat{u}_j^{(N)}|^2 = \sum_{0 \leq |k| \leq \alpha M} \hat{u}_j^{(N)*} ik \Big(\hat{G}_j[\mathbb{P}^{(M)} \boldsymbol{u}^{(N)}] - \hat{G}_j[\boldsymbol{u}^{(N)}] \Big) \tag{3.27}$$

$$-(\frac{\acute{\nu}_j}{M} - \frac{\bar{\nu}_j}{N}) \sum_{\alpha M < |k| \leq \beta} k^2 |\hat{u}_j^{(N)}|^2 -$$

$$(\frac{\acute{\nu}_j}{M} - \frac{\acute{\nu}_j}{N}) \sum_{\beta < |k| \leq M} k^2 |\hat{u}_j^{(N)}|^2 = \sum_{\alpha M < |k| \leq M} \hat{u}_j^{(N)*} ik \Big(\hat{G}_j[\mathbb{P}^{(M)} \boldsymbol{u}^{(N)}] - \hat{G}_j[\boldsymbol{u}^{(N)}] \Big) \tag{3.28}$$

where the repeated j indices *do not* imply a summation. These expressions for evaluating the viscosity parameters are functions of the solution itself. Thus the closed system of equations (3.14), (3.11) and (3.27-3.28) comprises a numerical method with non-linear (in $\boldsymbol{u}_N$), multiscale viscosities. In implementing this method the viscosities are evaluated based on the solution obtained from the previous time-step. However once the numerical viscosity is determined this term is treated implicitly.

3.7 Numerical Example

As an example we apply the proposed method to Burgers equation in one dimension. In this case, in (3.1-3.2), $n = 1$, $\boldsymbol{f} = 0$, $\boldsymbol{G}(\boldsymbol{u}) = u^2/2$, $\boldsymbol{D} = \nu_1 = 5 \times 10^{-5}$, and $\boldsymbol{u}_0 = -\sin x$.

The solution to this problem evolves in two distinct phases. In the first phase ($t < \pi/2$), the smooth sine curve steepens. In wavenumber space, this corresponds to transfer of energy from the $k = 1$ mode to higher wavenumbers. This phase culminates in the formation of a shock (or an inverted N-wave) at $t \approx \pi$, whose approximate width is $l = 1.6 \times 10^{-4}$ units. All the dissipation in the system is concentrated near the shock. In the wavenumber space, the formation of the shock corresponds to a $1/k$ spectrum that extends to the dissipation wavenumber, where it steepens. In the second phase, the magnitude of the N-wave reduces as $1/(1+t)$ as the strength of the shock weakens. In wavenumber space, this corresponds to the lowering of the entire spectra at the rate of $1/t$. These stages of the solution are presented in Figures 3.1 and 3.2, where we have shown a well-resolved numerical solution of

the problem. Note that $E(k) \equiv |\hat{u}_k|$ represents the magnitude of the Fourier coefficients of the solution.

In order to asses the performance of the proposed method we consider the following numerical solutions

1. A Fourier-Galerkin solution obtained by solving (3.10-3.11) or (3.12-3.13) on a fine grid in which the shock is resolved. Following terminology used in turbulence modeling we refer to this benchmark solution as the direct numerical solution (DNS). The number of modes used for computing the DNS solution is $N = 65,536$. This corresponds to a mesh size $h = 4.79 \times 10^{-5}$, which is smaller than the shock width $l = 1.6 \times 10^{-4}$. In Figures 3.1 and 3.2 we have plotted this solution in physical and wavenumber spaces at various instances during the interval $]0, 5[$.

2. A Fourier-Galerkin solution obtained by solving (3.10-3.11) or (3.12-3.13) on a coarse grid with $N = 64$. In this case the finest resolved scale ($h = 4.9 \times 10^{-2}$) is much coarser than the scale at which dissipation occurs ($l = 1.6 \times 10^{-4}$).

3. A vanishing spectral viscosity solution on a coarse grid with $N = 64$. This method is represented by (3.14), where $\bar{\boldsymbol{D}} = \bar{\nu}_1 = 0$, and $\acute{\boldsymbol{D}}$ is non-zero. In particular we choose $\alpha = 1/2$ and $\acute{\boldsymbol{D}} = \acute{\nu}_1 = 0.25\alpha$. This choice for $\acute{\nu}_1$ is based on the guideline provided in [39].

4. A dynamic multiscale viscosity solution on a coarse grid with $N = 64$. This method is given by (3.14), where $\alpha = 1/2$ and the viscosity coefficients are determined using (3.27-3.28). In calculating these coefficients the solution from the previous time-step is used.

3.7.1 Comparison

The viscosity parameters of the dynamic multiscale method are chosen such that the method satisfies conditions that are necessary to ensure that the resulting numerical solution has the same Fourier coefficients as the continuous solution. This stipulation may be interpreted as a criterion used to design the numerical method. In the following comparison we assess how close the method comes to achieving this criterion. We also assess its performance in relation to other methods.

In Figures 3.3-3.6, we have plotted $E(k)$ for the three numerical methods and the truncated DNS solution at four distinct times. The DNS serves as a benchmark solution. At $t = 0.5$ we observe that there is little difference in the numerical methods and the DNS. At $t = 1.5$, when the shock is about to form differences appear. A significant pile-up of energy near the cut-off wavenumber is observed in the coarse Fourier-Galerkin solution. For the vanishing spectral viscosity solution, this pile-up is reduced. However the solution is seen to oscillate about the DNS at wavenumbers close to the separation between the coarse and fine scales ($k = 32$). The multiscale solution has much smaller oscillations at these wavenumbers and only slightly underestimates the spectrum at higher wavenumbers. At time $t = 2$, we observe that the pile-up at high wavenumbers in the Fourier-Galerkin solution has polluted the results at lower wavenumbers. The vanishing spectral viscosity solution continues to be

accurate at the lower wavenumbers, however the oscillations close to $k = 32$ appear to have increased. The dynamic multiscale viscosity solution is accurate at the lower wavenumbers. The oscillations near $k = 32$ persist, however they are less pronounced than those for the vanishing spectral viscosity solution. At $t = 5$ we observe that Galerkin solution is completely inaccurate, the oscillations in the vanishing spectral viscosity solution have increased and propagated to lower wavenumbers, where as the dynamic multiscale solution has retained its accuracy.

In Figure 3.7, we have plotted the viscosity parameters $\bar{\nu}_1/N$ and $\acute{\nu}_1/N$ for the vanishing spectral viscosity method and the dynamic multiscale method as a function of time. The coarse scale parameter for the vanishing spectral viscosity method is zero and is not shown, whereas the fine scale parameter which is non-zero and constant is shown. For the dynamic multiscale method we observe that both the coarse and fine scale parameters are zero till $t \approx 1$. This represents the time it takes for the energy to spill out to the wavenumbers near the cutoff wavenumber. Thus the numerical method (correctly) imposes no viscosity till this time. Thereafter, the fine scale parameter is seen to rise, and after a while the coarse scale parameter follows suite. A couple of observations are noteworthy: 1) Unlike the vanishing spectral viscosity method, the viscosity in the coarse scales in the dynamic multiscale method is not zero, thus the method is qualitatively different; 2) The viscosity in the coarse and the fine scales is active for different periods of time, and also has different values. In particular, the fine scale viscosity is about 5/3 of the coarse scale value.

Next we compare the accuracy with which the numerical methods predict the decay of kinetic energy with time. We define the relative error in the resolved kinetic energy as follows

$$\epsilon_{\text{ke}}(t) = \frac{\left(\sum_{|k|\leq 64} \left(\hat{u}^{(64)}\right)^2 - \sum_{|k|\leq 64} \left(\hat{u}\right)^2\right)}{\left(\sum_{|k|\leq 64} \left(\hat{u}\right)^2\right)}. \tag{3.29}$$

In Figure 3.8 we have plotted $\epsilon_{\text{ke}}(t)$ for all the numerical methods. We observe that at $t \approx 1$, that is when the spectra begins to spill beyond the numerical cut-off wavenumber, the Fourier-Galerkin solution overestimates the kinetic energy. By $t \approx 2.5$ its kinetic energy is about two times the actual value. Both the vanishing spectral viscosity and the dynamic multiscale methods are much more accurate. In Figure 3.9 we have compared the performance of these two methods. We observe that the vanishing spectral viscosity solution overestimates the kinetic energy and that the error is seen to increase with time. At $t = 5$ the total error is about 2.7%. The multiscale solution underestimates the kinetic energy however the error is less (about 0.2% at $t = 5$) and remarkably it does not appear to increase with time.

One of the attractive features of the vanishing spectral viscosity method is that in the limit $\nu \to 0$, it converges to the unique solution that satisfies the entropy production inequality, while *retaining spectral accuracy in the coarse modes.* This leads us to consider that while the dynamic multiscale method may be more accurate in predicting quantities such as the overall spectrum and the resolved kinetic energy, the vanishing spectral viscosity method may be more accurate in capturing the evolution of the coarse modes since it imposes no additional viscosity on these modes. In order to verify this in Figure 3.10, we have plotted

the error in the $k = 1$ mode, scaled by the exact value, as a function of time. That is

$$\epsilon_1(t) = \frac{\hat{u}^{(64)}(1,t) - \hat{u}(1,t)}{|\hat{u}(1,t)|}. \tag{3.30}$$

We consider the DNS solution to be the exact value. We observe that at $t \approx \pi$ the error in the coarse Fourier-Galerkin solution rises steeply, whereas the error in the other two methods is smaller. In Figure 3.11, we exclude the Fourier-Galerkin solution. We observe that error the vanishing spectral viscosity solution rises steadily beyond $t \approx 1$. At $t = 5$ the error is about 1%. The error in the dynamic multiscale method is much smaller and appears not to increase with time. At $t = 5$ it is about 0.04%. We have observed similar behavior for other coarse modes ($k = 1, \cdots, 10$). Thus contrary to what might be expected, we observe that *dynamic method (with a non-zero viscosity in the coarse modes) is more accurate than the vanishing spectral viscosity method in predicting the evolution of the coarse modes.* We attribute this observation to the hypothesis that the ideal model, which would replicate the effects of the missing scales on the retained scales exactly, may possess a non-zero viscosity at small wavenumbers. We are presently verifying this hypothesis analytically and numerically.

3.8 Conclusions

We have proposed a new dynamic multiscale viscosity method for the spectral approximation of conservation laws in the limit of small or vanishing viscosities. Within this method the numerical approximation is split into coarse and fine scales, and likewise the projected spectral equations are also split into coarse and fine scale equations. Thereafter different numerical viscosities are applied in the coarse and fine scale equations. These viscosities are determined using a condition that must be satisfied if the resulting numerical solution is to be optimal in a user-defined sense.

We have applied this method to the one-dimensional Burgers equation. We have compared the resulting solution with the Fourier-Galerkin solution and the vanishing spectral viscosity solution computed using the same number of modes. As a benchmark we have used a well-resolved Fourier-Galerkin solution. In all comparisons we have found that the dynamic multiscale solution is the most accurate. In addition we have observed that the relative errors in this solution appear not to grow in time.

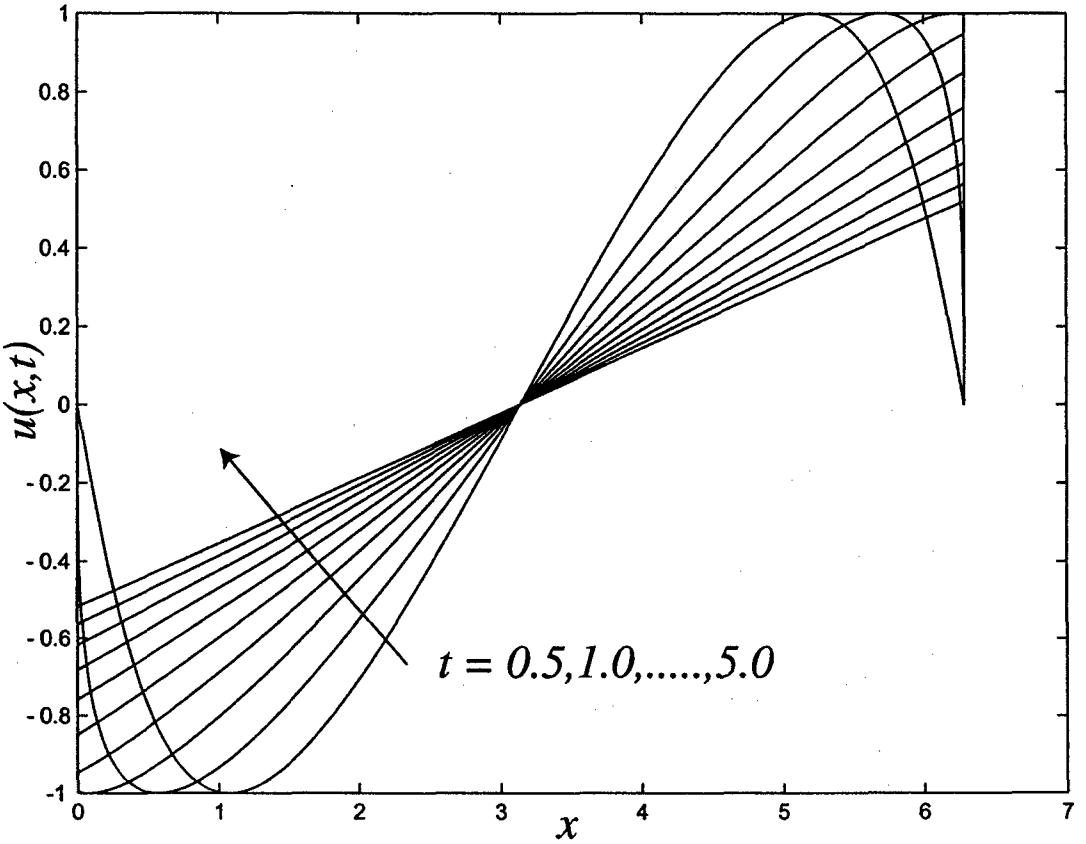

Figure 3.1: Well resolved numerical solution (DNS) at $t = 0.5, 1.0, 1.5, 2.0, 2.5, 3.0, 3.5, 4.0, 4.5$ and 5.0 (arrow indicates increasing time).

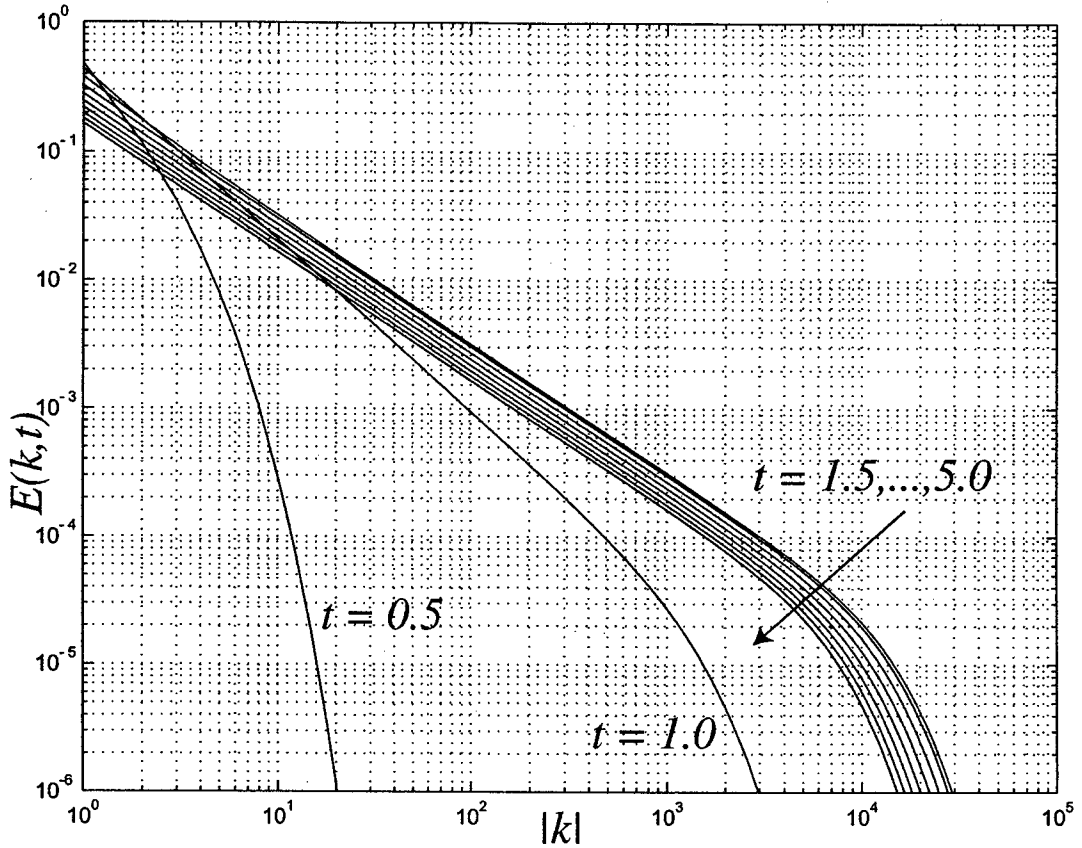

Figure 3.2: $E(k)$ for the well resolved numerical solution (DNS) at $t = 0.5, 1.0, 1.5, 2.0, 2.5, 3.0, 3.5, 4.0, 4.5$ and 5.0 (arrow indicates increasing time).

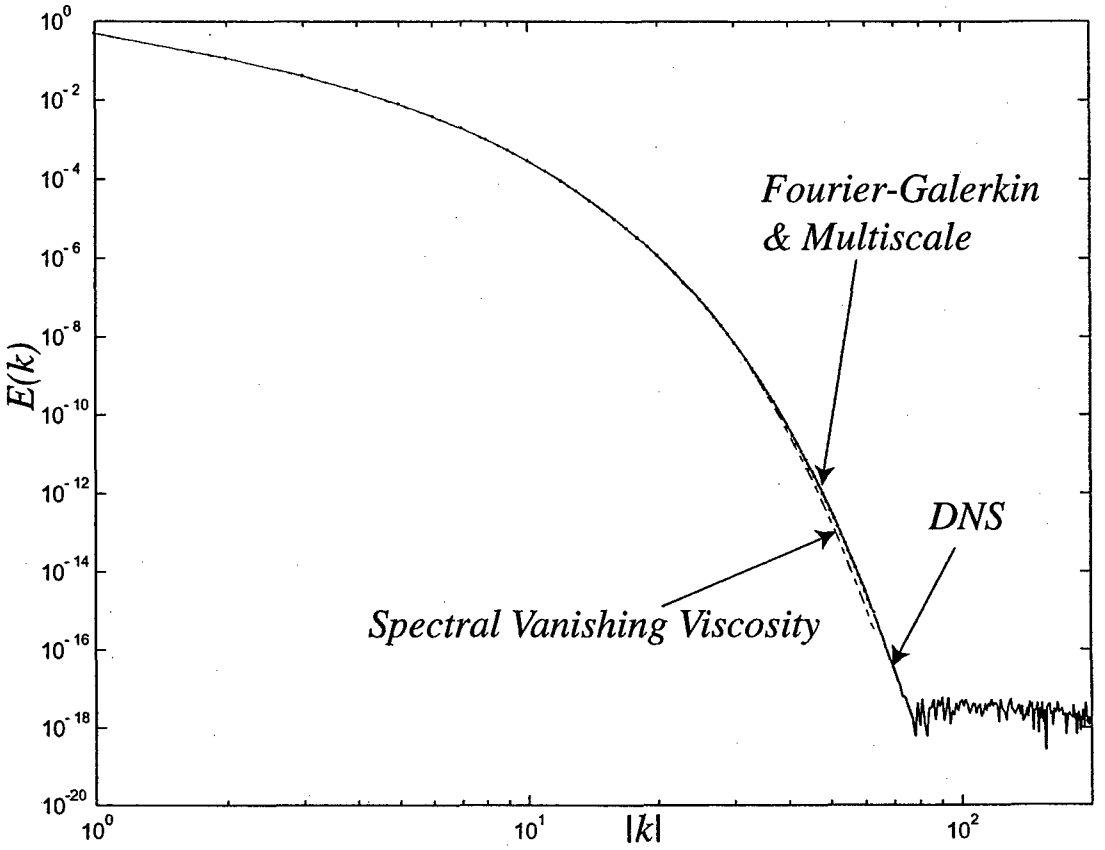

Figure 3.3: $E(K)$ for the solution of the numerical methods and the DNS at $t = 0.5$.

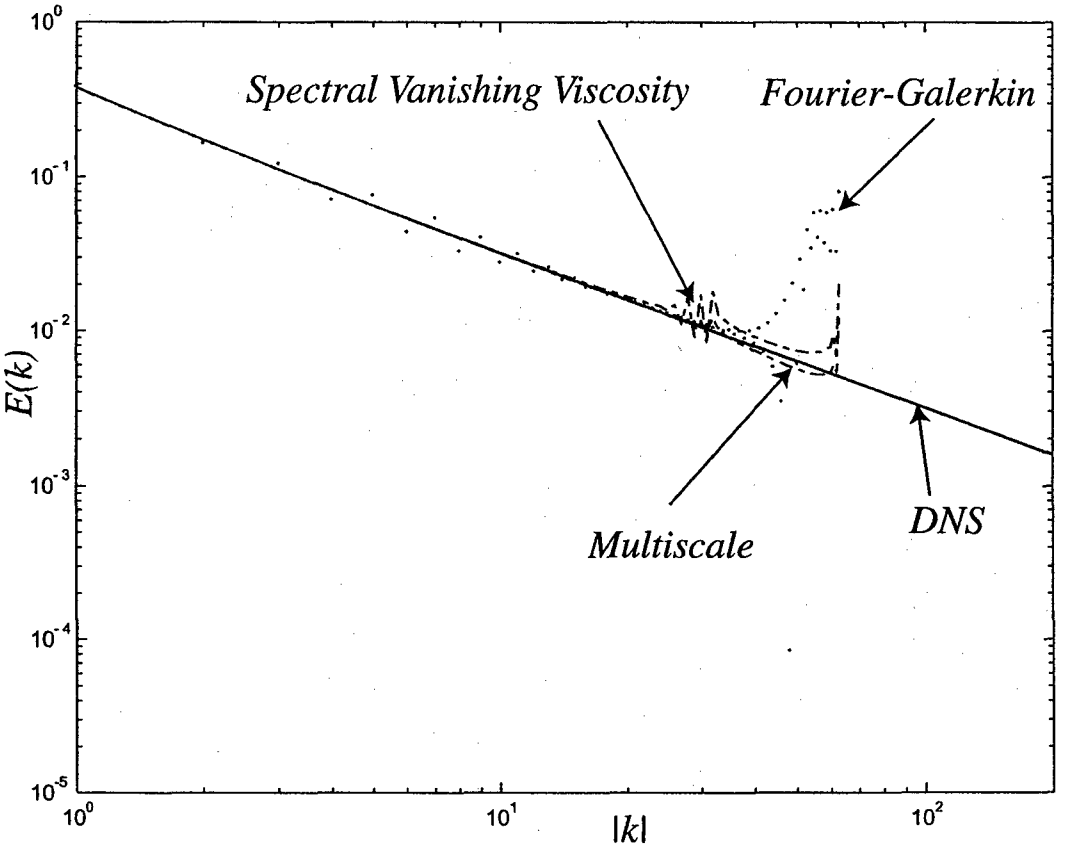

Figure 3.4: $E(k)$ for the solution of the numerical methods and the DNS at $t = 1.5$.

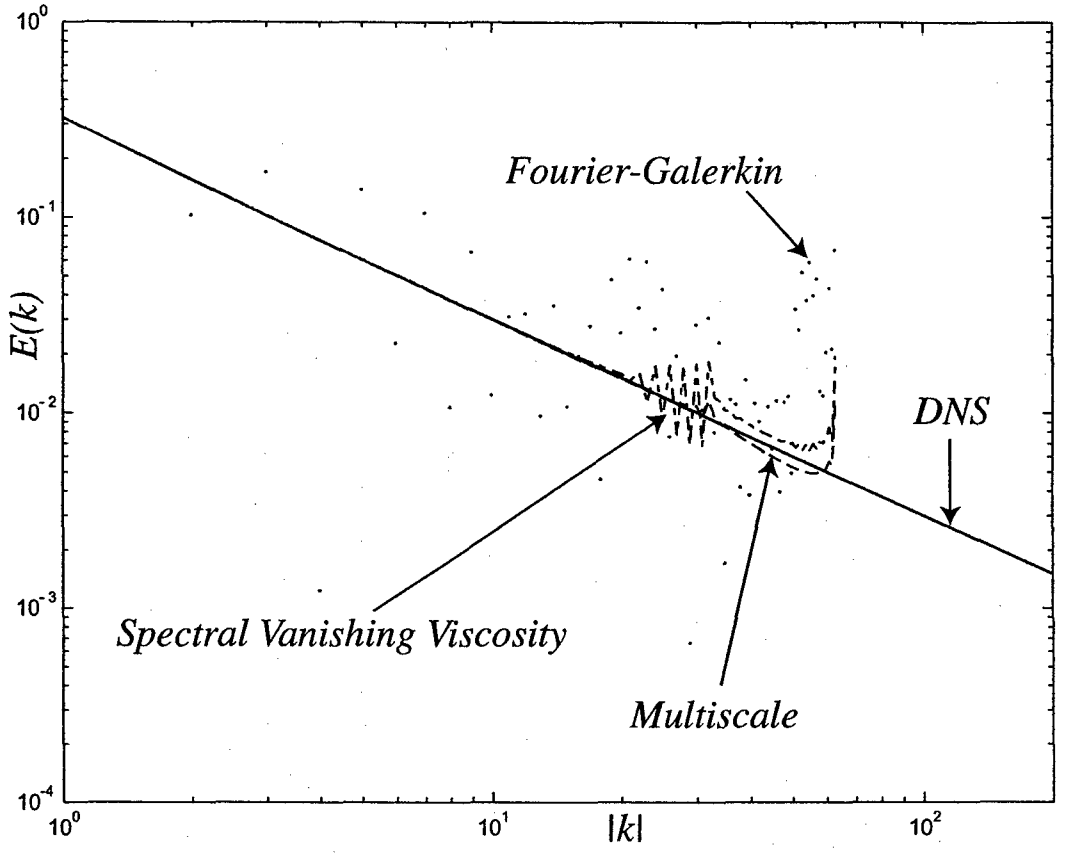

Figure 3.5: $E(k)$ for the solution of the numerical methods and the DNS at $t = 2.0$.

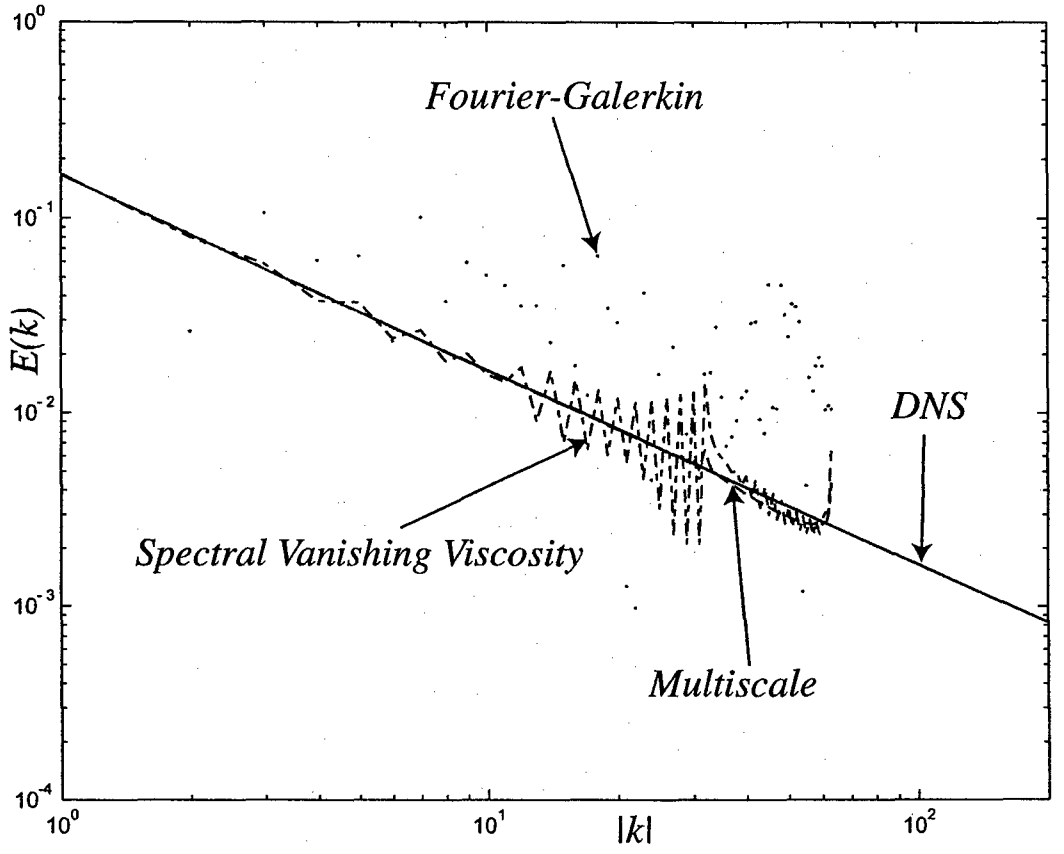

Figure 3.6: $E(k)$ for the solution of the numerical methods and the DNS at $t = 5.0$.

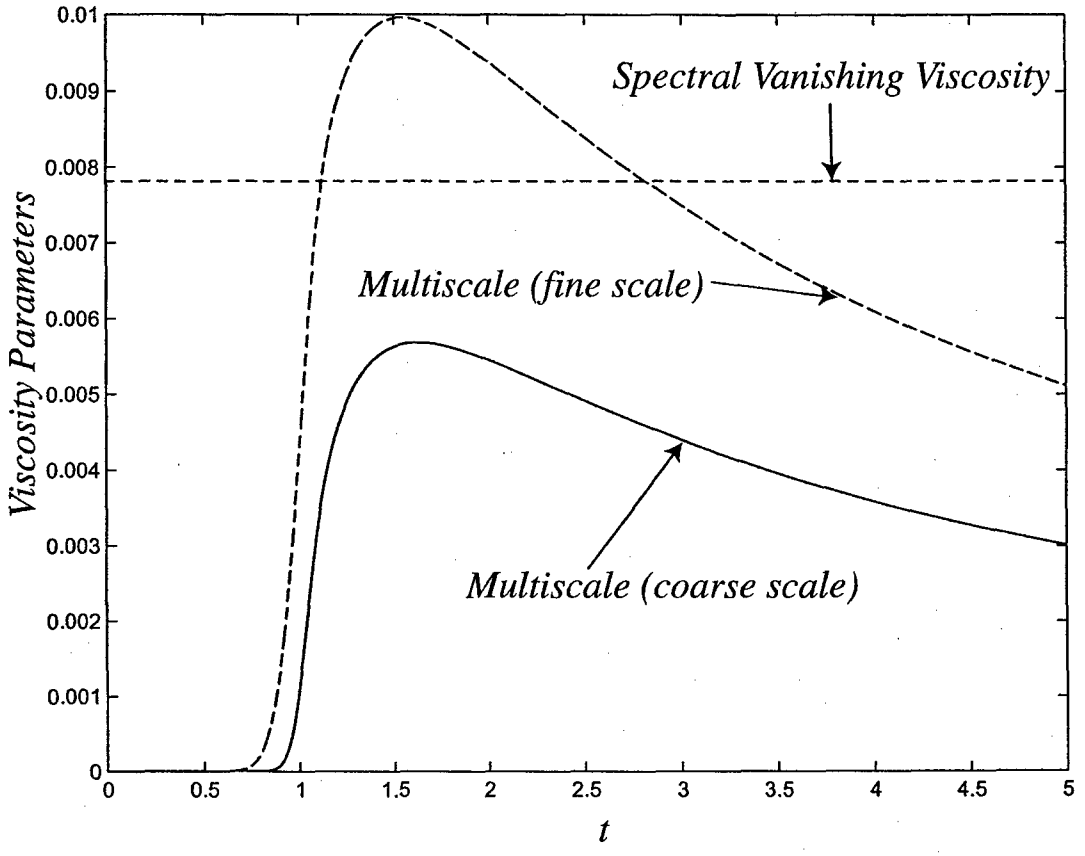

Figure 3.7: Numerical viscosities for the spectral vanishing viscosity method and the dynamic multiscale method as a function of time.

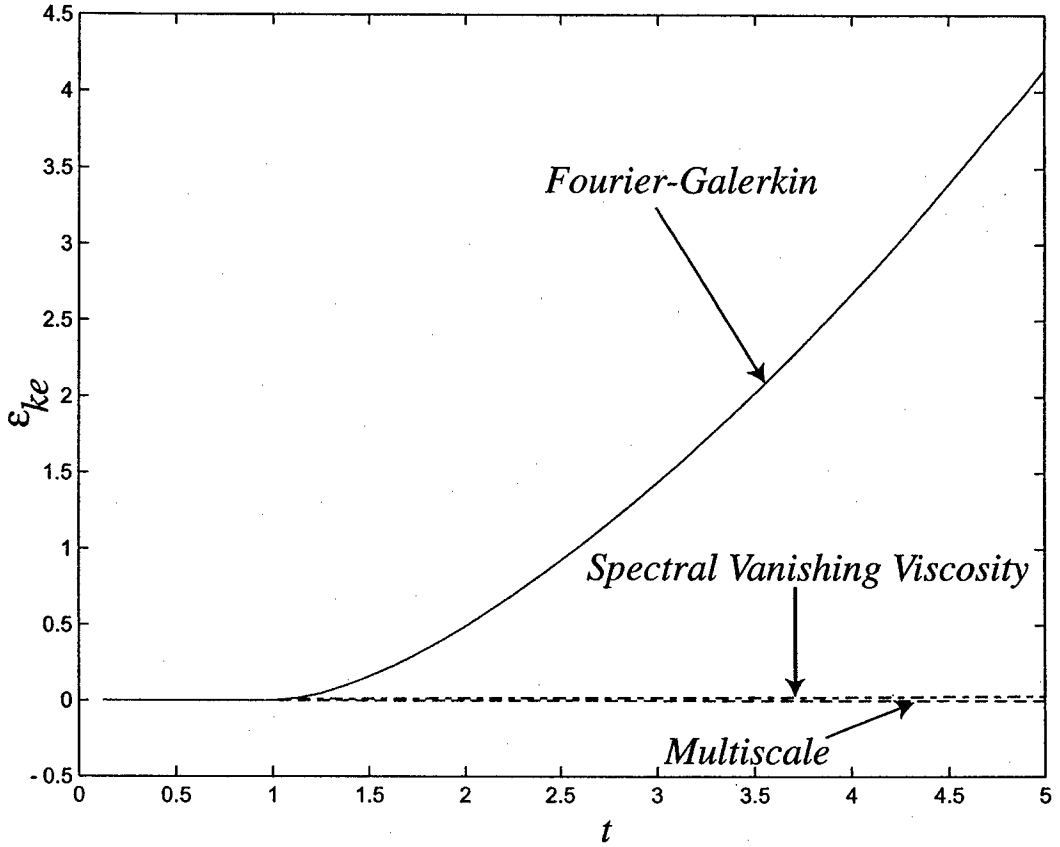

Figure 3.8: Scaled error in the resolved kinetic energy of the numerical methods as a function of time.

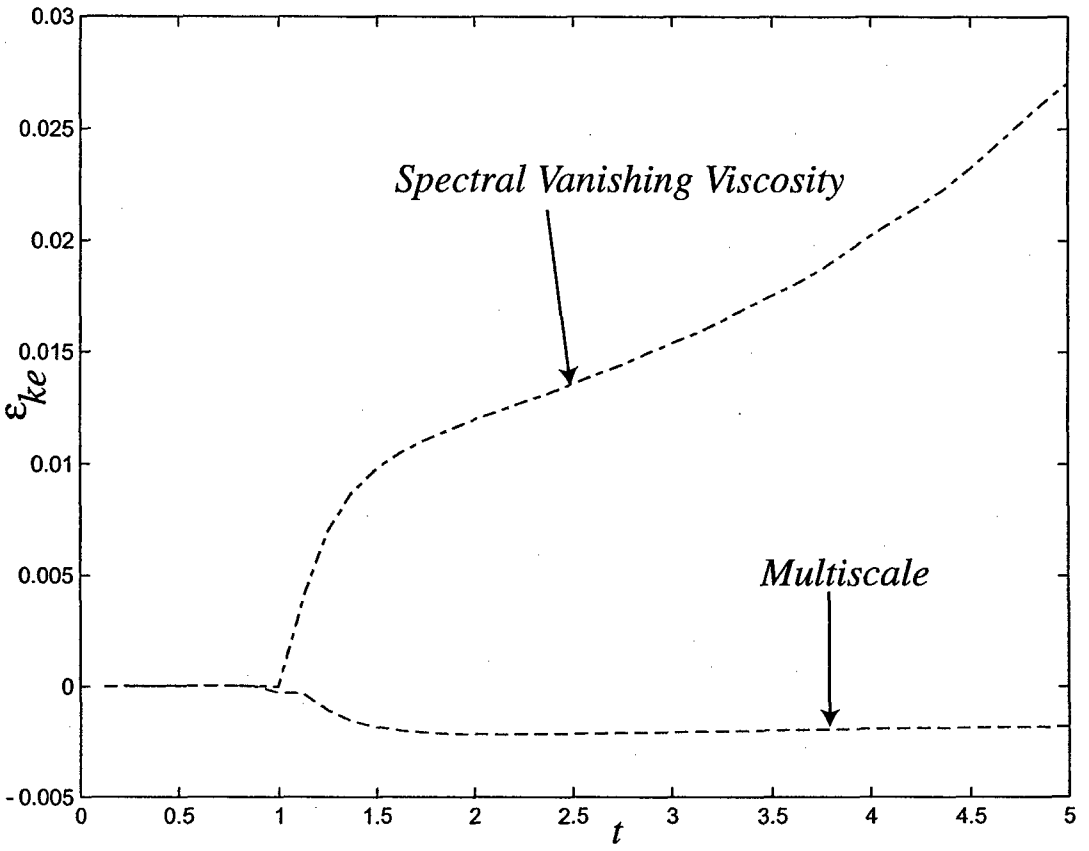

Figure 3.9: Scaled error in the resolved kinetic energy of the spectral vanishing viscosity method and the dynamic multiscale method as a function of time.

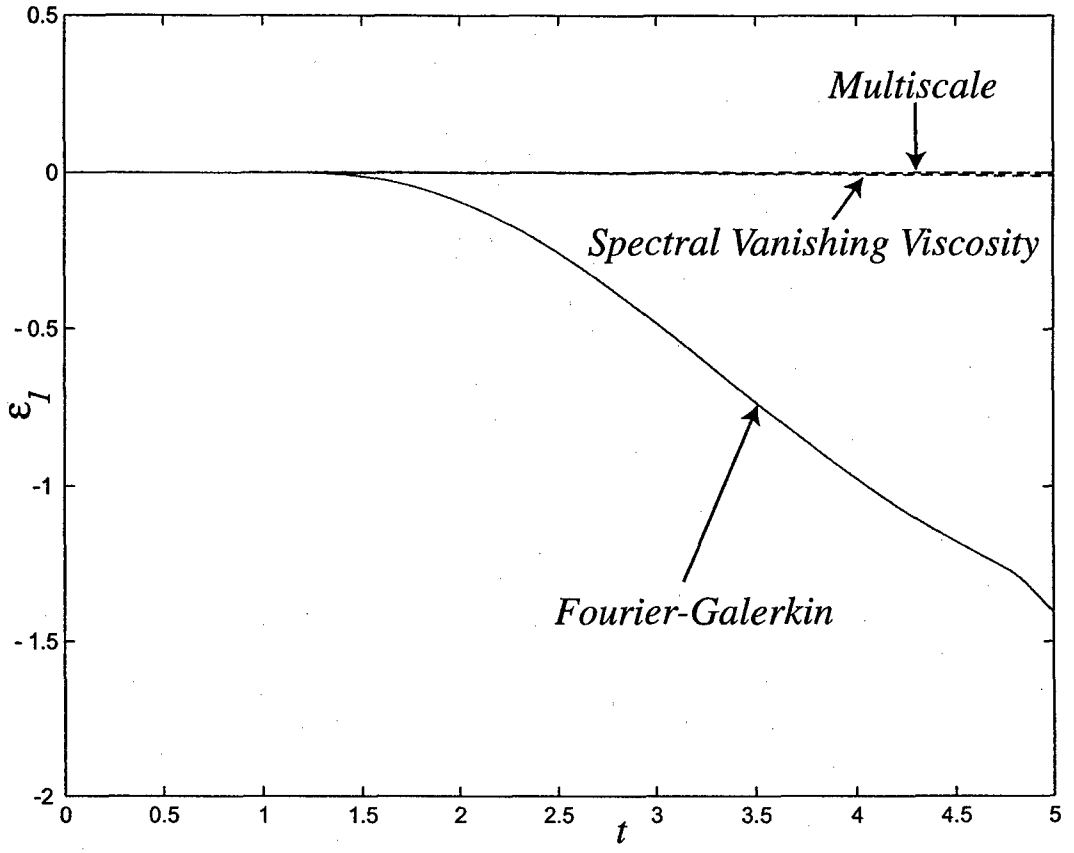

Figure 3.10: Scaled error in the $k = 1$ mode of the numerical methods as a function of time.

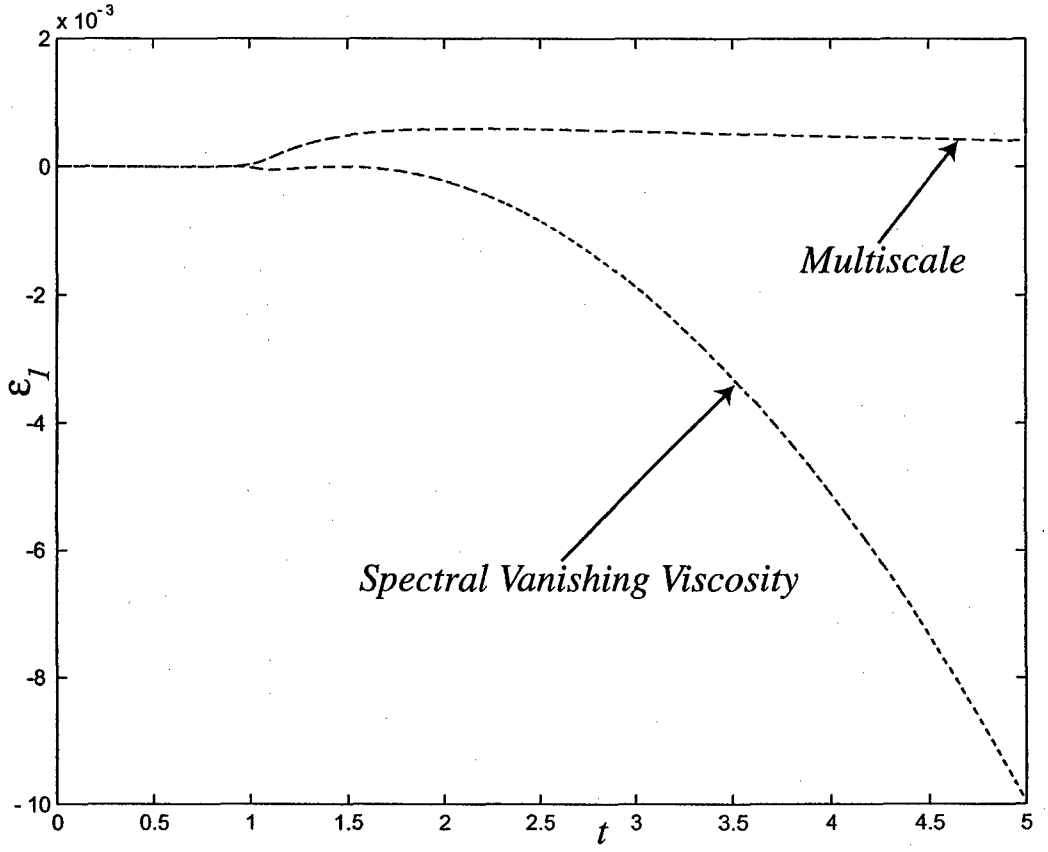

Figure 3.11: Scaled error in the $k = 1$ mode of the spectral vanishing viscosity method and the dynamic multiscale method as a function of time.

Chapter 4

Variational Germano Identity Applied to Large Eddy Simulation

4.1 Introduction

The typical formalism for performing large eddy simulation (LES) of turbulent flows involves spatially filtering the strong form of the Navier-Stokes equations. The width of the filter is chosen in accordance with the resolution of the computational grid on which the numerical solution is sought. The filtering operation yields a system of equations for the filtered variables in which certain terms that involve the unfiltered variables appear. These terms are replaced by models, which are functionals of the filtered variables only, and a closed system for the filtered variables is obtained.

In [14], a different formalism for performing LES was introduced. In this new approach, instead of spatially filtering the strong form of the Navier-Stokes equations, a weak or a variational form was used as a starting point. It was recognized that the approximation of the weak form by the Galerkin method involved approximating infinite-dimensional function spaces by their finite-dimensional counterparts. It was argued that for typical turbulent flows, which tend to have a large range of energetic structures of different sizes, finite dimensional spaces could not faithfully represent all the features of the exact solution. In the few select cases where this would be feasible, the Galerkin solution would correspond to the direct numerical simulation of the problem. On the other hand, in most cases of practical interest, LES models that represent the effect of the missing scales will be required. This formalism was then used to develop a multiscale model (in reality, a two-scale model) for the resolved scales. This model consisted of a Smagorinsky-type term constructed from the resolved, fine-scale velocity components and applied to the fine-scale equations and no model in the coarse scale equations. Several applications of this model with encouraging results have now been reported (see for example [12, 13, 41]).

While the variational formulation of LES has lead to encouraging results, there is one aspect of this formulation that is still missing. This is the development of dynamic *variational LES models*. In the context of filter-based LES modeling, dynamic LES models rely on the Germano identity to evaluate model parameters as part of the simulation (dynamically) [15]. Dynamic LES models have been particularly successful in modeling flows where the statistics

of turbulence vary in space and time, such as flows with intermittent, transitional or decaying turbulence and flows with boundary layers. In this manuscript, we derive the variational counterpart of the Germano identity and demonstrate how it may be used to determine LES model parameters in a variational context.

Our derivation of the variational counterpart of the Germano identity is similar to its derivation in the filtered case. There are however important differences in the final result. These differences emanate from differences in the definition of an ideal LES model in the variational and the filter-based formulations and are highlighted in our development. In fact, we have discovered that the variational formulation of the Germano identity has applications beyond the realm of large eddy simulation. In [16] we have demonstrated how it may be used to determine parameters of a generic numerical method. So far in addition to its application to turbulence (described in this chapter), we have applied it to the determine parameters in a residual-based finite element method solution of the linear advection-diffusion problem [16] and to determine the multiscale viscosity parameters in the spectral approximation of Burgers equation [17].

The layout of the remainder of this chapter is as follows: In the following section we introduce the incompressible Navier Stokes equations. In Section 3, we review the filter-based Germano identity. Thereafter in Section 4, we introduced the variational formulation of LES and also derive the variational counterpart of the Germano identity. In Section 5, we apply it to the specific problem of determining the Smagorinsky parameter in the spectral approximation of the decay of homogeneous isotropic turbulence. In Section 6, we present numerical results and end with conclusions in Section 7.

4.2 Incompressible Navier Stokes Equations

We consider the motion of an incompressible fluid in $Q = \Omega \times]T_1, T_2[$, where Ω is the spatial domain and $]T_1, T_2[$ is the time period of interest. The strong form of the problem is given by

$$\begin{aligned} \boldsymbol{u}_{,t} + \nabla \cdot (\boldsymbol{u} \otimes \boldsymbol{u}) + \nabla p - \nu \nabla^2 \boldsymbol{u} &= \boldsymbol{f}, \text{ in } Q & (4.1) \\ \nabla \cdot \boldsymbol{u} &= 0, \text{ in } Q. & (4.2) \end{aligned}$$

In the above equations $\boldsymbol{U} = [\boldsymbol{u}, p]^T$, where $\boldsymbol{u}$ is the fluid velocity field and p is the pressure. In addition, ν is the kinematic viscosity and the symbol $\otimes$ denotes the outer product of two vectors. The boundary of Ω is denoted by $\partial\Omega$. For simplicity the boundary condition on $\boldsymbol{U}$ is assumed to be either periodic or homogeneous. The initial, divergence-free velocity field is given by

$$\boldsymbol{u}(\boldsymbol{x}, 0) = \boldsymbol{u}_0(\boldsymbol{x}). \quad (4.3)$$

4.3 Filtered Form of the Germano identity

In this section we provide a summary of the derivation the filtered form of the Germano identity (for details see [15]). This will be contrasted with the its variational counterpart in the following section.

We apply a spatial filter to (4.1) and (4.2) to arrive at

$$(\mathbb{F}^h \boldsymbol{u})_{,t} + \nabla \cdot \mathbb{F}^h(\boldsymbol{u} \otimes \boldsymbol{u}) + \nabla(\mathbb{F}^h p) - \nu \nabla^2(\mathbb{F}^h \boldsymbol{u}) = \mathbb{F}^h \boldsymbol{f}, \text{ in } Q \quad (4.4)$$

$$\nabla \cdot \mathbb{F}^h \boldsymbol{u} = 0, \quad \text{in } Q \quad (4.5)$$

where $\mathbb{F}^h \boldsymbol{u}$ is the filtered version of $\boldsymbol{u}$ and $\mathbb{F}^h$ is a filter of width h and we have assumed that filtering and spatial differentiation commute. Note that (4.4) and (4.5) are not closed in $\mathbb{F}^h \boldsymbol{u}$ as (4.4) still involves the unfiltered velocity $\boldsymbol{u}$ in the quadratic term. Thus (4.4) may be replaced by

$$(\mathbb{F}^h \boldsymbol{u})_{,t} + \nabla \cdot (\mathbb{F}^h \boldsymbol{u} \otimes \mathbb{F}^h \boldsymbol{u}) + \nabla(\mathbb{F}^h p) - \nu \nabla^2(\mathbb{F}^h \boldsymbol{u}) - \nabla \cdot \boldsymbol{m}(\mathbb{F}^h \boldsymbol{u}; h, \boldsymbol{c}) = \mathbb{F}^h \boldsymbol{f}, \text{ in } Q \quad (4.6)$$

where $\boldsymbol{m}(\mathbb{F}^h \boldsymbol{u}; h, \boldsymbol{c})$ is a model term that depends only on the filtered velocity field $\mathbb{F}^h \boldsymbol{u}$ (and not $\boldsymbol{u}$), the filter width h and a vector of parameters $\boldsymbol{c}$. For a fixed choice of $\boldsymbol{c}$, (4.6) and (4.5) represent a closed system in $\mathbb{F}^h \boldsymbol{u}$ and $\mathbb{F}^h p$.

From (4.6) and (4.4) we conclude that the ideal model term is given by

$$\boldsymbol{m}(\mathbb{F}^h \boldsymbol{u}; h, \boldsymbol{c}) = (\mathbb{F}^h \boldsymbol{u}) \otimes (\mathbb{F}^h \boldsymbol{u}) - \mathbb{F}^h(\boldsymbol{u} \otimes \boldsymbol{u}) \text{ in } Q, \quad (4.7)$$

as this choice allows the filtered velocity and pressure fields $[\mathbb{F}^h \boldsymbol{u}, \mathbb{F}^h p]$ to be the solution of (4.6) and (4.5).

To derive the filtered form of the Germano identity we consider a coarser spatial filter $\mathbb{F}^H$, with $H > h$. Using the argument made in the previous paragraph, we conclude that at this scale the ideal model is given by

$$\boldsymbol{m}(\mathbb{F}^H \boldsymbol{u}; H, \boldsymbol{c}) = (\mathbb{F}^H \boldsymbol{u}) \otimes (\mathbb{F}^H \boldsymbol{u}) - \mathbb{F}^H(\boldsymbol{u} \otimes \boldsymbol{u}) \text{ in } Q. \quad (4.8)$$

Note that we have assumed that the functional dependence of the model on the filtered solution and the filter width as well as the parameters $\boldsymbol{c}$ is unchanged. By subtracting (4.7) filtered at the H scale from (4.8), and assuming that $\mathbb{F}^H = \mathbb{F}^H \mathbb{F}^h$, we arrive at the Germano identity, viz,

$$\boldsymbol{m}(\mathbb{F}^H \boldsymbol{u}; H, \boldsymbol{c}) - \mathbb{F}^H(\boldsymbol{m}(\mathbb{F}^h \boldsymbol{u}; h, \boldsymbol{c})) = (\mathbb{F}^H \boldsymbol{u}) \otimes (\mathbb{F}^H \boldsymbol{u}) - \mathbb{F}^H((\mathbb{F}^h \boldsymbol{u}) \otimes (\mathbb{F}^h \boldsymbol{u})) \text{ in } Q \quad (4.9)$$

This expression only involves the filtered velocity fields and does not contain any unfiltered quantity. It was first introduced in [15] and since then has found wide application in determining parameters (denoted by $\boldsymbol{c}$ in our case) in LES models. Note that strictly speaking this relation is valid only for the exact filtered field, which is also unknown during a numerical simulation. However, in typical applications the numerical approximation of the filtered field is used in this relation.

The derivation of the Germano identity described above is simplified by making the assumptions that spatial differentiation and filtering operations commute and that $\mathbb{F}^H \mathbb{F}^h = \mathbb{F}^H$. Neither of these assumptions are typically valid for flows that are inhomogeneous (wall bounded flows for example). For such flows, the assumption of commutativity of differentiation and filtering introduces errors in the modeled equations which can be quite large (see for example [42] and [43]). We are not aware of a filtered form of the Germano identity that accounts for these errors. However filters that minimize these errors have been

proposed (see for example [44]). The assumption $\mathbb{F}^H\mathbb{F}^h = \mathbb{F}^H$ may be avoided altogether by utilizing the composite filter $\mathbb{F}^H\mathbb{F}^h$ in (4.8) instead $\mathbb{F}^H$. Note that the width of this composite filter (denoted by $\bar{H}$) may not equal to H and is determined separately. In this case, (4.9) is replaced by

$$\begin{aligned} \boldsymbol{m}(\mathbb{F}^H\mathbb{F}^h\boldsymbol{u}; \bar{H}, \boldsymbol{c}) - \mathbb{F}^H(\boldsymbol{m}(\mathbb{F}^h\boldsymbol{u}; h, \boldsymbol{c})) &= (\mathbb{F}^H\mathbb{F}^h\boldsymbol{u}) \otimes (\mathbb{F}^H\mathbb{F}^h\boldsymbol{u}) \\ &\quad -\mathbb{F}^H((\mathbb{F}^h\boldsymbol{u}) \otimes (\mathbb{F}^h\boldsymbol{u})) \text{ in } Q. \end{aligned} \tag{4.10}$$

4.4 Variational Germano identity

We now derive the variational form of the Germano identity. Note that even though our derivation mimics the derivation of the filtered version described in the previous section, *it is not restricted to homogeneous flows or uniform meshes.* At every step we will point out the salient differences between the filtered and the variational approaches.

4.4.1 Variational Formulation of LES

We begin with a weak or a variational formulation of the Navier Stokes equations (see [29] for example) given by: Find $\boldsymbol{U}(\cdot, t) = [\boldsymbol{u}(\cdot, t), p(\cdot, t)]^T \in \mathcal{V}$, such that

$$B(\boldsymbol{W}, \boldsymbol{U}) = (\boldsymbol{W}, \boldsymbol{F}), \qquad \forall \boldsymbol{W} = [\boldsymbol{w}, q]^T \in \mathcal{V}, \forall t \in]T_1, T_2[, \tag{4.11}$$

where the semi-linear form $B(\cdot, \cdot)$ and is defined as

$$B(\boldsymbol{W}, \boldsymbol{U}) = (\boldsymbol{w}, \boldsymbol{u}_{,t}) - (\nabla \boldsymbol{w}, \boldsymbol{u} \otimes \boldsymbol{u}) + (\boldsymbol{w}, \nabla p) + 2\nu(\nabla^S \boldsymbol{w}, \nabla^S \boldsymbol{u}) - (\nabla q, \boldsymbol{u}), \tag{4.12}$$

and where

$$(\boldsymbol{W}, \boldsymbol{F}) = (\boldsymbol{w}, \boldsymbol{f}). \tag{4.13}$$

In the equations above $(\cdot, \cdot)$ is used to denote the L_2 inner product in Ω and $\nabla^S \boldsymbol{u} = \frac{1}{2}(\nabla \boldsymbol{u} + \nabla \boldsymbol{u}^T)$.

The infinite dimensional function space $\mathcal{V}$ is defined as

$$\mathcal{V} = \left\{ \boldsymbol{V} = [\boldsymbol{v}, r]^T | \boldsymbol{v} \in H^1(\Omega); r \in L_2(\Omega) \right\}, \tag{4.14}$$

where $H^1(\Omega)$ denotes the Sobolev space of vector-valued functions that are square-integrable and whose derivatives are also square-integrable. This implies that the energy and the enstrophy of the weak solutions remain finite. Also $L_2(\Omega)$ denotes the space of scalar functions that are square-integrable. In addition, we assume that the boundary conditions (though not explicitly stated) are built into the definition of $\mathcal{V}$.

Let $\mathcal{V}^h \subset \mathcal{V}$ be a finite dimensional subspace. The Galerkin method when applied to (4.11) yields the following equation for the approximate solution $\boldsymbol{U}^h$. Find $\boldsymbol{U}^h(\cdot, t) \in \mathcal{V}^h$, such that

$$B(\boldsymbol{W}^h, \boldsymbol{U}^h) = (\boldsymbol{W}^h, \boldsymbol{F}), \qquad \forall \boldsymbol{W}^h \in \mathcal{V}^h, \forall t \in]T_1, T_2[. \tag{4.15}$$

Remarks

1. Since $\mathcal{V}^h$ is a subspace of $\mathcal{V}$, (4.11) implies that the exact solution $\boldsymbol{U}$ satisfies
$$B(\boldsymbol{W}^h, \boldsymbol{U}) = (\boldsymbol{W}^h, \boldsymbol{F}), \qquad \forall \boldsymbol{W}^h \in \mathcal{V}^h, \forall t \in]T_1, T_2[. \tag{4.16}$$
2. The Galerkin solution essentially corresponds to a Direct Numerical Simulation (DNS) solution of the original problem. If the space $\mathcal{V}^h$ is incapable of representing the large inertial scales of motion as well as the fine dissipative scales, then this solution is inaccurate. It may be improved upon by adding a model term to the terms that appear in the Galerkin approximation.

The addition of a model term to the Galerkin approximation leads to the following variational equation : Find $\boldsymbol{U}^h(\cdot, t) \in \mathcal{V}^h$, such that
$$B(\boldsymbol{W}^h, \boldsymbol{U}^h) + M(\boldsymbol{W}^h, \boldsymbol{U}^h; h, \boldsymbol{c}) = (\boldsymbol{W}^h, \boldsymbol{F}), \qquad \forall \boldsymbol{W}^h \in \mathcal{V}^h, \forall t \in]T_1, T_2[. \tag{4.17}$$
In (4.17), $M(\boldsymbol{W}^h, \boldsymbol{U}^h; h, \boldsymbol{c})$ is the model term that is linear in $\boldsymbol{W}^h$ and non-linear in $\boldsymbol{U}^h$. It also depends on the mesh size h and a vector of parameters $\boldsymbol{c}$. The equation above is the variational counterpart of (4.6). Also note that due to the presence of the model term, the solution of (4.17) and the Galerkin solution are distinct.

We now introduce the concept of an optimal solution in the space $\mathcal{V}^h$. For this we define a *restriction operator* $\mathbb{P}^h : \mathcal{V} \to \mathcal{V}^h$, such that $\mathbb{P}^h \boldsymbol{U} \in \mathcal{V}^h$ is the optimal representation of $\boldsymbol{U}$ in $\mathcal{V}^h$. For example, $\mathbb{P}^h \boldsymbol{U}$ may be the nodal interpolant or a suitable projection (L_2 or H^1 in our case) of $\boldsymbol{U}$ in $\mathcal{V}^h$, in which case $\mathbb{P}^h$ will be the interpolation or the projection operator, respectively. We would like to select our model term in (4.17) such that the solution $\boldsymbol{U}^h$ is optimal. Thus requiring $\boldsymbol{U}^h = \mathbb{P}^h \boldsymbol{U}$ in (4.17) we have
$$M(\boldsymbol{W}^h, \mathbb{P}^h \boldsymbol{U}; h, \boldsymbol{c}) = (\boldsymbol{W}^h, \boldsymbol{F}) - B(\boldsymbol{W}^h, \mathbb{P}^h \boldsymbol{U}), \qquad \forall \boldsymbol{W}^h \in \mathcal{V}^h, \forall t \in]T_1, T_2[. \tag{4.18}$$
Using (4.16) in (4.18) we arrive at
$$M(\boldsymbol{W}^h, \mathbb{P}^h \boldsymbol{U}; h, \boldsymbol{c}) = B(\boldsymbol{W}^h, \boldsymbol{U}) - B(\boldsymbol{W}^h, \mathbb{P}^h \boldsymbol{U}), \qquad \forall \boldsymbol{W}^h \in \mathcal{V}^h, \forall t \in]T_1, T_2[. \tag{4.19}$$
This equation defines the model required to generate the optimal solution. By comparing the definition of the ideal model in the variational context (4.19) with its counterpart in the filtered approach (4.7) we find:

1. In the filtered case only the *non-linear* terms in the Navier Stokes equations contribute to the definition of the ideal model. In the variational case every term in the semi-linear form contributes.

2. In the filtered case it is assumed that for the ideal model, (4.7) is satisfied pointwise. Thus the residual of (4.7) when multiplied with any weighting function and integrated over Ω is equal to zero. In contrast to this (4.19) holds only for weighting functions contained in $\mathcal{V}^h$. Thus the constraint on the model term in the variational case is weaker. In particular, in the variational case *the effect of the model on weighting functions outside of $\mathcal{V}^h$ is irrelevant.*

3. In the filtered case the model term is a *tensor*. In the variational case it appears in the weak form just as a *vector* would appear.

These differences in the definition of the ideal model in the variational and filtered approaches are important and will *lead to different forms of the Germano identity.*

4.4.2 The variational Germano Identity

Next we consider another function space $\mathcal{V}^H$ such that $\mathcal{V}^H \subset \mathcal{V}^h \subset \mathcal{V}$. We also define a restriction operator $\mathbb{P}^H$ such that $\mathbb{P}^H : \mathcal{V} \to \mathcal{V}^H$ and $\mathbb{P}^H \boldsymbol{U} \in \mathcal{V}^H$ is the optimal representation of $\boldsymbol{U}$ in $\mathcal{V}^H$. We assume that the operators $\mathbb{P}^h$ and $\mathbb{P}^H$ are related and hence the same form of the model term yields optimal solutions in $\mathcal{V}^h$ and $\mathcal{V}^H$. The finite dimensional, modeled variational equation for this space is given by: Find $\boldsymbol{U}^H(\cdot, t) \in \mathcal{V}^H$, such that

$$B(\boldsymbol{W}^H, \boldsymbol{U}^H) + M(\boldsymbol{W}^H, \boldsymbol{U}^H; H, \boldsymbol{c}) = (\boldsymbol{W}^H, \boldsymbol{F}), \qquad \forall \boldsymbol{W}^H \in \mathcal{V}^H, \forall t \in]T_1, T_2[, \quad (4.20)$$

where the same vector of parameters appears in (4.20) and (4.17). Hence the model that yields the optimal solution $\boldsymbol{U}^H = \mathbb{P}^H \boldsymbol{U}$, satisfies

$$M(\boldsymbol{W}^H, \mathbb{P}^H \boldsymbol{U}; H, \boldsymbol{c}) = B(\boldsymbol{W}^H, \boldsymbol{U}) - B(\boldsymbol{W}^H, \mathbb{P}^H \boldsymbol{U}), \qquad \forall \boldsymbol{W}^H \in \mathcal{V}^H, \forall t \in]T_1, T_2[. \quad (4.21)$$

Returning to (4.19), we note that it holds for all $\boldsymbol{W}^h \in \mathcal{V}^h$, and hence is also valid for all $\boldsymbol{W}^H \in \mathcal{V}^H$. Thus we have

$$M(\boldsymbol{W}^H, \mathbb{P}^h \boldsymbol{U}; h, \boldsymbol{c}) = B(\boldsymbol{W}^H, \boldsymbol{U}) - B(\boldsymbol{W}^H, \mathbb{P}^h \boldsymbol{U}), \qquad \forall \boldsymbol{W}^H \in \mathcal{V}^H, \forall t \in]T_1, T_2[. \quad (4.22)$$

Subtracting (4.22) from (4.21) we arrive at

$$\begin{aligned} M(\boldsymbol{W}^H, \mathbb{P}^H \boldsymbol{U}; H, \boldsymbol{c}) - M(\boldsymbol{W}^H, \mathbb{P}^h \boldsymbol{U}; h, \boldsymbol{c}) \;&=\; B(\boldsymbol{W}^H, \mathbb{P}^h \boldsymbol{U}) - B(\boldsymbol{W}^H, \mathbb{P}^H \boldsymbol{U}), \\ &\qquad \forall \boldsymbol{W}^H \in \mathcal{V}^H, \forall t \in]T_1, T_2[. \quad (4.23) \end{aligned}$$

In addition if the restriction operators are such that

$$\mathbb{P}^H = \mathbb{P}^H \mathbb{P}^h, \quad (4.24)$$

then $\mathbb{P}^H \boldsymbol{U} = \mathbb{P}^H (\mathbb{P}^h \boldsymbol{U})$ and (4.23) reduces to

$$\begin{aligned} M(\boldsymbol{W}^H, \mathbb{P}^H (\mathbb{P}^h \boldsymbol{U}); H, \boldsymbol{c}) - M(\boldsymbol{W}^H, \mathbb{P}^h \boldsymbol{U}; h, \boldsymbol{c}) \;&=\; B(\boldsymbol{W}^H, \mathbb{P}^h \boldsymbol{U}) - B(\boldsymbol{W}^H, \mathbb{P}^H (\mathbb{P}^h \boldsymbol{U})), \\ &\qquad \forall \boldsymbol{W}^H \in \mathcal{V}^H, \forall t \in]T_1, T_2[. \quad (4.25) \end{aligned}$$

Equation (4.25) is the *variational counterpart of the Germano identity.* It involves only the optimal solution $\mathbb{P}^h \boldsymbol{U}$ in the space $\mathcal{V}^h$. It is easy to verify that the condition (4.24) holds for several restriction operators including L^2 or H^1 projectors and interpolation operators.

At this stage it is instructive to compare this equation with its filtered counterpart (4.9).

1. In the filtered case only the *non-linear* terms contribute to the right hand side of the Germano identity. In the variational case every term contributes.

2. In the filtered case it is assumed that the Germano identity is satisfied pointwise, thus when the residual of (4.9) is multiplied by any weighting function and integrated over Ω, the result is zero. In contrast to this (4.19) holds only for weighting functions contained in $\mathcal{V}^H$, indicating that there is less usable information in the variational Germano identity. This is direct consequence of the fact that fewer constraints are placed on the model term in the variational approach than in the filtered approach.

3. In the filtered case the Germano identity is a tensor relation. In the variational case it is a weak form of a vector equation. It this aspect the variational Germano identity is closer to the vector level identity studied in [45].

It is easy to see that the differences described above can be traced back to differences in the definition of the ideal model term in the variational and filtered cases.

While utilizing this identity in a numerical method we will replace $\mathbb{P}^h\boldsymbol{U}$ with the numerical solution $\boldsymbol{U}^h$. In that case the modeled system is given by (4.17) and

$$M(\boldsymbol{W}^H, \mathbb{P}^H\boldsymbol{U}^h; H, \boldsymbol{c}) - M(\boldsymbol{W}^H, \boldsymbol{U}^h; h, \boldsymbol{c}) = B(\boldsymbol{W}^H, \boldsymbol{U}^h) - B(\boldsymbol{W}^H, \mathbb{P}^H\boldsymbol{U}^h), \quad \forall \boldsymbol{W}^H \in \mathcal{V}^H, \forall t \in]T_1, T_2[. \quad (4.26)$$

The equation above may then be used to determine the parameters $\boldsymbol{c}$ in the model term. This modeled system, that is (4.17) and (4.26), has the following special property: *If (4.24) holds, then it permits as its solution the optimal solutions $\mathbb{P}^h\boldsymbol{U}$ and $\mathbb{P}^H\boldsymbol{U}$ on the spaces $\mathcal{V}^h$ and $\mathcal{V}^H$ respectively.*

Equation (4.26) represents as many equations as the dimension of $\mathcal{V}^H$. Very often the number of parameters to be determined (that is the number of components of $\boldsymbol{c}$) is much smaller than this number. Motivated by what is done in the traditional dynamic models, we propose the following methods to reduce the dimension of these equations.

Dissipation method This method is motivated by the approach described in [15] for the filter-based Germano identity. It involves setting $\boldsymbol{W}^H = \mathbb{P}^H\boldsymbol{U}^h$ in (4.26) to arrive at

$$M(\mathbb{P}^H\boldsymbol{U}^h, \mathbb{P}^H\boldsymbol{U}^h; H, \boldsymbol{c}) - M(\mathbb{P}^H\boldsymbol{U}^h, \boldsymbol{U}^h; h, \boldsymbol{c}) = B(\mathbb{P}^H\boldsymbol{U}^h, \boldsymbol{U}^h) - B(\mathbb{P}^H\boldsymbol{U}^h, \mathbb{P}^H\boldsymbol{U}^h), \quad \forall t \in]T_1, T_2[. \quad (4.27)$$

The equation above represents a scalar relation that may be used to determine a *single* parameter in the model.

Least squares method This method is based on the approach developed in [27] for the filter-based Germano identity. In this case we set $\boldsymbol{W}^H = \boldsymbol{\phi}_A$, $A = 1, \cdots, \dim(\mathcal{V}^h)$, to arrive at

$$M(\boldsymbol{\phi}_A, \mathbb{P}^H\boldsymbol{U}^h; H, \boldsymbol{c}) - M(\boldsymbol{\phi}_A, \boldsymbol{U}^h; h, \boldsymbol{c}) = B(\boldsymbol{\phi}_A, \boldsymbol{U}^h) - B(\boldsymbol{\phi}_A, \mathbb{P}^H\boldsymbol{U}^h), \quad A = 1, \cdots, \dim(\mathcal{V}^h), \forall t \in]T_1, T_2[\quad (4.28)$$

Thereafter we evaluate the $\boldsymbol{c}$ that minimizes the sum of the square of the residual of (4.28) for each A.

4.5 Decay of Homogeneous Isotropic Turbulence

In this section we apply the variational Germano identity to calculate the time-dependent viscosity parameter for the Smagorinsky model during the decay of homogeneous isotropic turbulence.

The strong form of the problem is given by (4.1) & (4.3), where $\Omega =]0, L[^3$ and its boundary comprises of six faces, $\Gamma_j(0)$, $\Gamma_j(L)$, $j = 1, 2, 3$, where

$$\Gamma_j(c) = \{\boldsymbol{x} \in \partial\Omega \mid x_j = c\} \tag{4.29}$$

It is assumed the boundary conditions are periodic, that is

$$\boldsymbol{u}(\boldsymbol{x} + L\boldsymbol{e}_j, t) = \boldsymbol{u}(\boldsymbol{x}, t), \quad \boldsymbol{x} \in \Gamma_j(0), \quad t \in]T_1, T_2[\tag{4.30}$$

where $\boldsymbol{e}_j$ is the Cartesian basis vector in the x_j direction.

The equivalent weak form is given by (4.11). We solve this problem using a Fourier-spectral discretization. The space of weak solutions and weighting functions, $\mathcal{V}$, is given by

$$\mathcal{V} = \Big\{ \boldsymbol{V} \mid \boldsymbol{V} = \sum_{(L\boldsymbol{k}/2\pi)\in\mathbb{Z}^3} \hat{\boldsymbol{V}}_{\boldsymbol{k}} e^{i\boldsymbol{k}\cdot\boldsymbol{x}};\ \hat{\boldsymbol{V}}^*_{-\boldsymbol{k}} = \hat{\boldsymbol{V}}_{\boldsymbol{k}};$$
$$\sum_{(L\boldsymbol{k}/2\pi)\in\mathbb{Z}^3} |\hat{\boldsymbol{v}}_{\boldsymbol{k}}|^2(1 + |\boldsymbol{k}|^2) < \infty;\ \sum_{(L\boldsymbol{k}/2\pi)\in\mathbb{Z}^3} |\hat{r}_{\boldsymbol{k}}|^2 < \infty \Big\}. \tag{4.31}$$

In the equation above, $\hat{\boldsymbol{V}}_{\boldsymbol{k}}$ are the Fourier-coefficients of $\boldsymbol{V}$ for a given wave-vector $\boldsymbol{k}$, the superscript $*$ denotes the complex-conjugate of a quantity and for a vector $\boldsymbol{s}$, $|\boldsymbol{s}| \equiv \sqrt{\boldsymbol{s}^* \cdot \boldsymbol{s}}$. The terms within the curly brackets imply that velocity fields contained in $\mathcal{V}$ are real-valued and belong to $H^1(\Omega)$ (the energy and the enstrophy of the flow are finite for $t \in]T_1, T_2[$), and that the pressure is real-valued and square integrable. Note that the periodic boundary conditions are also built into the definition of $\mathcal{V}$.

The modeled system of equations is given by (4.17), where the finite dimensional space is given by

$$\mathcal{V}^h = \{\boldsymbol{V} \in \mathcal{V}; \hat{\boldsymbol{V}}_{\boldsymbol{k}} = \boldsymbol{0}, |\boldsymbol{k}| > k^h\} \tag{4.32}$$

and the model term, which represents the Smagorinsky eddy viscosity model [30], is given by

$$M(\boldsymbol{W}^h, \boldsymbol{U}^h; h, c) = 2(c_1 h)^2(\nabla^S \boldsymbol{w}^h, |\nabla^S \boldsymbol{u}^h| \nabla^S \boldsymbol{u}^h). \tag{4.33}$$

Note that in (4.32), $|\boldsymbol{k}| = \sqrt{\boldsymbol{k}^* \cdot \boldsymbol{k}}$. The unknown parameter c_1 in the Smagorinsky model is to be determined using the variational Germano identity. It is assumed that c_1 is independent of the spatial coordinate $\boldsymbol{x}$, and varies only in time. We consider the use of the dissipation method (4.27) and the least squares method (4.28) in determining this parameter. In order to utilize these relations we first define the space $\mathcal{V}^H$ and the restriction operator $\mathbb{P}^H$. Following (4.32) we have

$$\mathcal{V}^H = \{\boldsymbol{V} \in \mathcal{V}; \hat{\boldsymbol{V}}_{\boldsymbol{k}} = \boldsymbol{0}, |\boldsymbol{k}| > k^H\}, \tag{4.34}$$

where $H > h$ and $k^H < k^h$. We select $\mathbb{P}^H$ to be the L_2 projector of $\mathcal{V}$ into $\mathcal{V}^H$. Thus $\mathbb{P}^H \boldsymbol{V}$, where $\boldsymbol{V} \in \mathcal{V}$, is given by

$$(\boldsymbol{W}^H, \mathbb{P}^H \boldsymbol{V}) = (\boldsymbol{W}^H, \boldsymbol{V}), \quad \forall \boldsymbol{W}^H \in \mathcal{V}^H. \tag{4.35}$$

Using (4.34) and the orthogonality of the Fourier modes in Ω, from the above equation we have

$$\mathbb{P}^H \boldsymbol{V} = \sum_{|\boldsymbol{k}| \leq k^H} \hat{\boldsymbol{V}}_{\boldsymbol{k}} e^{i\boldsymbol{k}\cdot\boldsymbol{x}} = \mathbb{F}^H \boldsymbol{V}, \tag{4.36}$$

where $\mathbb{F}^H$ represents a sharp cut-off filter in the wavenumber space. Note that while the operation of $\mathbb{P}^H$ is defined only on elements of $\mathcal{V}$, $\mathbb{F}^H$ may operate on any scalar, vector or tensor with a finite L_2 norm.

We are also interested in comparing the expressions for the Smagorinsky parameter obtained using the variational counterpart of the Germano identity with those obtained from the filtered version of this identity. In order to be consistent in this comparison we choose the filtering operator to be the sharp cut-off filter in wavenumber space.

Dissipation method We are now in a position to estimate the Smagorinsky parameter. We first consider the dissipation method applied to the variational Germano identity. Using (4.33), (4.12) and (4.36) in (4.27) we arrive at

$$c_1 = \sqrt{\frac{1}{2}\frac{(\boldsymbol{S}^H, \boldsymbol{u}^H \otimes \boldsymbol{u}^H) - (\boldsymbol{S}^H, \boldsymbol{u}^h \otimes \boldsymbol{u}^h)}{H^2(\boldsymbol{S}^H, |\boldsymbol{S}^H|\boldsymbol{S}^H) - h^2(\boldsymbol{S}^H, |\boldsymbol{S}^h|\boldsymbol{S}^h)}}, \forall t \in]T_1, T_2[, \tag{4.37}$$

where $\boldsymbol{u}^H = \mathbb{F}^H \boldsymbol{u}^h$, $\boldsymbol{S}^h = \nabla^S \boldsymbol{u}^h$ and $\boldsymbol{S}^H = \nabla^S \boldsymbol{u}^H$. In deriving the above relation we have made use of the L_2 orthogonality of Fourier modes to eliminate all the bilinear terms in (4.27).

The dissipation method when applied to filtered form of the Germano identity yields (see for example [15]),

$$c_1 = \sqrt{\frac{1}{2}\frac{(\boldsymbol{S}^h, \boldsymbol{u}^H \otimes \boldsymbol{u}^H) - (\boldsymbol{S}^H, \boldsymbol{u}^h \otimes \boldsymbol{u}^h)}{H^2(\boldsymbol{S}^h, |\boldsymbol{S}^H|\boldsymbol{S}^H) - h^2(\boldsymbol{S}^H, |\boldsymbol{S}^h|\boldsymbol{S}^h)}}, \forall t \in]T_1, T_2[. \tag{4.38}$$

In comparing (4.37) and (4.38) the following observations may be made:

1. For both the variational and the filtered approach ((4.37) and (4.38), respectively) the contribution from the linear terms on the right hand side of the Germano identity to the numerator in the expression for c_1, is zero. In the filtered case, this is a consequence of the Germano identity itself, whereas in the variational case this is due to the special orthogonal properties of the basis functions and the restriction operator.

2. The first term in the numerator and the denominator of the variational equation (4.37) contains $\boldsymbol{S}^H$ in the weighting function slot, which is replaced by $\boldsymbol{S}^h$ in the filtered equation (4.38). This is the only difference between these two expressions and it is a direct consequence of the fact that in the variational case constraints are imposed on the ideal model only for weighting functions contained in a finite dimensional subspace, whereas in the filtered case constraints are imposed for all weighting functions.

3. The fact that the filtered Germano identity represents a tensor relation and the variational Germano identity represents a vector relation, does not lead to any differences in the final expression for c_1 when using the dissipation method. This is because in the filtered case, when using the dissipation method, the equation for c_1 is obtained by contracting the Germano identity with the rate of strain tensor and integrating the resulting scalar equation over Ω. Using integration by parts it can be shown that this is identical to contracting the divergence of the filtered Germano identity with the velocity field and integrating the resulting scalar equation in Ω, which in turn amounts to interpreting the Germano identity as a vector relation.

Least squares method In order to estimate c_1 using the least squares method applied to the variational form of the Germano identity we set

$$\boldsymbol{W}^H = \boldsymbol{e}_j e^{-i\boldsymbol{k}\cdot\boldsymbol{x}}, \quad j = 1,2,3,4; |\boldsymbol{k}| < k^H, \tag{4.39}$$

in (4.26) and then use (4.33), (4.12), (4.36) and the L_2 orthogonality of Fourier modes to arrive at

$$2c_1^2 \mathbb{F}^H \nabla \cdot \mathcal{M} = \mathbb{F}^H \nabla \cdot \mathcal{N}, \quad \forall t \in]T_1, T_2[. \tag{4.40}$$

where

$$\mathcal{M} = h^2 |\boldsymbol{S}^h| \boldsymbol{S}^h - H^2 |\boldsymbol{S}^H| \boldsymbol{S}^H, \tag{4.41}$$
$$\mathcal{N} = \boldsymbol{u}^h \otimes \boldsymbol{u}^h - \boldsymbol{u}^H \otimes \boldsymbol{u}^H, \tag{4.42}$$

and as before $\boldsymbol{u}^H = \mathbb{F}^H \boldsymbol{u}^h$, $\boldsymbol{S}^h = \nabla^S \boldsymbol{u}^h$ and $\boldsymbol{S}^H = \nabla^S \boldsymbol{u}^H$. Selecting c_1 such that sum of the squares of the residual of (4.40) is minimized, we arrive at

$$c_1 = \sqrt{\frac{1}{2} \frac{(\mathbb{F}^H \nabla \cdot \mathcal{N}, \mathbb{F}^H \nabla \cdot \mathcal{M})}{(\mathbb{F}^H \nabla \cdot \mathcal{M}, \mathbb{F}^H \nabla \cdot \mathcal{M})}}, \forall t \in]T_1, T_2[. \tag{4.43}$$

The least squares approach when applied to the filtered from of the Germano identity yields (see [27])

$$c_1 = \sqrt{\frac{1}{2} \frac{(\mathcal{N}, \mathcal{M})}{(\mathcal{M}, \mathcal{M})}}, \forall t \in]T_1, T_2[, \tag{4.44}$$

where

$$\mathcal{M} = \mathbb{F}^H (h^2 |\boldsymbol{S}^h| \boldsymbol{S}^h) - H^2 |\boldsymbol{S}^H| \boldsymbol{S}^H, \tag{4.45}$$
$$\mathcal{N} = \mathbb{F}^H (\boldsymbol{u}^h \otimes \boldsymbol{u}^h) - \boldsymbol{u}^H \otimes \boldsymbol{u}^H. \tag{4.46}$$

In comparing the expressions for the parameter derived using the variational and the filtered versions of the least squares approach, that is (4.43) and (4.44), the following observations may be made:

1. In this case also for both the variational and the filtered approaches the contribution from the linear terms to the Germano identity is zero. In the filtered case, this is a consequence of the identity itself, whereas in the variational case this is due to the properties of the basis functions and the restriction operator.

2. The definitions of $\mathcal{N}$ and $\mathcal{M}$ for the variational and filtered cases are similar. However, in the variational case in equation (4.43), these tensors are operated upon by the sharp cut-off filter $\mathbb{F}^H$, whereas in the filtered case ((4.45) & (4.46)), $\mathbb{F}^H$ acts on only one term in these tensors. This difference may be traced back to the observation that in the variational approach the ideal model is constrained to satisfy a given relation only for a finite subset of weighting functions, whereas in the filtered case it is required to satisfy the relation for every weighting function.

3. The inner products that appear in the definition of c_1 in the variational case (4.43) involve the divergence of the tensors $\mathcal{N}$ and $\mathcal{M}$, whereas in the filtered case (4.44) they involve the tensors themselves. This is because the expression for the ideal model and the Germano identity are vector relations in the variational case, whereas they are tensor relations in the filtered case.

4.6 Numerical Examples

In this section we evaluate the performance of the variational Germano identity in predicting the time dependent Smagorinsky constant during the large eddy simulation of the decay of homogeneous isotropic turbulence. We compare the following methods:

1. The Dynamic Smagorinsky method, where the Smagorinsky parameter c_1 is obtained using the dissipation method applied to the variational Germano identity (4.37).

2. The Dynamic Smagorinsky method with the least squares form of the variational Germano identity (4.43).

3. The Dynamic Smagorinsky method with the dissipation form of the filtered Germano identity (4.38).

4. The Dynamic Smagorinsky method with the least squares form of the filtered Germano identity (4.44).

In the first problem we consider the decay of turbulence from a Taylor micro-scale Reynolds number (Re_λ) of 90 to about 60 and compare the LES solutions to a benchmark DNS calculation. In the second problem Re_λ decays from 716 to 626 and we compare the LES results with experimental data. In both cases we perform the simulations using a Fourier-spectral code. We advance in time using a third-order Runge-Kutta scheme. The nonlinear terms (convective acceleration term and the model term) are evaluated on a grid of size $(3N/2)^3$. The effect of molecular viscosity is accounted for exactly by utilizing an appropriate integrating factor for each ODE [33].

4.6.1 $Re_\lambda = 90$

We compute the DNS solution with 256^3 modes. For this solution we use a random initial condition with an energy spectrum given by $E(k) = (q^2/2A)(k^4/k_p^5)\exp(-2(k/k_p)^2)$, where the initial turbulent kinetic energy, $\frac{q^2}{2} = \frac{3}{2}$, and the spectrum is peaked at $k_p = 3$. The length of the side of the cube, $L = 2\pi$ and the kinematic viscosity $\nu = 0.005$. The same spectrum was used in [31] to study the decay of low Reynolds number homogeneous isotropic turbulence. The phase of the modes for the initial velocity field is chosen randomly and each mode satisfies the divergence-free condition. The solution is allowed to evolve according to the Navier-Stokes equations till a spectra with a physical $k^{-5/3}$ range is obtained at $t = T_1 \approx 2.2$. The evolution of the kinetic energy on a cross-section of the 256^3 DNS is shown in the video clip. The animation starts from the random initial condition and ends at $t = T_1$. At this instant the Taylor-microscale Reynolds number is ≈ 90. This velocity field is used as an initial condition for all LES calculations, which are performed with $k^h/(2\pi/L) = 32$ and $k^h/k^H = 2$. The DNS and LES solutions are evolved till $t = T_2 = 3$ which corresponds to $Re_\lambda = 60$ and the results compared.

In Figure 4.1, we have plotted the variation of the Smagorinsky parameter c_1 as a function of time for the LES methods. We observe that coefficient predicted by the filtered dissipation approach is much higher than all the other coefficients. The coefficient predicted by the filtered least squares approach is smaller than the dissipation approach. We also observe that the coefficient predicted by the variational dissipation approach is very close to the filtered least squares approach and that the coefficients predicted by the two variational methods (dissipation and least squares) are closer to each other when compared to the coefficients predicted by the two filtered methods.

It is worth pointing out that all the LES methods considered here differ from each other only in the way the Smagorinsky parameter is evaluated. Hence the differences observed in the values of this parameter are solely responsible for any difference in the final solutions.

In Figure 4.2, we have plotted the variation of the total resolved kinetic energy ($|\boldsymbol{k}| \leq 32$) for the benchmark DNS solution and the LES solutions as a function of time. We observe that to begin with all the models are overly dissipative. However they improve with time. We also observe that the filtered dissipation approach, which attains the largest viscosity (see Figure 4.1), is the most dissipative, whereas the performance of all the other methods is virtually indistinguishable.

In Figure 4.3, we compare the energy spectra at $t = T_2 = 3$. We observe that all the methods under-predict the energy in the fine scale modes. This in turn, lowers the transfer of energy from the coarse scale modes to the fine scale modes leading to an over-prediction of the energy in the coarse scale modes. We observe that the method with the largest value of the Smagorinsky parameter, namely the filtered dissipation approach, is the least accurate, whereas the one with the smallest parameter, the filtered least squares approach is the most accurate. The variational dissipation approach yields results that are very similar to the filtered least squares approach, whereas the variational least squares is somewhat more inaccurate (though not as inaccurate as the filtered dissipation approach).

4.6.2 $Re_\lambda = 716$

In this section we compare the performance of the LES methods at a higher value of Reynolds number. We utilize the experiment reported in [46] as the benchmark solution. In our simulations, the length of the side of the cube $L = 5.12$, the kinematic viscosity $\nu = 1.5074 \times 10^{-4}$ and the initial spectra is given by equation (6) in [46]. A divergence-free velocity field with random phases is used to initialize all LES calculations which are performed with $k^h/(2\pi/L) = 32$ and $k^h/k^H = 2$. The LES calculations are allowed to evolve till $t = 0.1267$, when correlations between the velocity coefficients across different modes have been established and the Smagorinsky parameters predicted by the various dynamic procedures have attained a steady non-zero value. The velocity field is then rescaled so that the spectra attains its original value. This velocity field is used initial condition for the LES simulations. Using this approach the effect of the transient associated with the Smagorinsky parameter starting from zero (due to random phases) is eliminated.

In Figure 4.4, we have plotted the variation of the Smagorinsky coefficient as a function of time. Note that in this figure time is measured in the x/M units used in [46]. We note that when compared with Figure 4.1, the values of the parameters in this figure are generally higher. This may be attributed to a more extensive inertial range for the simulation reported in Figure 4.4. We also observe that as before the filtered dissipation approach predicts the largest value of the Smagorinsky parameter and the filtered least squares approach predicts the smallest value. The variational methods predict values that are very close to each other. These value are closer to the value for filtered least squares approach than to the filtered dissipation approach.

In Figure 4.5, we have plotted the Energy spectra at $t = T_2 = 0.506$ for the LES simulations and the experimental result. This time corresponds to $x/M = 48$ in Kang et al's experiment. We observe that the filtered dissipation approach has significantly under-predicted the spectra at high wavenumbers. On the other hand, the filtered least squares approach is somewhat under-dissipative leading to a slight pile-up of energy at high wavenumbers. The results for the two variational methods (dissipation and least squares) lie in between the two filtered methods and are about as accurate as the filtered least squares method.

4.6.3 Summary and explanation of numerical results

Based on the results presented in this section (at $Re_\lambda = 90$ and 716) the following comments may be made regarding the variational and the filtered forms of the Germano identity.

1. The variational form yields values of parameters that are less sensitive to the method utilized in calculating them (dissipation or least squares).

2. The dissipation approach is observed to yield accurate results in the variational case, whereas in the filtered case it is overly dissipative.

3. The results for the variational dissipation approach are about as accurate as that of the filtered least squares approach. However the costs associated with implementing this approach are lower. Thus it may represent a new, easier method for evaluating a "more accurate" Smagorinsky parameter.

From the numerical results presented in the previous section we observe that the value of the Smagorinsky parameter calculated using the filtered dissipation approach is the highest. We now provide an explanation for this. We conduct an *a-priori* analysis using the DNS field at $Re_\lambda = 90$. We compare the expression for the filtered dissipation approach with its variational counterpart. The difference between the numerators in these two expressions is given by

$$(\boldsymbol{S}^h - \boldsymbol{S}^H, \boldsymbol{u}^H \otimes \boldsymbol{u}^H) = \int_{k^H}^{k^h} T_n(k) dk \tag{4.47}$$

where

$$T_n(k) = -\int_{\Gamma_k} \hat{\boldsymbol{u}}^*_{\boldsymbol{k}} \cdot \mathrm{FT}[\nabla \cdot (\boldsymbol{u}^H \otimes \boldsymbol{u}^H)]_{\boldsymbol{k}} d\Gamma_k. \tag{4.48}$$

and $k = |\boldsymbol{k}|$. In the integral above, Γ_k denotes the surface of a sphere of radius k in the wavenumber space. Similarly, the difference between the denominator in (4.38) and (4.37) is given by

$$(\boldsymbol{S}^h - \boldsymbol{S}^H, |\boldsymbol{S}^H|\boldsymbol{S}^H) = \int_{k^H}^{k^h} T_d(k) dk \tag{4.49}$$

where

$$T_d(k) = -\int_{\Gamma_k} \hat{\boldsymbol{u}}^*_{\boldsymbol{k}} \cdot \mathrm{FT}[\nabla \cdot (|\boldsymbol{S}^H|\boldsymbol{S}^H)]_{\boldsymbol{k}} d\Gamma_k. \tag{4.50}$$

In Figure 4.6, we have plotted T_n and T_d, scaled by their maximum values, as a function of k. We observe that T_d rapidly drops to zero beyond k^H. As a result the denominators in the expressions for c_1 for the filtered and the variational dissipation approach are about the same. On the other hand, the decay in T_n is much more gradual and the numerator for the filtered approach is substantially larger. This leads to a larger value of c_1 for the filtered formulation.

It is worth noting that the cause of this discrepancy between the filtered and the variational formulations is the difference in the definition of an ideal model. In the filtered formulation, an ideal model is assumed to represent the subgrid term pointwise, that is for all weighting functions. *This leads to a Germano identity wherein contribution from a model applied at a cutoff wavenumber of k^H, to modes greater than k^H, is also included.* This is not the case for the variational formulation. In this case an ideal model represents the effect of the subgrid terms only on a select number of weighting functions with wavenumbers smaller than the cutoff wavenumber. As a result there are no terms in the Germano identity which contain the effect of the model beyond the cutoff wavenumber. We note that this difference between these two approaches is present for all flows and will carry over to more complex, inhomogeneous flows.

For the least squares approach, we observe that the difference in the Smagorinsky parameter evaluated using the filtered and the variational formulations is smaller. This is remarkable considering that the terms responsible for the differences observed in the

dissipation approach, are also present in the least squares approach ($\boldsymbol{u}^H \otimes \boldsymbol{u}^H$ in the numerator of the filtered formulation versus $\mathbb{F}^H(\boldsymbol{u}^H \otimes \boldsymbol{u}^H)$ in the numerator of the variational formulation). However there is one crucial difference. The numerators in the least squares approach contain the inner product of these terms with "other" terms, whose Fourier coefficients beyond k^H have been verified to be either very small (for the filtered formulation) or identically zero (for the variational formulation). As a result, in this case, the differences in $\boldsymbol{u}^H \otimes \boldsymbol{u}^H$ and $\mathbb{F}^H(\boldsymbol{u}^H \otimes \boldsymbol{u}^H)$ beyond k^H do not play a significant role determining the Smagorinsky parameter.

It is important to bear in mind that in the least squares approach, the divergence operator, which is present in the variational formulation and absent from the dissipation formulation is another source of differences. The precise effect of this operator on the Smagorinsky parameter will be investigated in the future.

4.7 Conclusions

In this chapter we have derived the variational counterpart of the Germano identity for the incompressible Navier-Stokes equations. This identity provides a means of determining model parameters within the variational formulation of LES and is analogous to the Germano identity derived in [15] for the filter-based LES formulation. We have identified the following differences among the variational and the filtered versions of the Germano identity and traced their origin to differences in the definition of an ideal model in the two cases:

1. Linear terms in the Navier-Stokes equations contribute to the variational formulation and not to the filter-based formulation.

2. The variational formulation holds only for a finite dimensional space of weighting functions, whereas the filter-based formulation holds pointwise.

3. The variational formulation is essentially a vector relation, while the filter-based formulation is a tensor relation.

In light of the third point above, we have noted that the variational Germano identity is similar to (though not the same as) the vector-level Germano identity discussed in [45].

We have applied the variational Germano identity to determine the Smagorinsky parameter in the decay of homogeneous isotropic turbulence and compared its performance with the filter-based formulation. We have found it to be accurate and robust, in that the value of the parameter is less sensitive to the exact approach (dissipation or least-squares) used in evaluating it. The example described in this chapter represents an initial result of the application of the variational Germano identity. Other interesting applications to be pursued in the future include determining multiscale parameters in the variational multiscale formulation and determining parameters in cases (such as when using the finite element method) where contributions from linear terms are non-zero.

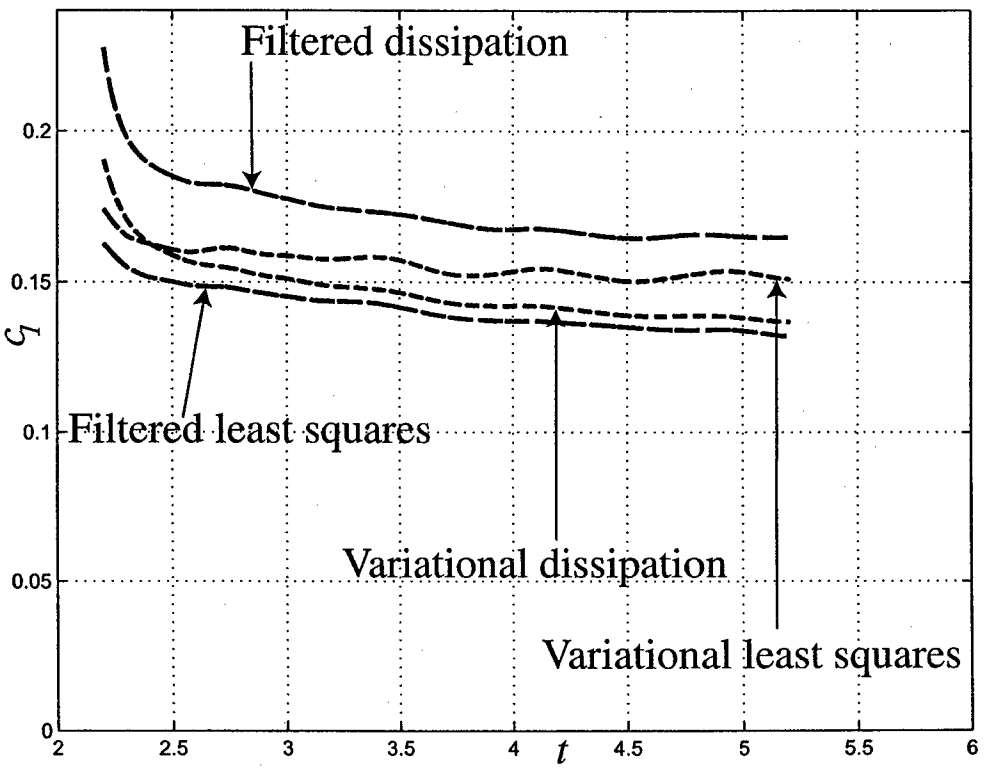

Figure 4.1: Variation of the Smagorinsky parameter c_1 with time for the low Reynolds number simulation.

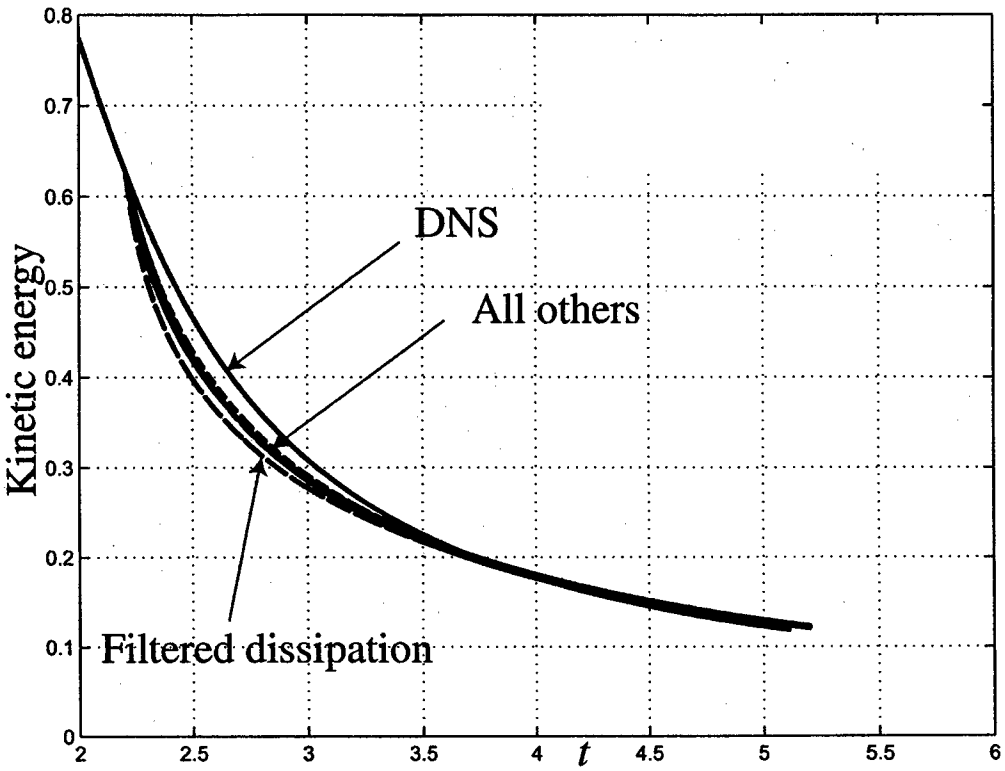

Figure 4.2: Variation of the resolved kinetic energy ($|\boldsymbol{k}| < 32$) with time for the low Reynolds number simulation.

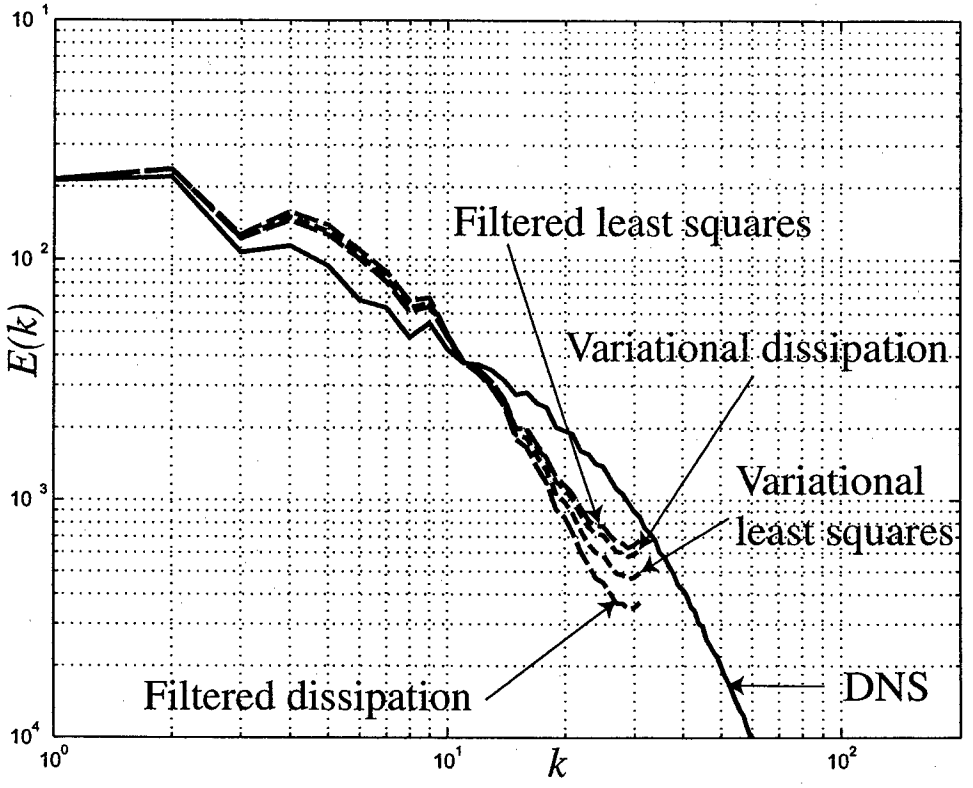

Figure 4.3: Energy spectra at $t = T_2 = 3$ for the low Reynolds number simulation.

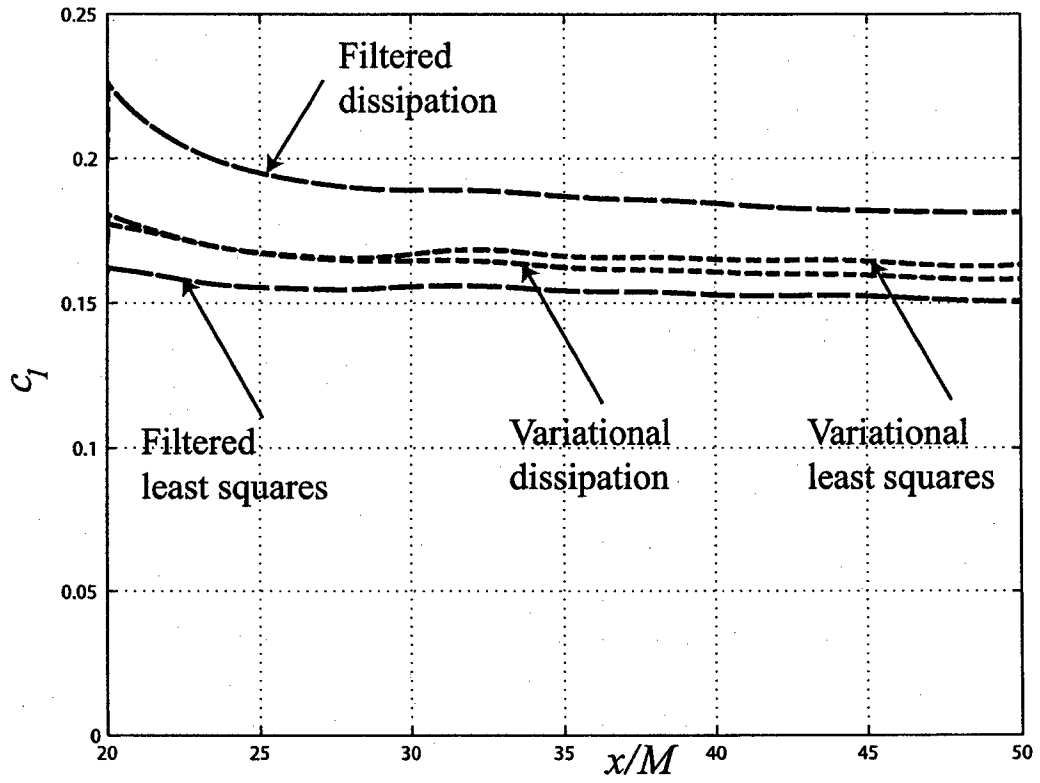

Figure 4.4: Variation of the Smagorinsky parameter c_1 with time for the high Reynolds number simulation.

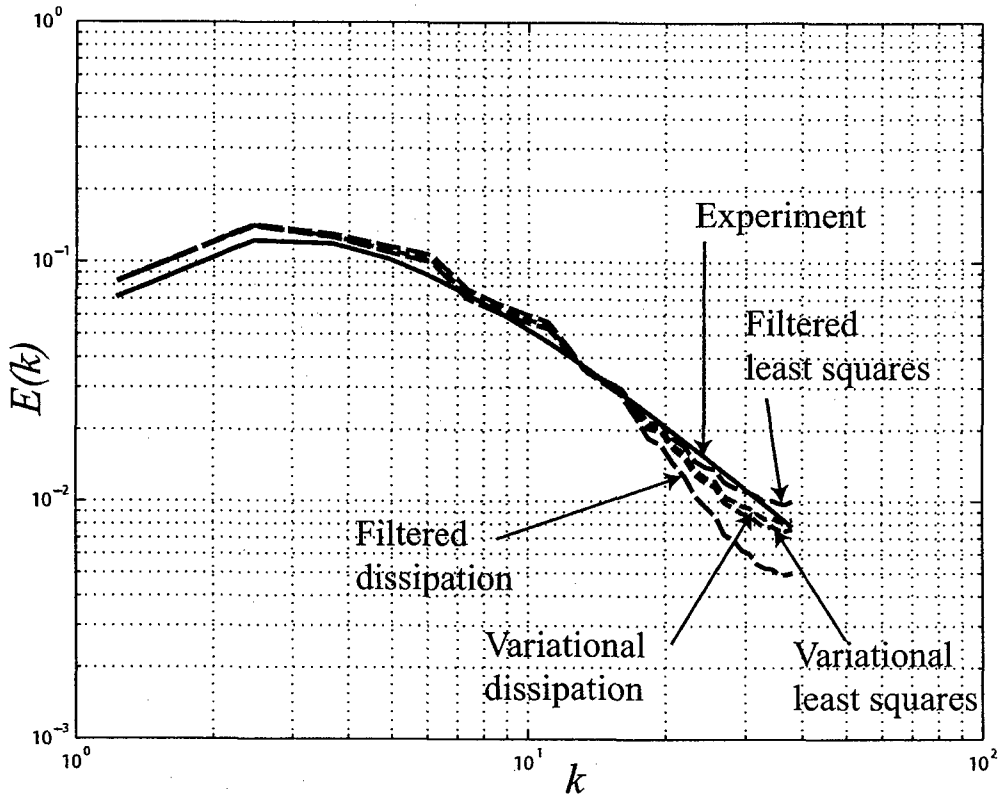

Figure 4.5: Energy spectra at $t = T_2 = 0.506$ for the high Reynolds number simulation.

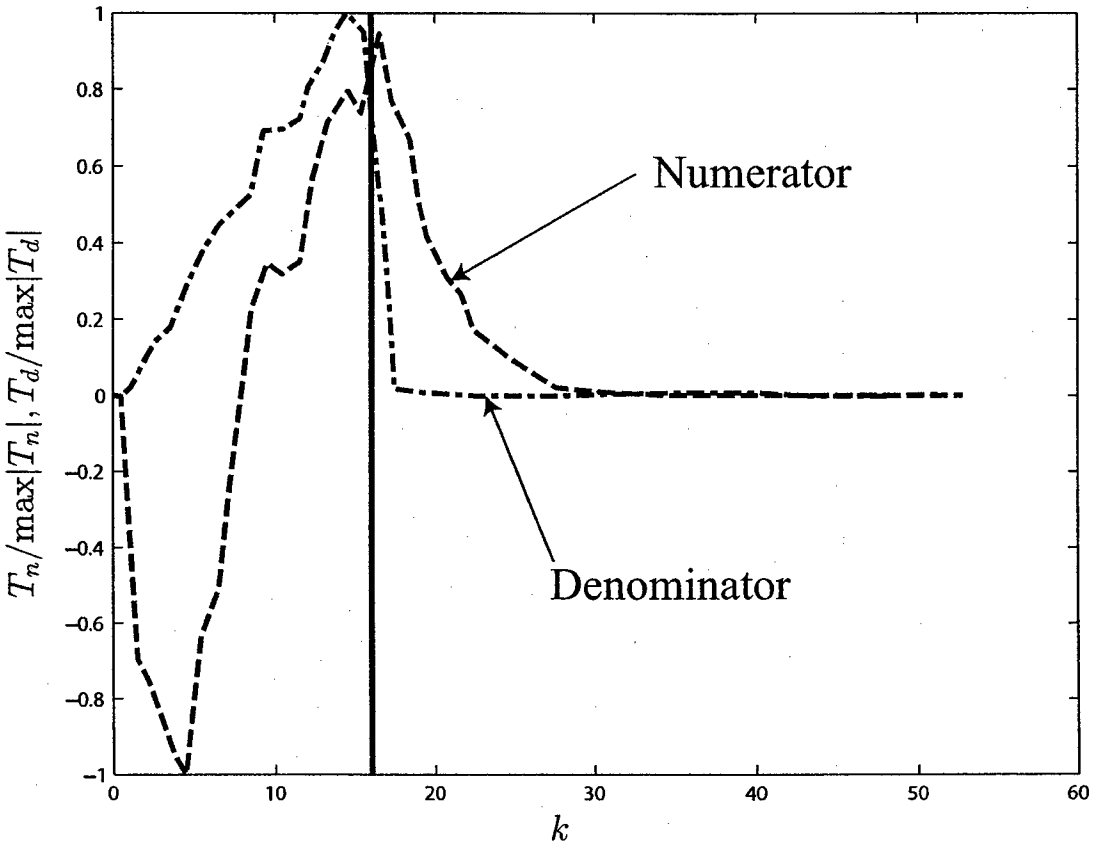

Figure 4.6: Scaled values of T_n and T_d versus wavenumber $k = |\boldsymbol{k}|$. The solid, vertical line represents $k = k^H$.

Chapter 5

Variational Germano Identity Applied to Computing Hydrodynamic Noise

5.1 Introduction

In this chapter we assess the performance of the LES models developed as part of this research program in computing far-field noise. We consider the simple case of homogeneous isotropic turbulence and apply Lighthill's acoustic analogy to compute noise. This decouples the problem into two parts. In the first part we solve the incompressible Navier Stokes equations to determine the fluctuating (turbulent) velocity field. For this purpose we consider sustained turbulence which is driven by a forcing at low wavenumbers. We solve this problem on a fine mesh, where the dissipation length scale is resolved, and then on a much coarser mesh where various LES models are employed to represent the effect of the missing scales.

The velocity field from the turbulent problem is used to construct quadrupole sources which drive the acoustic problem. The acoustic problem is transformed into the frequency domain and then solved. Since we are dealing with an unbounded domain with simple sources, an analytical solution to this problem is feasible. This solution is constructed and used to determine the far-field acoustic pressure intensity as a function frequency and wavenumber. The acoustic intensity is computed for sources obtained from the highly resolved turbulent simulation (the Direct Numerical Solution, DNS) and those obtained from LES models. The acoustic intensity for the LES models is compared to that of the DNS and conclusions about their efficacy are drawn. This rather simple framework provides a useful means to categorize the performance of LES models in predicting turbulence generated noise.

In the following section we derive an expression for the far-field acoustic intensity corresponding to a homogeneous isotropic turbulence field. Thereafter we present results comparing the performance of various LES models.

5.2 Expression for the Far-Field Acoustic Intensity

The use of LES velocity data in Lighthill's acoustic analogy allows for the computation of the far-field acoustic pressure for low Mach number flows. The effect of the hydrodynamic

fluid motion appears as a quadrapole source term in the wave equation

$$\left(\frac{1}{c^2}\frac{\partial^2}{\partial t^2} - \nabla^2\right) p = \nabla \cdot \nabla \cdot \tau \tag{5.1}$$

$$\tau = u \otimes u \tag{5.2}$$

where c is the speed of sound in the ambient medium. The Helmholtz equation is obtained by taking the Fourier transform in time of the wave equation, such that $p(x,t) = \int_{-\infty}^{\infty} \check{p}(x,\omega) e^{-i\omega t} d\omega$.

$$-\left(k^2 + \nabla^2\right) \check{p} = \nabla \cdot \nabla \cdot \check{\tau} \tag{5.3}$$

where $\check{\tau}$ is the Fourier transform in time of τ and $k = \frac{\omega}{c}$.

Writing the solution in terms of a Green's function, the pressure becomes:

$$\check{p}(x,\omega) = \int_{\Omega_y} G(x;y) \nabla_y \cdot \nabla_y \cdot \check{\tau}(y,\omega) d\Omega_y \tag{5.4}$$

For an unbounded domain, the Green's function is

$$G(x;y) = \frac{1}{4\pi} \frac{e^{-ik|x-y|}}{|x-y|} \tag{5.5}$$

The integral in (5.4) can be approximated assuming that x is in the far-field. The acoustic pressure as a function of k, ω and x is then:

$$\tilde{p}(x,k,\omega) = -k^2 \frac{e^{-ik|x|}}{4\pi|x|} \xi \otimes \xi : T(k\xi,\omega) \tag{5.6}$$

where $\xi = \frac{x}{|x|}$ is the unit vector parallel to x and $T(k\xi,\omega)$ is the space-time Fourier transform, with wavenumber $k\xi$ and frequency ω, of $\tau = u \otimes u$ calculated from the incompressible velocity field. This quantity is readily available from the incompressible Navier-Stokes calculation provided a long enough time series of velocity data can be stored for calculating the Fourier transform in time of the source term.

Since the turbulence is isotropic, an ensemble average of the acoustic pressure is equivalent to an average over all directions, ξ, of one realization of the acoustic pressure. By averaging the acoustic pressure over all directions, a two variable function of the scaled noise intensity as a function of k and ω is obtained.

$$(4\pi|x|)^2 \left\langle \check{p}^2(x,k,\omega) \right\rangle = \left\langle \left((k\xi) \otimes (k\xi) : T(k\xi,\omega)\right)^2 \right\rangle \tag{5.7}$$

That is the the scaled, far-field acoustic intensity is determined by the quantity $\left\langle \left((k\xi) \otimes (k\xi) : T(k\xi,\omega)\right)^2 \right\rangle$.

5.3 Evaluation of LES Models

In Figure 5.1, a comparison is made between DNS and several LES schemes with regards to the scaled acoustic intensity. Figure 5.1(a) shows the results from the DNS velocity field while 5.1(d) shows the result from a LES with a constant Smagorinsky parameter. A large improvement is observed when the variational Germano identity is used to determine the Smagorinsky parameter (see Figure 5.1(b)). The best results are obtained when the variational Germano identity is used to determine the parameter of a one parameter multiscale model where the model is only applied to fine scale Fourier modes (Figure 5.1(c)).

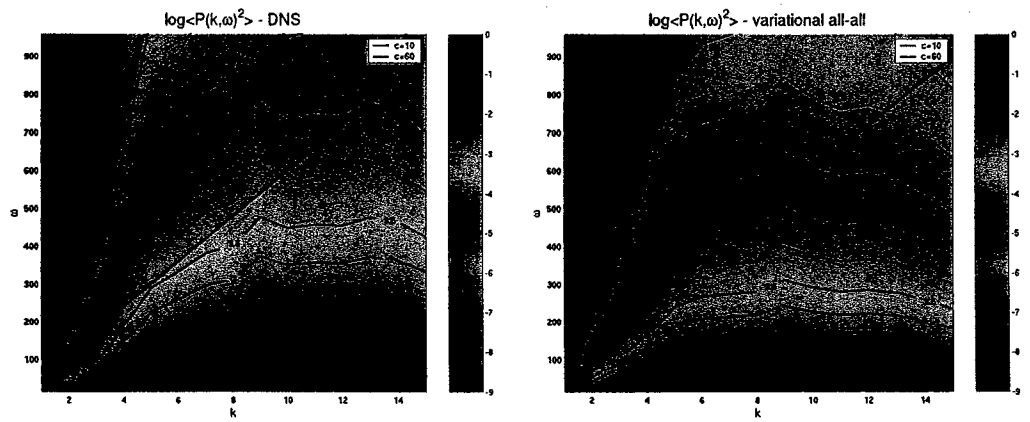

(a) DNS

(b) variational dynamic Smagorinsky

(c) variational multiscale

(d) static Smagorinsky

Figure 5.1: Comparison between DNS and LES of the normalized acoustic pressure intensity as a function of $|k|$ and ω.

From the plots in Figure 5.1, the acoustic pressure frequency spectrum for a particular medium is obtained by choosing a sound speed and taking a section of the plot along $k = \omega/c$. In each plot, lines are added corresponding to values of $c = 10$ and 50. These values of c correspond to a Mach number of about $M = 0.1$ and $M = 0.02$ which is well within the

low-Mach number limit.

When an LES is performed, the Lighthill source term is only partially known. The contribution from the fine scales is not available. To correct for this, the modeled subgrid stress has been included in the source term such that, for the Smagorinsky model, $\tau = \left(u^h \otimes u^h + 2\sqrt{2}(C_s h)^2 |\nabla^s u^h| \nabla^s u^h\right)$. In the results described above we have included this term.

Bibliography

[1] M. J. Lighthill. On Sound Generated Aerodynamically I. General Theory. *Proceedings of the Royal Society of London. Series A, Mathematical and Physical Sciences*, **211A, 1107**:564–587, 1952.

[2] M. J. Lighthill. On Sound Generated Aerodynamically II. Turbulence as a Source of Sound. *Proceedings of the Royal Society of London. Series A, Mathematical and Physical Sciences*, **222, 1148**:1–32, 1954.

[3] A.A. Oberai, F. Roknaldin, and T.J.R. Hughes. Computational Procedures for Determining Structural Acoustic Response due to Hydrodynamic Sources. *Computer Methods in Applied Mechanics and Engineering*, **190(3-4)**:345–361, 2000.

[4] A.A. Oberai, F. Roknaldin, and T.J.R. Hughes. Computation of Turbulent Trailing-edge Noise for a Finite-chord Airfoil. *AIAA journal*, **40(1)**:2206–2217, 2002.

[5] J. E. Ffowcs Williams and L. H. Hall. Aerodynamic Sound Generation by Turbulent Flow in the Vicinity of a Scattering Half Plane. *Jounal of Fluid Mechanics*, **40(4)**:657–670, 1970.

[6] D. G. Crighton and F. G. Leppington. On the Scattering of Aerodynamic Noise. *Journal of Fluid Mechanics*, **46(3)**:577–597, 1971.

[7] D. M. Chase. Sound Radiated by Turbulent Flow off a Rigid Half-Plane Obtained from a Wavevector Spectrum of Hydrodynamic Pressure. *Journal of the Acoustical Society of America*, **52(3)**:1101–1123, 1971.

[8] K. L. Chandiramni. Diffraction of Evanescent waves, with Applications to Aerodynamically Scattered Sound and Radiation from Unbaffled Plates. *Journal of Acoustical Society of America*, **55(1)**:18–29, 1973.

[9] M. S. Howe. Trailing Edge Noise at Low Mach Numbers. *Journal of Sound and Vibration*, **225(2)**:211–238, 1998.

[10] M. S. Howe. Edge-source Acoustic Green's Function for an Airfoil of Arbitrary Chord, with Application to Trailing-edge Noise. *Quarterly Journal of Mechanics and Applied Mathematics*, **54(1)**:139–155, 2001.

[11] M. Wang and P. Moin. Computation of Trailing-edge Flow and Noise Using Large-eddy Simulation. *AIAA Journal*, **38(12)**:2201–2209, 2000.

[12] T.J.R. Hughes, L. Mazzei, A.A. Oberai, and A.A. Wray. The Multiscale Formulation of Large Eddy Simulation: Decay of Homogeneous Isotropic Turbulence. *Physics of Fluids*, **13**(2):505–512, 2001.

[13] T.J.R. Hughes, A.A. Oberai, and L. Mazzei. Large Eddy Simulation of Turbulent Channel Flows by the Variational Multiscale Method. *Physics of Fluids*, **13**(6):1784–1799, 2001.

[14] T.J.R. Hughes, L. Mazzei, and K.E. Jansen. Large Eddy Simulation and the Variational Multiscale Method. *Computing and Visualization in Science*, **3**:47–59, 2000.

[15] M. Germano, U. Piomelli, P. Moin, and W.H. Cabot. A Dynamic Subgrid-scale Eddy Viscosity Model. *Physics of Fluids*, **3(7)**:1760–1765, 1991.

[16] A.A. Oberai and J. Wanderer. A Dynamic Approach for Evaluating Parameters in a Numerical Method. *International Journal for Numerical Methods in Engineering*, **62**:50–71, 2005.

[17] A.A. Oberai and J. Wanderer. A Dynamic Diffusivity Method for the Spectral Approximation of Conservation Laws. *Computer Methods in Applied Mechanics and Engineering*, in press, 2005.

[18] A.A. Oberai and J. Wanderer. Variational Formulation of the Germano Identity for the Navier-Stokes Equations. *Journal of Turbulence*, 6, 2005.

[19] J. Wanderer and A.A. Oberai. Evaluation of the VMS models in prediciting turbulence induced noise. *in preperation*, 2006.

[20] T. J. R. Hughes, G. R. Feijóo, L. Mazzei, and J.-B. Quincy. The Variational Multiscale method–A Paradigm for Computational Mechanics. *Computer Methods in Applied Mechanics and Engineering*, **166(1-2)**:3–24, 1998.

[21] P.E. Barbone and I. Harari. Nearly H-1-optimal finite element methods. *Computer Methods in Applied Mechanics and Engineering*, **190(43-44)**:5679–5690, 2001.

[22] T. J. R. Hughes. Multiscale Phenomena: Green's functions, The Dirichlet-to-Neumann formulation, subgrid scale models, bubbles, and the origins of stabilized methods. *Computer Methods in Applied Mechanics and Engineering*, **127**:387–401, 1995.

[23] F. Brezzi, L. Franca, T. J. R. Hughes, and A. Russo. $b = \int g$. *Computer Methods in Applied Mechanics and Engineering*, **145**:329–339, 1997.

[24] E. Oñate. Derivation of Stabilized Equations for Numerical Solution of Advective-Diffusive Transport and Fluid Flow Problems. *Computer Methods in Applied Mechanics and Engineering*, **51(1-2)**:233–265, 1997.

[25] F. Brezzi, P. Houston, D. Marini, and E. Suli. Modeling subgrid viscosity for advection-diffusion problems. *Computer Methods in Applied Mechanics and Engineering*, **190(13-14)**:1601–1610, 2000.

[26] S. Ghosal, T.S. Lund, P. Moin, and K. Akselvoll. A Dynamic Localization Model for Large-Eddy Simulation of Turbulent Flows. *Journal of Fluid Mechanics*, **286**:229–255, 1995.

[27] D.K. Lilly. A Proposed Modification of the Germano Subgrid-scale Closure Method. *Physics of Fluids A*, **4(3)**:633–635, 1992.

[28] A. N. Brooks and T. J. R. Hughes. Streamline upwind/petrov-galerkin formulations for convection dominated flows with particular emphasis on the incompressible navier-stokes equations. *Computer Methods in Applied Mechanics and Engineering*, **32(1-3)**:199–259, 1982.

[29] C. Foais, O. Manley, R. Rosa, and R. Temam. *Navier-Stokes Equations and Turbulence.* Cambridge University Press, Cambridge, 2001.

[30] J. Smagorinsky. General Circulation Experiments with the Primitive Equations. I. The Basic Experiment. *Monthly Weather Review*, **91**:99–164, 1963.

[31] N. Mansour and A. Wray. Decay of Isotropic Turbuelnce and Low Reynolds Number. *Physics of Fluids*, **6(2)**:808–814, 1994.

[32] D. K. Lilly. On the Application of the Eddy Viscosity Concept in the Inertial Subrange of Turbulence. Technical report, NCAR manuscript 123, Boulder, CO, 1966.

[33] R.S. Rogallo. Numerical Experiments in Homogeneous Turbulence. Technical Report Tech. Memo. TM 81315, NASA, 1981.

[34] G. B. Whitham. *Linear and Nonlinear Waves.* John Wiley and Sons, New York, NY, 1974.

[35] P. D. Lax. *Hyperbolic systems of Conservation Laws and the Mathematical Theory of Shock Waves.* Society for Industrial and Applied Mathematics, Philadelphia, PA, 1972.

[36] R. J. LeVeque. *Numerical Methods for Conservation Laws.* Birkhauser Veralg, Basel, 2nd edition, 1992.

[37] C. Canuto, M.Y. Hussaini, A. Quarteroni, and T.A. Zang. *Spectral Methods in Fluid Dynamics.* Springer-Verlag, Berlin-Heidelberg, 1988.

[38] J. von Neumann and R. D. Richtmyer. A Method for Numerical Calculations of Hydrodynamical Shocks. *Journal of Applied Physics*, **21**:232–237, 1950.

[39] E. Tadmor. Convergence of Spectral Methods for Nonlinear Conservation Laws. *SIAM Journal of Numerical Analysis*, **26(1)**:30–44, 1989.

[40] J.-L Guermond. Subgrid Stabilization of Galerkin Approximations of Linear Monotone Operators. *IMA Journal of Numerical Analysis*, **21(1)**:165–197, 2001.

[41] S.S. Collis. The DG/VMS Method for Unified Turbulence Simulation. AIAA Paper, No. 2002-3124, 2002.

[42] S. Ghosal and P. Moin. The Basic Equations for the Large Eddy Simulation of Turbulent Flows in Complex Geometry. *Journal of Computational Physics*, **118**:24–37, 1995.

[43] G.P. Galdi and W.J. Layton. Approximation of the Larger Eddies in Fluid Motions. II. A Model for Space-Filtered Flow. *Mathematical Models & Methods in Applied Sciences*, **10**:343–350, 2000.

[44] A.L. Marsden, O.V. Vasilyev, and P. Moin. Construction of Commutative Filters for LES on Unstructured Meshes. *Journal of Computational Physics*, **174**:584, 2002.

[45] Y. Morinishi and O.V. Vasilyev. Vector Level Identity for Dynamic Subgrid Scale Modeling in Large Eddy Simulation. *Physics of Fluids*, **14(10)**:3616–3623, 2002.

[46] H.S. Kang, S. Chester, and C. Meneveau. Turbulence in an Active-Grid-Generated Flow and Comparisons with Large-Eddy Simulation. *Journal of Fluid Mechanics*, **480**:129–160, 2003.